UCRL-19073 errata
cy. 2

RECEIVED
LAWRENCE
RADIATION LABORATORY
OCT 9 1969
LIBRARY AND
DOCUMENTS SECTION

MAGNETIC PROPERTIES OF THE NICKEL-RHODIUM SYSTEM

Eric R. Katz
(Ph.D. Thesis)

August 1969

AEC Contract No. W-7405-eng-48

TWO-WEEK LOAN COPY

This is a Library Circulating Copy
which may be borrowed for two weeks.
For a personal retention copy, call
Tech. Info. Division, Ext. 5545

UCRL-19073
cy. 2

LAWRENCE RADIATION LABORATORY
UNIVERSITY of CALIFORNIA BERKELEY

DISCLAIMER

This document was prepared as an account of work sponsored by the United States Government. While this document is believed to contain correct information, neither the United States Government nor any agency thereof, nor the Regents of the University of California, nor any of their employees, makes any warranty, express or implied, or assumes any legal responsibility for the accuracy, completeness, or usefulness of any information, apparatus, product, or process disclosed, or represents that its use would not infringe privately owned rights. Reference herein to any specific commercial product, process, or service by its trade name, trademark, manufacturer, or otherwise, does not necessarily constitute or imply its endorsement, recommendation, or favoring by the United States Government or any agency thereof, or the Regents of the University of California. The views and opinions of authors expressed herein do not necessarily state or reflect those of the United States Government or any agency thereof or the Regents of the University of California.

TABLE OF CONTENTS

ABSTRACT ---------- v

I. INTRODUCTION ---------- 1

II. EXPERIMENTAL DETAILS ---------- 8

A. Alloy Preparation ---------- 8

B. Analysis of Samples ---------- 11

C. Microwave Experiment ---------- 13

D. Magnetostatic Measurements ---------- 18

III. INTRODUCTION TO THE BAND THEORY OF MAGNETISM ---------- 24

A. Exchange and the Molecular Field Approximation ---------- 24

B. Stoner Theory ---------- 38

C. Hurwitz - Van Vleck Description ---------- 56

IV. MAGNETOSTATIC MEASUREMENTS IN Ni-Rh ---------- 61

A. Saturation Moment and Paramgnetic Susceptibility ---------- 61

B. Comparison with Theory - Solution of Stoner Equation ---------- 73

C. Low Temperature Variation of Magnetization Elementary Excitations in Band Ferromagnets ---------- 84

D. Magnetic Isotherms - Magnetocrystalline Anisotropy ---------- 99

V. MAGNETIC RESONANCE STUDIES ---------- 116

A. Background ---------- 116

B. Data and Discussion ---------- 126

C. Spectroscopic Splitting Factor ---------- 143

VI. SUMMARY AND CONCLUSIONS ---------- 145

ACKNOWLEDGEMENTS ---------- 147

REFERENCES ---------- 148

FIGURE CAPTIONS ---------- 153

UNIVERSITY OF CALIFORNIA

February 9, 1970

Lawrence Radiation Laboratory
Berkeley, California

ERRATA

TO: Recipients of UCRL-19073

FROM: Technical Information Division

SUBJECT: Eric R. Katz' Ph.D. Thesis entitled:
MAGNETIC PROPERTIES OF THE NICKEL-RHODIUM SYSTEM
Date of thesis: August 1969

Please make the following corrections on subject report:

1. Replace abstract with attached corrected.

2. p. 30, line just above Eq. 3.1.6 reads:"In the effect..." should read:"In the effective ..."

3. p. 79,Eq. 4.2.40 should read : $\eta(\Delta c) = \eta_o + \eta_1 \cdot \Delta + \ldots$

4. p. 84,line 5 should read: "by applying Fermi..."

5. p. 86, 2nd paragraph , line 3 should read "These are collective..."

6. p. 98, last paragraph, line 4 should read: "wave contribution, varying as $T^{3/2}$..."; line 5 should read: "particle contribution, varying as T^2."

7. p. 111, Eq. 4.422 should read: "....$\vec{L}\cdot\vec{S} = A\,\vec{L}\cdot\vec{S}$

MAGNETIC PROPERTIES OF THE NICKEL-RHODIUM SYSTEM

Eric R. Katz

Inorganic Materials Research Division, Lawrence Radiation Laboratory,
and Department of Physics,
University of California, Berkeley, California

ABSTRACT

Magnetostatic and magnetic resonance studies have been performed on a number of alloys in the Ni-Rh binary system. These alloys exhibit ferromagnetic behavior for nickel concentrations exceeding 63 atomic per cent, and paramagnetic behavior for the more dilute alloys. The earlier work of Crangle and Parsons, in which the saturation magentization and Curie temperature as a function of composition were measured, was extended. The magnetization as a function of temperature in the range $4.2°K < T < 320°K$ was measured in the presence of an externally applied field. These results were compared with the theory developed by Stoner and Wohlfarth, who attempted to explain the behavior of weakly ferromagnetic systems by treating the magnetic electrons as forming a band. Our results do not agree with the predictions of this overly simplified theory. The magnetocrystalline anisotropy was determined from magnetic isotherm measurements, and the observed composition dependence followed the expected form. The spin relaxation rate was determined from the magnetic resonance data and compared with the composition dependence of the magnetocrystalline anisotropy, again using the Stoner model. Again the observations failed to obey the behavior predicted by this model. Another model, similar to the Anderson model of dilute magnetic alloys, was proposed, which explains all our data in a qualitative way.

MAGNETIC PROPERTIES OF THE NICKEL-RHODIUM SYSTEM

Eric R. Katz

Inorganic Materials Research Division, Lawrence Radiation Laboratory,
and Department of Physics,
University of California, Berkeley, California

ABSTRACT

Magnetostatic and magnetic resonance studies have been performed on a number of alloys in the Ni-Rh binary system. These alloys exhibit ferromagnetic behavior for nickel concentrations exceeding 63 atomic per cent, and paramagnetic behavior for the more dilute alloys. The earlier work of Crangle and Parsons, in which the saturation magnetization and Curie temperature as a function of temperature in the range $4.2^{\circ}K. < T < 320^{\circ}K$ was measured in the presence of an externally applied field. These results were compared with the theory developed by Stoner and Wohlfarth, who attempted to explain the behavior of weakly ferromagnetic systems by treating the magnetic electrons as forming a band. Our results do not agree with the predictions of this overly simplified theory. The magnetocrystalline anisotropy was determined from magnetic isotherm measurements, and the observed composition dependence followed the expected form. The spin relaxation rate was determined from the magnetic resonance data and compared with the composition dependence of the magnetocrystalline anisotropy, again using the Stoner model. Again the observations failed to obey the behavior predicted by this model. Another model, similar to the Anderson model of dilute magnetic alloys, was proposed, which explains all our data in a qualitative way.

I. INTRODUCTION

The nature of the ferromagnetic state in the 3-d transition metals is not yet understood. The basic problem is explaining the nature of the 3-d electrons themselves, which are the ones responsible for the magnetic behavior. The descriptions of these electrons lies somewhere between the limits of the two well known models, a nearly free electron gas, and the tight binding approximation. Thus, these electrons are very difficult to treat in a quantitative manner.

Historically, the treatment of magnetism has proceeded along two lines: the localized moment, or Heisenberg model, and the band picture.

The localized moment picture has been applied quite successfully to ferromagnetic insulators and to rare-earth ferromagnets[1], thus it has received a greater amount of attention.

In this familiar model, the metal is thought of as containing incomplete inner shells (d or f) whose electrons couple together in each atom, according to Hund's rule into a state with net spin angular momentum, $\vec{S}$, and associated magnetic moment. Spins on neighboring atoms, due to overlap of their wave functions, may couple together ferromagnetically, the strength of this coupling interaction being determined by the overlap, or exchange integral, J, between neighboring sites.

This model leads to quantitative relationships between the ferromagnetic transition temperature T_c and the strength of the exchange interaction, and describes spin waves, critical fluctuations, saturation magnetization at low temperature, paramagnetic susceptibility, specific heat, scattering (elastic and inelastic) of neutrons, and magnetic resonance properties.

However, this approach breaks down when it is applied to the 3-d transition metals. First, the observed value of the saturation magnetization at absolute zero for these metals leads to magnetic moments per atom far different from those corresponding to an integral number of electrons, as required by the Heisenberg model. Second, there is a large deviation in the size of the magnetic moment per atom as derived from saturation magnetization measurements, and from the magnitude of the Curie-Weiss susceptibility constant.

Other discrepencies include the following: Large electronic specific heat in these materials (e.g., the electronic specific heat of magnetic nickel is about ten times as great as that of non-magnetic copper). This indicates that the magnetic electrons are mobile. The presence of high field differential susceptibility, which is difficult to explain in a local moments model without resorting to various spiral magnetic structures. This susceptibility has been observed in various materials. However, neutron diffraction studies of these materials have ruled out any such structure. This type of susceptibility follows quite naturally from the band approach[2]. Hall effect measurements[3] indicate d-electrons contribute to conductivity, i.e., that they are mobile.

In favor of the localized moment picture was thought to be the $T^{3/2}$ temperature dependence of the saturation magnetization at low temperature, and the inelastic neutron scattering (below, and somewhat above T_c), explainable by spin wave theory, which was thought to result only from localized moments. However, recent works, which we shall discuss, have shown that spin-wave-like excitations also can exist in a running wave (band) model of a ferromagnet, and in fact, the band approach also

provides accurate description of the experimental neutron scattering data.

The band approach treats the magnetic electrons as running waves, forming bands. This approach can be thought of as a generalization of the picture used to describe the Pauli spin susceptibility in a conduction electron gas. Such a description is provided in Introduction to Solid State Physics[4].

A very useful approach to this problem was made by Stoner, which we will describe in Section III. His theory makes qualitative predictions about such a system, using only a very small number of parameters to describe the system.

In order to test the applicability of his theory, it was desirable to find a magnetic system in which one could experimentally vary these parameters, and then compare the results of this variation with the predictions of the theory. For reasons which we shall describe, we felt that the nickel-rhodium binary alloy system is describable by the Stoner theory, and that the variation in alloy composition provides the desired variation in the parameters describing this system.

The Ni-Rh system forms a continuous range of FCC solid solutions[5] which exhibit ferromagnetic behavior for concentrations of nickel exceeding a critical value of about 63 atomic per cent[6].

Crangle and Parsons[7], as part of a study of the magnetization of binary alloys of cobalt and nickel with elements of the Pd and Pt group, noted that the saturation moment of the Ni-Rh system first increased with increasing rhodium concentration, reaching a maximum near 5 per cent rhodium, then decreased continuously to 0 at about 37 per cent rhodium. They attempted to explain the initial increase in magnetization using

several simple models, including the rigid-band model. This model supposes the shapes and relative positions of the d and s bands remain essentially unchanged by the addition of rhodium. Thus, the density of states functions describing these bands also remains constant, and the sole effect of alloying is to contribute additional carriers to these two bands.

The initial increase of magnetization with low Rh concentration corresponds to about 2 holes in the d-band per Rh atom added, as compared to the one hole per atom expected from the atomic configurations of Ni and Rh. Of course, this model provides no explanation of the decreasing moment as the Rh concentration is further increased. One must resort to the band picture for such an explanation. These authors also measured the Curie temperature as a function of Rh concentration, and found it to decrease continuously.

Bucher et al.[6] measured the high field differential susceptibility at 1.4°K. for this system, concentrating their efforts in the region around the critical concentration. They found a symmetric peak behaving roughly as the inverse of the deviation in alloy composition from its critical value. Further, they measured the electronic contribution to the heat capacity, and found a logarithmic peak at the critical concentration.

The explanation of this data cannot be made within the framework of the traditional, or localized moments, description of the magnetic state. We are thus forced to appeal to the band approach for such an explanation.

Therefore, we decided to use this system to test the applicability of some of the band approaches in describing a real system.

The first part of our experiments consisted of magnetostatic

measurements with various samples of differing composition, ranging from pure nickel, to a sample consisting of 57 per cent nickel and 43 per cent rhodium. These measurements included determination of the saturation magnetization at low temperatures, the susceptibility in the paramagnetic region as a function of temperature, and the determination of the magnetocrystalline anisotropy.

The second part of the experiment was an outgrowth of earlier work done by Salamon[8]. He performed magnetic resonance studies in pure nickel in the vicinity of the Curie point and above. He concerned himself primarily with the relaxation rate of the paramagnetic spins, which is obtained from the width of the resonance lines. He based his interpretation on a localized moments picture, in which, for very high temperatures, the relaxation mechanism is the exchange-narrowed pseudo-dipolar interaction[9], which is modified as the Curie temperature is approached from above by the onset of short range order and critical fluctuations[10].

We performed similar measurements on our alloys, both in the ferromagnetic and paramagnetic regions, with particular attention devoted to the paramagnetic region, where we determined the spectroscopic splitting factor and the relaxation rate, which we compare to the predictions of the band theory.

The organization of the remainder of this work will be as follows:

Chapter Two contains the description of the alloy preparation and analysis, as well as the descriptions of the experimental details. We also discuss the apparatus used in making the magnetostatic measurements, and the microwave spectrometer used for the resonance studies.

Chapter Three is an introduction to the band theory of magnetism. In the first subsection we show how certain simplifying assumptions regarding exchange lead to a molecular field approximation in an electron gas, and some of the consequences of this field. In the second subsection, we outline briefly the quantitative approach to this problem taken by Stoner, indicating the basic assumptions, the weaknesses, and the conclusions reached by this approach. We compare these predictions with previous experimental work. In the third subsection, we describe another approach in explaining the magnetic properties of the 3-d series, that of Hurwitz and Van Vleck. This model is able to treat effects of correlation, whereas, the Stoner model is not. However quantitative predictions are difficult with this approach.

In Chapter Four, we discuss our magnetostatic measurements. In the first subsection we discuss the concentration dependence of the saturation magnetization, the Curie temperature, and the magnitude of the paramagnetic susceptibility. Since the Stoner theory treats these quantities, we compare our data with the predictions of Stoner. Since quantitative predictions require detailed knowledge about the density of states function, we concentrate our attention on the region near the critical concentration, where certain expansions may be carried out, leading to predictions about the general relationships between various measured quantities. We find several discrepencies between the theoretical predictions and the observed data. In the second subsection we discuss the low temperature magnetization data for some of our samples. We trace the development of the theory of spin waves as it applies to band ferromagnets, as well as the more important band effects which

influence the temperature dependence of the magnetization, in the framework of the Stoner model. We then compare our data with the results of this theory, and find satisfactory agreement. In the third subsection we discuss our determination of the magnetocrystalline anisotropy versus alloy composition. We trace the development of the theory of anisotropy, indicating how this theory applies to a band system. We compare this theory to our data, and again find satisfactory agreement.

In Chapter Five, we discuss our magnetic resonance studies. We concentrate our attention on explaining the observed relaxation rates in the paramagnetic region, and relate this to the microscopic nature of the magnetic state. We indicate how the band theory must be modified to explain our observations.

In Chapter Six, we present a summary of our results and conclusions.

II. EXPERIMENTAL DETAILS

A. Alloy Preparation

Nickel and rhodium for an uninterrupted series of solid solutions[5], which solidify into a F.C.C. structure.

The alloys for the present studies were prepared from high purity nickel and rhodium powders. The rhodium powder was obtained from Leico Industries, New York, and was quoted by them as being 99.999% pure. The nickel powder was obtained from Electronic Space Products, Inc., Los Angeles, and was 99.99+% pure.

The powder sizes were measured under a metallurgical microscope, and the average particle grain size was found to be ≃ 1 micron diameter for both of the powders.

The alloys were prepared in batches of 1.6 grams. Desired atomic compositions were selected, and converted to ratios by weight. The powders were weighed out carefully, using a Mettler micro-balance, to an accuracy of ± .0003 gm. This corresponds to ± .02% by weight. The powders were then thoroughly mixed and put into a zirconia crucible. The zirconia cricibles were made by grinding down zirconia tubes, obtained from the Degussa Corp., Kearny, New Jersey. These tubes were 5 mm. I.D., 8 mm. O.D., and closed on one end. They were composed of a dense ceramic containing 97% ZrO_2 stabilized with 3% CaO. After being ground down to the proper length, they were baked at about 500°C for about 24 hours.

After the powder was put in the crucible, a tightly fitting cap was cemented on the crucible, using Astroceram, a general purpose ceramic cement. This did not provide a vacuum-tight seal, but was used to retard escape of nickel vapor from the crucible during the melting process.

The crucible was suspended in a high vacuum Abar resistance furnace, using a tantalum sheet which surrounds the hot zone as a resistance element. The furnace is equipped with Pt-Pt/Rh thermocouples, but temperature measurements were made with an optical pyrometer.

The furnace was evacuated with the powder and crucible inside to a pressure of less than 10^{-5} torr. The furnace was then heated to 500-600°C. and held there for five hours to set the ceramic cement. The temperature was increased to 1000-1100°C to de-gas the crucible and powder inside. After the pressure reached less than 3×10^{-6} torr, the furnace was held at this temperature for at least one additional hour.

The crucible was then heated in gradual steps to avoid any undo thermal stresses to the crucible according to the following program. Temperatures given are those read by an optical pyrometer, calibrated for a black-body radiator. Due to the non-perfect emissivity of the crucible material (manufacturer quotes e = 0.24) the actual temperatures are actually 100-150°C higher. The heating program was as follows:

T = 1550°C	held for 5 minutes
T = 1650°C	held for 3 minutes
T = 1850°C	held for 3 minutes
T = 1965°C	held for 7 minutes

(The melting point of Rh is 1966 $\pm$ 3°C , while nickel melts at 1453°C.)[11]

After holding the sample at the highest temperature for seven minutes, the heater power was shut off completely. The outside of the crucible dropped to 1600°C. in 14 seconds, and to 1400°C. in less than 30 seconds.

The sample was "quenched" as described in order to cross the solidus-liquidus transition region as quickly as possible, to make the

alloy as uniform as possible.

The crucible was allowed to cool to room temperature, and was then removed from the furnace. It was cracked open, and the alloy, in the form of a slug 5 mm. diameter X ≈ 8 mm. length was removed.

There was indication of a mild reaction between the inner surface of the crucible and the outer surface of the slug, which gave the slug a "glazed" appearance, but the reaction did not appear to penetrate into the slug.

The slug was placed in an alumina crucible and returned to the furnace for annealing. It was annealed at 1100°C. for a minimum of 72 hours. It was then removed from the furnace.

Thin disks, 5 mm. diameter by .010"-.020" were sliced off by means of a carborundum disk saw, for use in the magnetic resonance experiments. The remainder of the slug was turned down on a lathe into a cylinder, .105 inches diameter by .145 inches in length, for magnetization measurements.

B. Analysis of Samples

Several of the alloys were analyzed with an electron beam microprobe.

During this type of analysis, the sample is bombarded in a high vacuum with a narrow (approximately 1 micron diameter) beam of monoenergetic electrons. The resulting X-ray radiation is scanned for various wavelengths corresponding to K-alpha and L-alpha lines of the elements being scanned. These lines are detected using various crystals as X-ray diffration monochromators, followed by counters. The number of counts per fixed time interval is related to the concentration of the corresponding element in the alloy under investigation. The device is calibrated with known standards of pure elements, and corrected for background, X-ray fluorescence, etc.

Our alloys were scanned for nickel and rhodium. In addition, since the alloys were prepared in a zirconia crucible, they were also scanned for zirconium.

Since the production of X-rays excited by an electron beam is a random process, there is a statistical distribution in the counts received in each monochromator channel. Thus, from elementary statistics, the standard deviation in the number of counts in any channel is just the square root of the mean number of counts expected in that channel.

For the ten second interval used, our samples gave approximately 10,000 and 5,000 counts for nickel and rhodium, respectively. Thus the statistical uncertainty in the number of counts is on the order of one percent, and therefore the uncertainty in the concentration of each of these elements was also of this order of magnitude.

Thus the device was useful only for determining whether or not the alloy deviated significantly from the concentration of the ingredients, i.e., if there was excessive evaporation of one of the constituents, (nickel has the higher vapor pressure of the two, reaching 1-10 torr at the highest temperature reached during the melting) and whether or not there were large local fluctuations in the concentration.

The results of the microprobe indicated that the composition of the alloy was, within the limitations of the accuracy of the analysis, equal to the composition of the ingredients as they were weighed out before melting, and that there were no large (i.e. > 1%) fluctuations in the composition.

Further, the counts received in the zirconium channel were just equal to the zirconium channel background counts, within the statistical distribution expected, and indicated that the zirconium concentration was at least less than 0.1%.

Metallographic analyses of the samples were also attempted, but no suitable etchant could be found, so the crystal grain boundaries could not be revealed.

Such studies would be desirable, for one could then perform microprobe analysis on a particular grain, as a function of the distance from the grain center to the perimeter. Such a study would show whether the quench and subsequent anneal were sufficient to remove any composition gradients introduced by crossing the solidus-liquidus region in a finite length of time.

However, the results of the microprobe analyses which were performed indicate, at least, that no gross composition gradients exist.

C. Microwave Experiment

Ferromagnetic resonance (FMR) and electron paramagnetic resonance (EPR) measurements were performed using a standard Q-band magic-tee microwave spectrometer. This type of spectrometer has been described by Feher.[12]

The spectrometer used had been built originally for another experiment[13] and the modifications necessary for the present work were incorporated.

The cavity and sample unit are shown in figure 1. The cavity was maintained at the coolant temperature (either 77°K or 4.2°K).

The sample, in the form of a thin disk, was glued on the closed end of a hollow copper rod. Inside the rod was a Pt resistance thermometer around which was wound a non-inductive manganin heater coil. This temperature unit was loosely coupled to the coolant bath with three thin brass support struts.

Temperature control was achieved in either of two ways:

Long term constant temperature: The Pt thermometer was used as one arm of an AC bridge. A second arm was adjusted externally, and the imbalance in the bridge was used to drive the heater power supply. With this method, a few millidegrees stability for long term periods was easily attainable.

Slow sweep: Heater power was increased very slowly, so that the temperature rose continuously but slowly. The temperature change was less than a degree during the course of a particular magnetic resonance sweep.

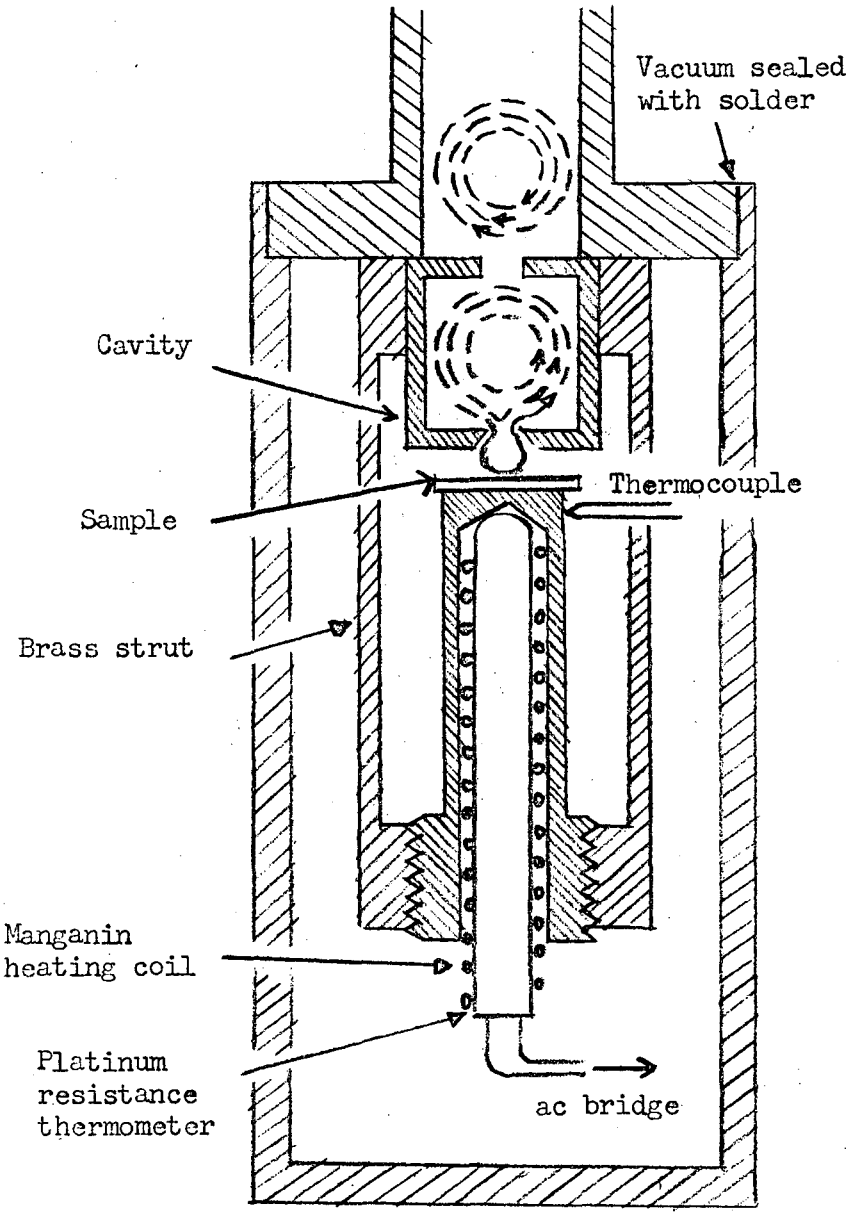
Vacuum sealed
with solder
Cavity
Thermocouple
Sample
Brass strut
Manganin
heating coil
Platinum
resistance
thermometer
ac bridge

Fig. 1

In both cases, temperature was monitored with a copper-constantan thermocouple. This was placed very close to the sample on the copper rod. In either mode of temperature control, the thermocouple gave accurate measurement of the temperature.

The cavity was excited in the TE101 mode using a standard klystron and power supply. Since the cavity was maintained at helium (or nitrogen) temperature during the course of a run, independent of sample temperature, the frequency remained constant, at 29.69 Gc./sec.

The sample, in the form of a thin disk, was placed very close to an iris in the cavity. The microwave field which bulged out of this iris impinged on the sample and caused an oscillating magnetic field parallel to the surface of the sample. Thus the sample was coupled to the microwave field of the cavity, though somewhat more weakly than if it were actually placed inside the cavity.

A slowly varied external D.C. magnetic field, H, was applied parallel to the surface of the sample, but perpendicular to at least one component of the RF magnetic field. This configuration of sample, microwave field, and static field exhibits a resonance in the power absorbed from the microwave field when the resonance condition

2.3.1 $$\omega_{RF} = \gamma(BH)^{1/2}$$

is met. Here

2.3.2 $$\gamma = g\mu_B/\hbar$$

where g is the gyromagnetic factor of the magnetic carriers, μ_B is the Bohr magneton, $\hbar$ is Planck's constant divided by 2π, and $B = (H+4\pi M)$ is the magnetic induction, and M is the magnetization of the sample. This result has been discussed, for example, by Kittel.[14] The microwave

power reflected back from the cavity was monitored with a standard crystal detector.

The Zeeman field was swept slowly from about 2 koe. to 13 koe. and then back. The output of a DC gaussmeter (rotating coil gaussmeter with a phase detector and filter providing a DC output voltage proportional to the instantaneous value of the magnetic field) was used to drive the X channel of an X-Y recorder, and the change in reflected microwave power was amplified and used to drive the Y channel.

For technical reasons, this experiment was a DC one, rather than the usual AC experiment, i.e. one often modulates the Zeeman field with a small AC component, and uses a phase detector to monitor the reflected power. The coherent signal observed is proportional to the amplitude of this audio modulation, multipied by the derivative of the line being swept, evaluated at the position of the resonance line corresponding to the instantaneous value of the Zeeman field. This signal is also inversely proportional to the width of the line. Due to the broad line widths incurred ($\Delta H_{\text{audio modulation}}/\text{Linewidth} \lesssim .01$) as well as mechanical resonances in the system (driven by the interaction of currents induced by the AC field with the DC field, causing mechanical vibrations coherent with the AC signal) the AC method became unfeasible.

The field was then swept yielding X-Y recorder traces of the resonance line. Data was read off these recorder traces and punched onto IBM cards in pairs: field value and power reflected.

For reasons to be discussed in a later section, the relaxation process contributing to the linewidth are expected to yield Lorentzian lineshapes.

Thus a general least-squares curve fitting program was used on a CDC 6600 computer to fit a general Lorentzian line shape with five parameters to the observed data. The five parameters were essentially Lorentzian dispersion amplitude, absorption amplitude, line center, line width, and position of baseline.

The reason that dispersion is introduced into an absorption experiment is that the dispersive part of the magnetic susceptibility (which in addition to the absorptive part, is also a function of the applied Zeeman field. In fact, the two are related by the Kramers-Kronig relations.[15]) affects the skin depth, which in turn, affects the surface impedance.

General expressions for losses in such systems (i.e. metallic systems in a microwave field) as a function of the in-phase and out-of-phase portions of the magnetic susceptibilities are discussed by Kittel.[14]

D. Magnetostatic Measurements

$M(H)|_T$ and $M(T)|_H$ measurements were made with basically the same equipment, involving only some minor modifications.

$M(T)|_H$ Measurements. The basic unit used is shown in figure 2. The sample to be measured is turned down on a lathe into a right circular cylinder, .105" diameter by .142" length. It was glued onto the end of a rod of the same diameter which had been turned down from a small piece of rack material, thus leaving gear teeth along one side. This was placed in the main body of the unit, which consists primarily of a brass cylinder, with a hole bored down the center through which the sample assembly could move. On one side of this was mounted a pinion gear, whose teeth mesh with those of the sample holder. A teflon backstop was attached to the rear of the unit, and a lucite coil form, wound with 5000 turns of 1.2 mil diameter wire, was attached to the front end. A teflon pad and cap were used to close the front end of the coil. These two teflon pieces were used to reproducibly limit the travel of the sample in and out of the coil as the pinion was turned. The whole unit was suspended by means of stainless steel clamps from the top of a brass can. The can was sealed vacuum tight with Wood's metal, and suspended in a dewar by means of four stainless steel tubes, soldered to the can on one end, and to the upper dewar flange on the other end. One of these four stainless steel tubes was positioned over the pinion gear, and a drive shaft was run through the upper flange, using an O-ring seal, down the tube to the pinion gear. Thus by turning the drive shaft from above, the sample could be driven in and out of the pickup coil.

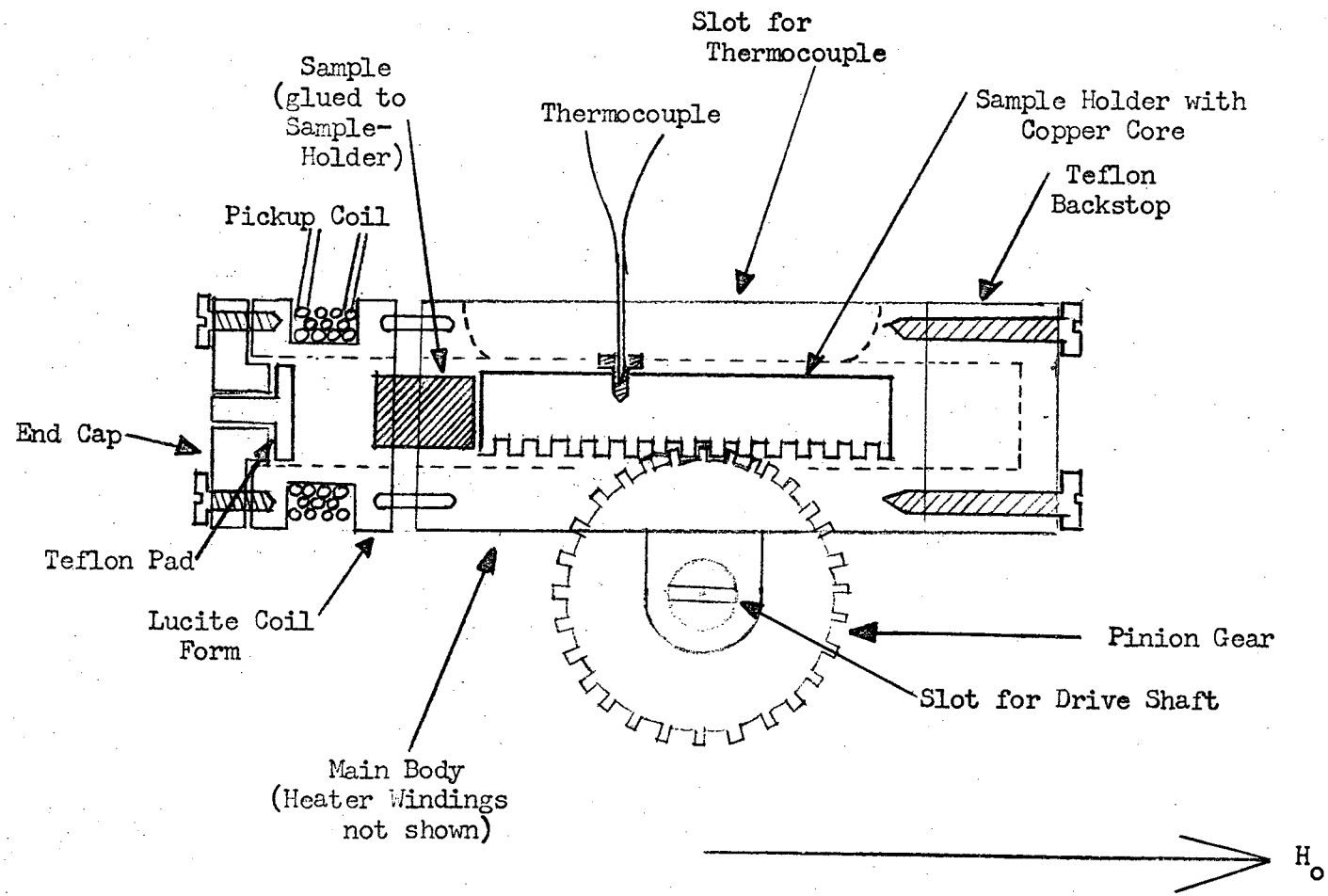
Slot for Thermocouple
Sample (glued to Sample-Holder)
Thermocouple
Sample Holder with Copper Core
Teflon Backstop
Pickup Coil
End Cap
Teflon Pad
Lucite Coil Form
Pinion Gear
Slot for Drive Shaft
Main Body (Heater Windings not shown)
H_o

Fig. 2

The other stainless steel tubes were used to run electrical connections down to the can, and as a vacuum line, through which the can could be evacuated.

From Faraday's Law, the EMF picked up by a coil inside of which the magnetic induction is changing is given by

$$2.4.1 \quad \varepsilon MF = -\frac{\partial}{\partial t} \int_{\substack{\text{area inside} \\ \text{coil windings}}} \vec{B} \cdot d\vec{A}$$

When the sample is outside the coil, the magnetic induction inside the coil is given by $B_{out} = H_o$, where H_o is the externally applied field (usually 8 koe. in these studies, to insure saturation). When the sample is inside the coil, the magnetic induction inside the sample is given by

$$2.4.2 \qquad \vec{B}_{in} = \vec{H}_{in} + 4\pi\vec{M}$$

where H_{in} is the field inside the sample. From elementary magnetostatics we can write this as:

$$2.4.3 \qquad \vec{B}_{in} = \vec{H}_o - N\vec{M} + 4\pi\vec{M}$$

where N is the demagnetizing factor of the cylindrical sample.

$$2.4.4 \quad \therefore \qquad \vec{B}_{in} = \vec{H}_o + (4\pi - N)\vec{M}$$

According to Bozorth,[16] for the dimensions of our samples the expected demagnetizing factor is about 2.4 oersteds/gauss-magnetization. (Our measured values came very close to this value.)

The field outside the sample volume, but inside the coil windings can be thought of as being due to fictitious surface poles induced on the sample end faces and which are proportional to the magnetization of the sample. These "fringing" fields are then also proportional to the

magnetization.

2.4.5 $\vec{B}_{Fringing} = M\vec{f}(\vec{x})$

where $\vec{f}(\vec{x})$ is some function of position depending upon sample size and shape. It is the same for all of our samples, since they were all identical in size and shape.

Thus the average induction inside the coil, with the sample in, is given by

2.4.6 $(\vec{B}_{in})_{average} = H_o$ + [other terms, each of which is proportional to the magnetization of the sample]

Thus, the net change in magnetic induction within the volume enclosed by the coil windings, when the sample is moved from outside the coil to inside the coil, is directly proportional to the magnetization of the sample.

Integrating Faraday's Law with respect to time, one finds

2.4.7 $\int (EMF)_{\substack{around\\windings}} dt_{coil} \propto \Delta B \propto M_{sample}$

To make the measurements the temperature around coil windings of the sample was varied by placing the can in a coolant (usually liquid helium at 4.2°K). Then power which was applied to the heater windings with a regulated current source was increased very slowly. The temperature was monitored with a copper-constantan thermocouple, mounted on the sample holder. The coil was connected in series to a helipot, and the total resistance which was the sum of the resistance of the coil windings and the helipot was monitored with a Wheatstone Bridge, and was maintained to within 1% of some predetermined constant value (about 3.3K) as the resistance of the coil windings changed, because of the temperature change.

The coil, now with the equivalence of fixed windings resistance, was connected to a low drift operational-amplifier current integrator, whose output is proportional to the time integral of the current (i.e., charge) through the input.

The sample was initially outside the coil. The output of the integrator circuit was set to zero. The gate to the integrator circuit was opened, the sample moved into the coil volume, and the gate to the integrator was closed. The output voltage from the integrator was measured with a Rubicon potentiometer and noted, along with the temperature. From equation 2.4.7, this voltage is directly proportional to the magnetization of the sample. This process was repeated at various values of temperature over the range we could cover, 4.2°K to about 320°K.

The overall system was calibrated with a pure nickel sample, whose values of magnetization are well known, due to Weiss and Forrer.[17]

Thus M(T) curves for all the samples could be measured.

$M(H)_T$ Measurements. The system was modified somewhat for these measurements. First, a bucking coil was wound, placed near the pickup coil but off axis, and connected in series opposition to the pickup coil. The EMF's induced in the two coils when H_o was changed cancelled each other to within about 1%. The remaining 1% was balanced out as follows:

The temperature was fixed. The sample was removed from the coil volume in the usual way. The gate to the integrator was opened and the field swept to some large value. The negative output of the integrator circuit was fed into one channel of an operational amplifier voltage adder. The output of the DC gaussmeter was fed into another channel, which had a variable coefficient. The coefficient was adjusted so that

changes in the magnetic field produced no changes in the output of the adder. This nulling adjustment had to be done in fields large enough to saturate the sample, since the pickup coil still picked up the change in magnetization of the sample, although only about 3% as strongly as with the sample in the coil.

With these adjustments, any change in H_o alone produced no change in the output of the circuit. The sample was then inserted in the coil, and the field swept from 0 to a value large enough so that M(H) was determined. Thus the instantaneous integral $\int_0^{t(H)} EMF(t')dt'$ was proportional to M(H) only.

The output of the DC gaussmeter was also used to drive the X channel of an X-Y recorder, and the output of the adder (now proportional to M(H)) was used to drive the Y channel. The value of the ordinate of these traces was noted (or extrapolated) at H=8 koe. Thus the graphs could be calibrated using the previous measurements of $M(T)|_H$.

Also, since the samples were ferromagnetic, the initial slope of the curves gave the demagnetizing factor, so that M as a function of the internal field could be determined. The values given by the slopes were very close to those predicted[16] for the sample geometry.

III. INTRODUCTION TO THE BAND THEORY OF MAGNETISM

A. Exchange and the Molecular Field Approximation

The subject of ferromagnetism among itinerant electrons is a very large if not well understood one. An excellent survey of the subject has been presented in a monumental work by Herring.[1] Especially enlightening, for our purposes, is Chapter Six of this work. It may be noteworthy to state that this book alone contains 478 references for the period preceeding its publication.

Needless to say, this paper could hardly begin to cover all the aspects of this tremendous field of study. However, a relatively brief survey, relevent to the experimental work done during the present studies, will be attempted.

Although this section may at first appear somewhat lengthy, it is felt that this presentation is, in fact, necessary in order to acquaint the reader with some of the more important ideas associated with this type of approach in explaining the magnetic properties of a large class of substances.

The subject probably began in 1929 with the publication of a paper by Bloch[18] in which he demonstrated the possibility of ferromagnetism among a band of (conduction) electrons, obeying Fermi-Dirac statistics, and interacting with each other via a Coulomb repulsion.

As is well known from elementary quantum mechanics, the total energy of a given pair of electrons, whose spatial wave functions overlap when their Coulomb repulsion interaction is considered, depends on whether the spins of these two electrons are parallel or anti-parallel. This result stems from the fact that the Fermi statistics, which the electrons

must obey, requires that the total wave function of the two electrons must be an antisymmetric linear combination of the individual electron wave functions (spin and spatial parts). Let us consider these two electrons as being in a metal. We imagine that we have solved the equations of motion for the electrons in the periodic potential of the lattice sites, neglecting for the time being, the effects of the electron-electron interaction. We assume there is sufficient nearest neighbor overlap between the atomic states to yield a solution of the Bloch running wave type. We then consider the effects of the electron-electron interaction as a perturbation, and calculate its effect on the energy of the system.

Since the spatial charge distribution between two electrons is different for the parallel and anti-parallel configurations, there will be a difference in the interaction energy. For our free electrons with a repulsive interaction, the interaction energy is lower when the two electrons are aligned parallel. This is because the exclusion principle automatically keeps the two electrons separated spatially if their spins are parallel, reducing the net amount of positive repulsive interaction energy with respect to the anti-parallel case. This is the origin of the so-called exchange energy.

Bloch calculated this exchange energy in his paper, and showed under what conditions, within the simplifying assumptions involved in our discussion thus far, this leads to ferromagnetism. He found, essentially, that one needs low density of electrons with large effective mass. For the unscreened Coulomb interaction, which, however, is never achieved in real metals, he found that the condition for ferromagnetism is:

3.1.1 $$r_s > 5.45$$

where r_s is the radius of a sphere just containing the volume associated with one electron in the lattice, expressed in units of the Bohr radius appropriate for the effective mass of the electron m^*. That is:

3.1.1 a) $$r_s = r_o/a_o$$

3.1.1 b) r_o = radius of sphere containing the volume associated with one electron

3.1.1 c) $$a_o = \hbar^2/m^* e^2$$

e is the electron charge

When this condition is met the exchange energy gained in aligning all the electrons parallel to one another more than offsets the increase in kinetic energy necessary to produce a magnetized state. To create such a state, we must raise electrons from the configuration where allowable k-states are doubly occupied, (one in each of the two allowed spin directions), to a configuration where k-states are only singly occupied (i.e., in one spin direction only, usually defined as the spin up direction). This configuration requires the filling of electrons in states of much higher k (and hence much higher K.E.) than the non-magnetic configuration.

However, in this calculation, Bloch neglected the effects of correlation. Not only does the electron-electron interaction change the energy of the system described by some (fixed) set of wave functions in the way just described, but it also modifies the wave functions themselves; in this case, in such a manner as to keep electrons farther apart than for the case of non-interacting electrons.

Thus, electrons which are anti-parallel and would be allowed to approach one another fairly closely (giving rise to relatively large interaction energy) in an uncorrelated model, are kept apart when correlation effects are included. The energy difference between the unparallel

state and the parallel state for two electrons, which was given by the exchange integral between the two states describing the electrons, is now greatly reduced. The problem of correlation plays an essential role in the calculation of the properties of a band of electrons, and determines for example, whether or not the electrons can even become ferromagnetic.

At the present time, it is not known whether a single band of electrons can produce ferromagnetism, when correlation is taken into account.

Although from a theoretical standpoint, it has not been proved whether or not a simple band system can become ferromagnetic, we will adopt a phenomenological approach, and assume it can.

For the present, let us neglect the effects of finite temperature, i.e., we restrict our discussion to absolute zero.

Then the normal paramagnetic state is one with half the electrons in the spin-up state, the other half in the spin-down state. For simplicity, we consider our crystal to be made up of N atoms, each contributing one electron to our band. Thus there are N electrons, which we assume are describable by Fermi-Dirac statistics. We further assume the effective mass approximation, so the density of states is proportional to $E^{1/2}$ (i.e., $N(E) = \text{constant} \times E^{1/2}$).

In this picture, the unmagnetized state of the system simply looks like figure 4a. The magnetized state looks like figure 4b, where the electrons fill all the allowable states of one sub-band, which has been depressed strongly in energy by the exchange interaction, the remaining electrons occupying states in the other sub-band. Then there is a net unbalance in the number of spins in the two spin directions, leading to a net magnetic moment. Due to the complete saturation one one sub-band, this case is termed strongly ferromagnetic. (To conform to the

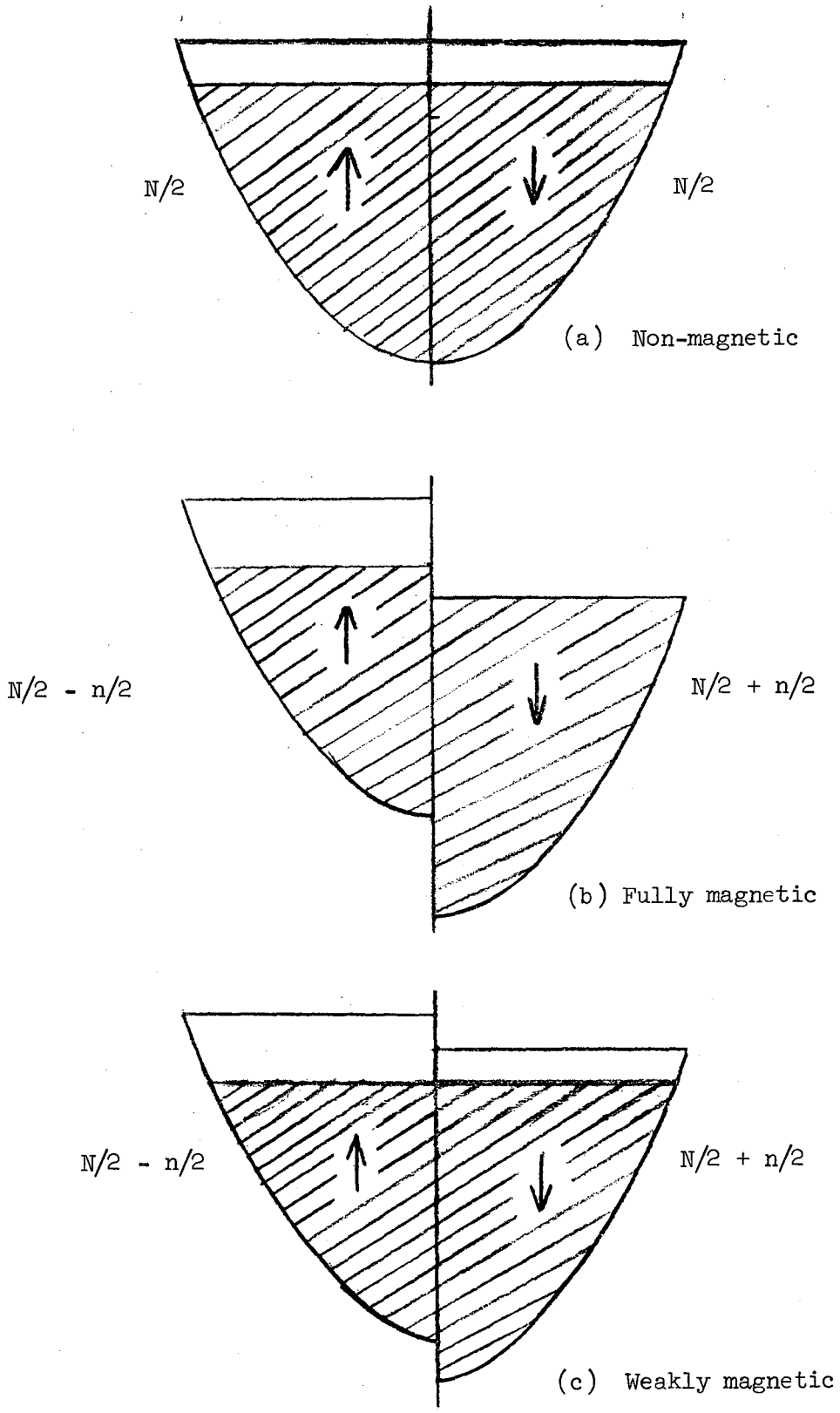
N/2
N/2
(a) Non-magnetic
N/2 - n/2
N/2 + n/2
(b) Fully magnetic
N/2 - n/2
N/2 + n/2
(c) Weakly magnetic

Fig. 4

3-d transition series, and to our alloys, we will assume that the d-bands are more than half full, so the carriers in this band are holes. Thus the magnetic properties come about from the fact that there are more holes, or vacancies, in one spin sub-band than the other. The treatment for the case when the d-band is less than half full, and the carriers are electrons, proceeds in a similar fashion.) Thus nickel, with a saturation magnetization corresponding to 0.6 Bohr magnetons per atom, arises from the fact that the d-band contains .54 holes per atom with a g-factor of 2.2 (yielding 1.1 Bohr magnetons per hole).

Another case may occur if the exchange interaction is too weak to depress one sub-band far enough to cause it to fill completely. This case is depicted in figure 4c. In this case, there is only partial transfer of carriers from one sub-band to the other, so that only a small fraction of the eligible magnetic carriers contribute to the net magnetization. That is, the net moment arises from the difference in the number of carriers in the two spin directions. For obvious reasons, this case is called the weakly ferromagnetic case, and as the exchange interaction strength is decreased, the magnetization decreases to zero. We will discuss this case in more detail later.

To see how this depression of one of the spin sub-bands comes about, we consider the effects of the exchange interaction in more detail.

We first develop the molecular field approximation for a band system, which turns out to be of great use.

If the electrons are describable by Bloch plane waves, the exchange interaction between any two electrons, one is the state describable by wave vector k, the other in a state k', is given by[25*]

---

*This result follows immediately from the overlap integral between two plane wave states. The result is the Fourier transform of the effective electron-electron interaction.

3.1.3 $$J(\vec{k}, \vec{k}') = \frac{1}{V} \frac{4\pi e^2}{|\vec{k} - \vec{k}'|^2}, \quad V = \text{volume of the crystal}$$

for the case of a bare Coulomb interaction, and by

3.1.4 $$J(\vec{k}, \vec{k}') = \frac{1}{V} \frac{4\pi e^2}{|\vec{k} - \vec{k}'|^2 + k_s^2}$$

for the more realistic case of a screened Coulomb interaction. The screening parameter K_s, which prevents divergence as $|\vec{k} - \vec{k}'| \to 0$ results from electron-electron effects (correlation), which tend to screen out the long range Coulomb effects by redistributing the electrons throughout the lattice. This screening parameter is treated by Kittel[25] and an order of magnitude estimate is given by

3.1.5 $$K_s^2 = 6\pi N e^2/E_f, \quad N = \text{number of electrons per unit volume}$$

where E_f is the Fermi energy.

In the effect mass approximation E_f is given by

3.1.6 $$E_f = \frac{\hbar^2(3\pi^2 N)^{2/3}}{2m^*}$$

Then the screening length becomes on the order of magnitude of an interatomic distance, which we call d_o.

In this case, K_s is large compared to most values of $|\vec{k} - \vec{k}'|$ occuring for pairs of electrons in a real metal, so we neglect the first term in the denominator of expression 3.1.4 in comparison to the screening term. Using the estimate

3.1.7 $$K_s \sim 1/d_o$$

and the fact that $V = N(d_o)^3$, we find

3.1.8 $$J_{av} \sim \frac{1}{N} \frac{4\pi e^2}{d_o} \sim J_{\text{interatomic}}/N$$

Although this can be considered little more than a dimensional argument, it does display an important feature of the exchange; namely, that the exchange between two itinerant electrons is roughly 1/N times an exchange interaction parameter describing two electrons at neighboring atomic sites. The 1/N factor arises from the fact that each electron is spread over all N atomic sites, with probability amplitude 1/N at each site. However, on the average, each site has the contributions from all N electrons in the band, so there is still one electron associated with each site.

We then write the exchange interaction between two electrons, one in the state k the other in state k' as

3.1.9 $$E_{exch}(\vec{k},\vec{k}') = -\frac{J}{N}\,\vec{S}_{\vec{k}} \cdot \vec{S}_{\vec{k}'}$$

where $\vec{S}_{\vec{k}}$ is the spin of the electron is state $\vec{k}$ and $\vec{S}_{\vec{k}'}$ is the spin of the electron in state $\vec{k}'$, and where we have supressed the k-dependence of the exchange interaction, for the time being, the justification being that the screening greatly reduces the k-dependence.

We then consider the change in energy of an individual electron in some state, $\vec{k}$, stemming from the exchange interaction with all the other electrons, as we go from the unmagnetized state to a magnetized state. In the unmagnetized state, there are N/2 electrons parallel to any given electron, and N/2 electrons antiparallel (neglecting 1, the electron in question, in comparison to N, the total number of electrons). Then the energy of this electron is

3.1.10 $$E_{total}(\vec{K}) = \epsilon_{\vec{k}} - \sum_{\vec{S}_{\vec{q}} \parallel \vec{S}_{\vec{k}}} \frac{J}{N}\,\vec{S}_{\vec{k}} \cdot \vec{S}_{\vec{q}} - \sum_{\vec{S}_{\vec{q}} \nparallel \vec{S}_{\vec{k}}} \frac{J}{N}\,\vec{S}_{\vec{k}} \cdot \vec{S}_{\vec{q}'}$$

$$= \epsilon_{\vec{k}} - \left(\frac{N}{2}\right)\frac{J}{N}\left(+\frac{1}{4}\right) - \left(\frac{N}{2}\right)\frac{J}{N}\left(-\frac{1}{4}\right)$$

$$= \epsilon_{\vec{k}}$$

Where we have summed equation 3.1.9 over all spin pairs, constructed from $\vec{S}_{\vec{k}}$ with the spins of all the other electrons in the lattice, and where the sum is broken into two sums, one involving the electrons in the crystal whose spins are parallel to the electron being considered, the other sum involving electrons whose spins are anti-parallel. Here, $\epsilon_{\vec{k}}$ is the kinetic energy of the electron in the state $\vec{k}$, and the dot product between the spins is +1/4 for parallel spins, and -1/4 for anti-parallel spins. Thus in the non-magnetic state, the gain in exchange energy for any particular electron from other electrons in the lattice parallel to it is just off-set by the loss from the equal number of electrons anti-parallel.

Now, let us consider the magnetized state, with (N/2 + n/2) electrons with spin up and (N/2 - n/2) electrons with spin down. Then the energy of our sample electron, if it has spin up, generalizing equation 3.1.10 is given by

3.1.11 $$E_{total}(\vec{k}\uparrow) = \epsilon_k - \frac{J}{N}\left(\frac{N}{2} + \frac{n}{2}\right)\left(\frac{1}{4}\right) - \frac{J}{N}\left(\frac{N}{2} - \frac{n}{2}\right)\left(-\frac{1}{4}\right)$$
$$= \epsilon_k - \frac{J}{4}\frac{n}{N}$$

and if it has spin down, its energy is given by

3.1.12 $$E_{total}(k\downarrow) = \epsilon_k + \frac{J}{4}\frac{n}{N}$$

However, we recall that the magnetization of our sample is, in this case, given by

3.1.13 $$M = \frac{n\mu}{V}$$

where μ is the magnetic moment carrier and V is the volume of the sample. Therefore

3.1.13a $$n = \frac{MV}{\mu}$$

Thus, electrons in states with their moment parallel to the overall mag-

netization of the sample have their energy lowered an amount proportional to the magnitude of the magnetization, while those electrons antiparallel to this direction have their energy raised by this amount. Since an externally applied magnetic field directed along the magnetization direction will have the same effect on the electron energies, we say that we may replace the exchange interaction by a (fictitious) magnetic field, proportional to both the exchange interaction strength, and the magnitude of the magnetization. The coefficient of magnetization (whose dimensions are the same as that of field, i.e. Oersteds) is usually much greater than unity. This approximation is known as the molecular field approximation.

We can now see how the magnetized state, as shown in figure 4b, c comes about. The unmagnetized state undergoes transfer of electrons among the spin states in a self-consistent way, so that the up-states are preferentially occupied, causing each of the k-up states to lower its total energy, and each of the k-down states to raise its energy. (Thus the k-up band shifts downward from its non-magnetic position while the spin down band moves up.) This allows electrons to spill over from the down sub-band into the up sub-band and distribute themselves as shown in the figures 4b or 4c.

One of the consequences of this molecular field, when it is not strong enough to bring about ferromagnetism, is an enhancement of the paramagnetic susceptibility, over its value were the exchange not present. More accurately, the molecular field decreases the inverse susceptibility by a constant term (independent of temperature if the molecular field coefficient is independent of temperature. Actually, for reasons which we shall discuss, the strength of the exchange interaction can become slightly temperature dependent, so that the molecular field constant does also).

The proof of this statement is trivial, and is demonstrated by Stoner[26], the proof being independent of the model chosen to describe the origin of the susceptibility in the first place. Then this theorem simply states

3.1.14 $$1/\chi(T) = 1/\chi_o(T) - \alpha$$

where χ is defined by $\vec{M} = \chi \vec{H}$

χ_o is the value in the absence of exchange

and α is defined by

$$\vec{H}_{mol.fld.} = \alpha\vec{M}$$

and $\vec{M}$ is the magnetization.

Having demonstrated the effects of the exchange interaction on the energy of the system, we now turn to a discussion of the magnetic susceptibility of our bands. We consider the magnetization of such a system in the presence of an external field, at T = 0.

We consider the free energy, F, of our system. Following our previous discussion, the magnetized state differs from the unmagnetized state by having distribution $(N/2+n/2\uparrow,\ N/2 - n/2\downarrow)$ instead of $(N/2\uparrow,\ N/2\downarrow)$. We rewrite the exchange energy in a slightly different form for this discussion.

3.1.15 $$E_{ex} = -J(\vec{S}_1 \cdot \vec{S}_2) \rightarrow J(1 - \vec{S}_1 \cdot \vec{S}_2) \equiv \text{constant} - J\,\vec{S}_1 \cdot \vec{S}_2$$

so that the exchange energy is shifted by a constant, and is equal to zero if the two spins are anti-parallel, and $-J/2N$ when the two spins are parallel. To calculate the change in internal energy due to exchange, on going from the unmagnetized state to the magnetized one, we calculate the change in the total number of parallel spin pairs. This is done easily, as follows:

Unmagnetized State

$$\left.\begin{array}{l}\text{Number of } \uparrow \text{ pairs} = (N/2)\cdot(N/2-1) \approx N^2/4 \\ \text{Number of } \downarrow \text{ pairs} = (N/2)\cdot(N/2-1) \approx N^2/4\end{array}\right\} \quad \text{total} = N^2/2$$

Magnetized State

$$\left.\begin{array}{l}\text{Number of } \uparrow \text{ pairs} = (N/2+n/2)(N/2+n/2-1) \approx \frac{N^2}{4}+\frac{nN}{2}+\frac{n^2}{4} \\ \text{Number of } \downarrow \text{ pairs} = (N/2-n/2)(N/2-n/2-1) \approx \frac{N^2}{4}-\frac{nN}{2}+\frac{n^2}{4}\end{array}\right\} \quad \text{total} = \frac{N^2}{2}+\frac{n^2}{2}$$

3.1.16 Change in number of parallel spin pairs $= n^2/2$

Then since each parallel spin pair reduces the internal energy by $J/2N$ we obtain

3.1.17 $$\Delta F_{exch} = \frac{-J}{2N}\cdot\frac{n^2}{2}$$

We next consider the kinetic energy. In order to effect this transfer, we must raise electrons to higher k-states. The <u>average</u> increase in K.E., of these electrons (i.e., the ones which are transferred), <u>per electron</u> is

3.1.18 $$\frac{1}{2}\,\frac{\text{number of electrons raised}}{\text{single sub-band density of states}} = \frac{1}{2}\,\frac{n/2}{1/2\cdot N(E)}$$

$$= \frac{1}{2}\,\frac{n}{N(E_f)}$$

where $N(E)$ is the density of states (for the entire crystal, evaluated in the non-magnetic state).

The number of electrons transferred is $n/2$. Thus the increase in K.E. of the system is

3.1.19 $$\Delta F_{K.E.} = +\frac{1}{4}\,\frac{n^2}{N(E_f)}$$

Finally, there is a term, $-1/2\ \vec{H}\cdot\vec{M}$ in the free energy describing the interaction of the system with the external field. Recalling also that

3.1.20 $$M = n\mu \qquad (\mu = \text{magnetic moment per electron})$$

we can write the free energy as a function of n, twice the number of electrons which are transferred.

3.1.21 $$F = \frac{1}{4}\frac{n^2}{N(E_f)} - \frac{J}{2N}\frac{n^2}{2} - \frac{1}{2}n\mu H$$

We require that this be a minimum, leading to the relation

3.1.22 $$\frac{\partial F}{\partial n} = 0 \Longrightarrow \frac{1}{2}\frac{n}{N(E_f)} - \frac{J}{2N} - \frac{1}{2}\mu H = 0$$

solving we find

3.1.23 $$n = \frac{\mu H}{\frac{1}{N(E_f)} - \frac{J}{N}} = \frac{\mu H N(E_f)}{1 - \frac{J}{N}N(E_f)}$$

3.1.24 $$\chi \equiv \frac{M}{H} = \frac{n\mu}{H} = \frac{\mu^2 N(E_f)}{1 - JN(E_f)/N}$$

defining $N(E_f)/N \equiv n(E_f)$ = density of states/atom

3.1.25 $$\chi = \frac{\mu^2 N(E_f)}{1-Jn(E_f)} \equiv \mu^2 N(E_f) \cdot S$$

where $\mu^2 N(E_f)$ is the value of the susceptibility when $J = 0$ and

$S \equiv$ Stoner enhancement factor $= \dfrac{1}{1-J \cdot n(E_f)}$

This result holds in general, provided the molecular field approximation is valid (i.e., the exchange interaction is independent of the electron states involved, etc.)

For a free electron gas, we have

3.1.26 $$N(E_f) = \frac{3N}{2E_f}$$

3.1.27 $$n(E_f) = \frac{3}{2E_f}$$

3.1.28 $$\chi = \frac{3N\mu^2}{k_b T_f} \cdot \left\{ \frac{1}{1 - \frac{3}{2} J/E_f} \right\}$$

where $E_f = k_b T_f$ defines the degeneracy temperature, and k_b is the Boltzmann constant. We see that as J approaches 0 (vanishingly small exchange interaction), the susceptibility approaches the usual Pauli paramagnetic susceptibility expression, which can be found in ISSP.[27] We also note that this expression diverges as $J \rightarrow \frac{2}{3} E_f$. The loss in kinetic energy is more than offset by the gain in exchange energy as we transfer electrons, and it becomes energetically favorable for the system to acquire a net magnetic moment, even in the absence of an externally applied magnetic field (i.e., the system becomes ferromagnetic).

B. Stoner Theory

It often becomes necessary to discuss the temperature variation of M or χ as a function of T or H quantitatively. One approach to this problem which has proven quite useful, was presented in a series of papers by Stoner in the 1930's.[28,29,30] He calculated the relative occupations of the 2 spin sub-bands, considering the effects of an externally applied magnetic field, and finite temperatures, under the following assumptions:

1. The electrons form a single band.
2. They obey Fermi-Dirac statistics.
3. The exchange can be treated by the molecular field approximation, i.e., we treat the electrons as being subjected to a fictitious field proportional to the magnetization, in addition to any externally applied fields.
4. We make the effective mass approximation. Then the density of state functions for each sub-band is proportional to the square root of the kinetic energy:

3.2.1 $$N(E_k) = \text{constant} \cdot E_k^{1/2}$$

Then the variable parameters in this model are:

1. The degeneracy energy or temperature $E_o = k_b \cdot T_o$ (also written $E_f = k_b \cdot T_f$) associated with the Fermi statistics. For more general band shapes, which have been considered subsequently, one then considers the density of states and its first and second derivatives, evaluated at the Fermi level: $N(E_f)$, $N'(E_f)$, and $N''(E_f)$.
2. The number of carriers in the magnetic (d-) band. This may be non-integral. e.g., for nickel it is taken to be .54 holes per atom.

3. The molecular field constant, or exchange interaction strength,

$J/N = k_b\theta'$

The molecular field is given by

3.2.2 $$H_{mf} = k_b\theta' \xi/\mu$$

where ξ is the fractional magnetization, (the number of unbalanced magnetic carriers, divided by the total number of carriers in the magnetic band) and μ is the magnetic moment per carrier. θ' has dimensions of temperature and in the limit of very narrow bands, $\theta' \rightarrow T_c$, the transition or Curie temperature. It is apparent that there are several weaknesses in this model. Some of them are:

1. Neglect of many body effects (correlation). For example, it has been shown that many body effects lead to spin-wave like excitations at low temperature, a point we will return to later.

2. Neglect of the effects of fluctuations. E.g., near T_c, short range order will make the molecular field approximation a bad one.

3. Effects of having real band shapes rather than the simple effective mass approximation. This affects the results of the theory quantitatively.

4. Dependence of Fermi degeneracy temperature (hence the statistics) and the exchange interaction on lattice spacing, which depends on temperature.

5. Presence of other bands. For example, finite temperatures excite interband transitions, changing the number of carriers in the magnetic band, and further serve to modify the exchange interaction strength.

In spite of these shortcomings, the Stoner theory has met with a great deal of success, and improvements have been added in the years following its first appearance, so that it now represents a fairly good

basis for describing some of the properties of an itinerant electron gas.

Stoner introduced a convenient notation, which we will follow. The basic equations which describe the system, from Fermi statistics are

3.2.3 $$\frac{1}{2}\, n\,(1 \pm \xi) = \int_0^\infty f\,(\epsilon, \eta^{\pm})\, N\,(\epsilon)\, d\epsilon$$

3.2.3a $$f(\epsilon,\eta) \equiv [\exp\{(\epsilon-\eta)/k_b T\} + 1]^{-1}$$

3.2.3b $$\eta^{\pm} = \epsilon_o \pm k_b\, \theta'\, \xi \pm \mu H$$

where

n = number of magnetic carriers (per atom)

N = number of atoms/volume

μ = magnetic moment per electron

= $g/2 \cdot \mu_b$ (g is the spectroscopic splitting factor, ≈ 2, and μ_b is the Bohr magneton)

$k_b\theta'$ = molecular field constant (k_b = Boltzmann constant)

$N(\epsilon)$ = density of states per atom

ϵ_o = chemical potential for the system (Fermi energy)

ξ = relative fractional magnetization

= $M(H,T)/Nn\mu$

= (number of unbalanced magnetic carriers)/(Total number of magnetic carriers)

ξ_o = relative fractional magnetization at $T = 0$

= $M(0,0)/Nn\mu$

T_c = Ferromagnetic transition (Curie) Temperature

Thus there are two equations, (corresponding to the plus and minus signs) and two unknowns, (ϵ_o and ξ). For solution of these equations, as we have stated previously, a parabolic band shape was assumed ($N(E)$ proportional to $E^{1/2}$).

Implicit in the solution is the Fermi-Dirac function

3.2.4 $$F_{3/2}(\eta) \equiv F(\eta) = 3/2 \int_0^\infty \frac{x^{1/2}\,dx}{e^{x-\eta}+1}$$

Applied to Ferromagnetism

For $K_b\theta'/\epsilon_o \geq 2/3$ the solution of these equations lead to spontaneous magnetization for sufficiently low temperatures.

What is remarkable, in this model, though, is that for $k\theta'/\epsilon_o$ in the range $2/3 \geq k_b\theta'/\epsilon_o \leq 2^{-1/3} \approx .793701$, one finds $0 \leq \xi_o \leq 1$. In other words, for a certain range of the interaction strength the band is only partially saturated. This corresponds to the limit of weak ferromagnetism. Then for $k_b\theta'/\epsilon_o > 2^{-1/3}$ we have $\xi_o = 1$; i.e., the exchange is strong enough to completely saturate the magnetization at low temperature.

Stoner lists the solution of the equations in inverse tabular form. For example, he lists k_bT/ϵ_o as a function of ξ_o and $\xi(T)$ in the range $2/3 \leq k_b\theta'/\epsilon_o \leq 2^{-1/3}$ (along with $k_b\theta'$ as a function of ξ_o) for equal spacings of ξ_o and $\xi(T)$ for the same range of $k_b\theta'/\epsilon_o$ for equally spaced values of $k_b\theta'/\epsilon_o$ and $\xi(T)$. This inverse solution was necessary in order to solve the equations numerically using the previously tabulated values of Fermi-Dirac function.

When these numerical relations are inverted, one obtains the dependence of M (actually ξ) on T for $T < T_c$, for various values of the relative exchange interaction parameter, $k_b\theta'/\epsilon_o$. One also obtains ξ_o as a function of $k_b\theta'/\epsilon_o$.

It is instructive to consider briefly, how this partial magnetization in the ferromagnetic state comes about. Let us consider the change in internal energy of the system (at T = 0) as we proceed continuously from the unmagnetized state, to a magnetized one, by transferring electrons. See figure 5.

There are, as we have indicated, two contributions to this energy.

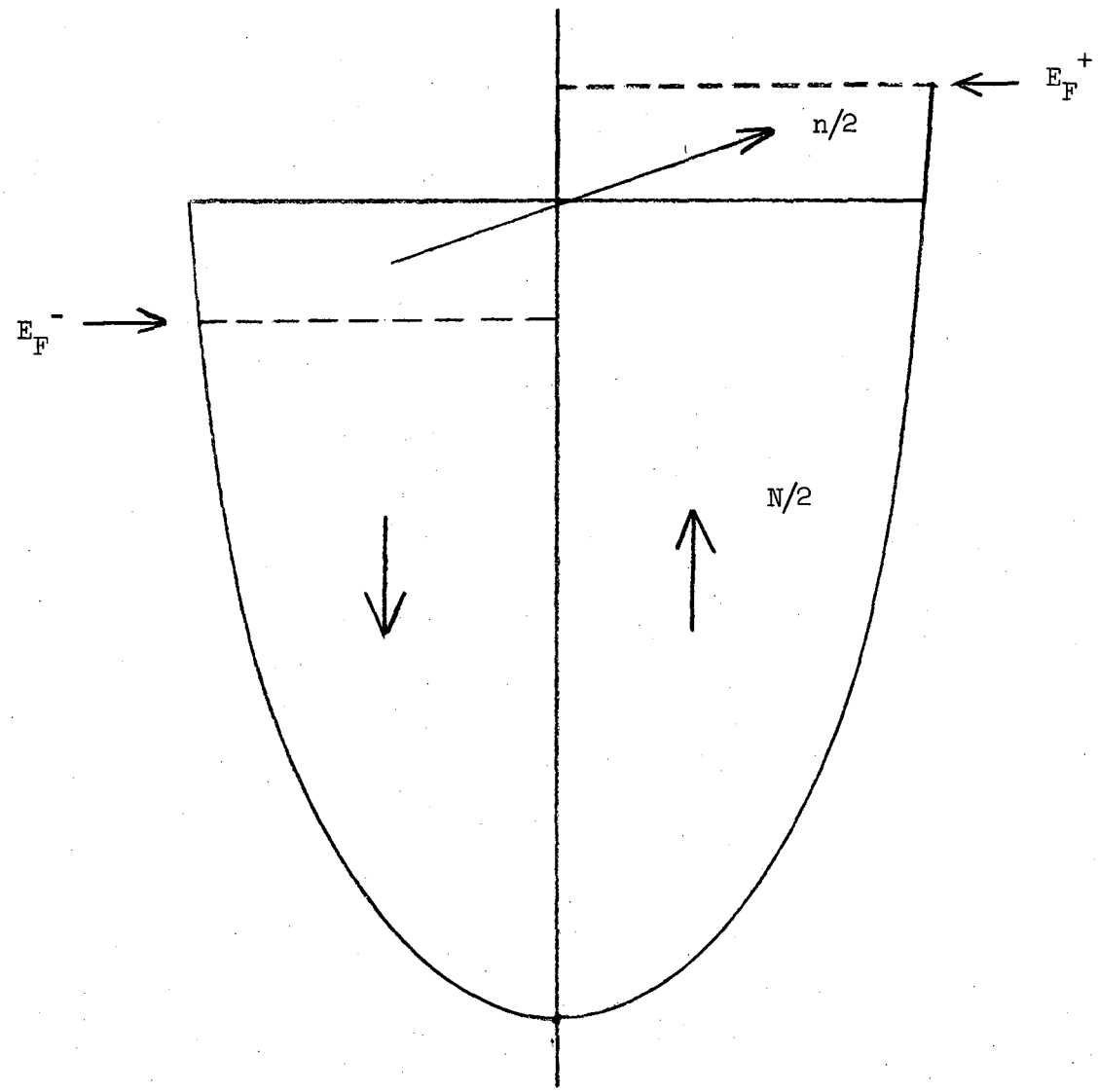

Fig. 5

(We are considering the ferromagnetic case, so there is no externally applied field.) One is the decrease in energy due to exchange, brought about by increasing the total number of parallel spin pairs. This must offset the second contribution which is the increase in kinetic energy due to the fact that we are raising electrons from states (slightly) below the Fermi level of one spin band, and are placing them in the higher un-occupied states (slightly) above the Fermi level in the other spin band.

In the effective mass approximation, the (new) Fermi level of each of these sub-bands in proportional to $(N\pm)^{2/3}$ where N+ and N- refers to the number of electrons in the spin up or spin down (sub) bands, respectively. Thus

3.2.5 $$E_f^{\pm} \propto [N/2 \pm n/2]^{2/3}$$

Now the average energy per electron in each of these sub-bands is well known to be $2/3\ E_f^{\pm}$. The total number of electrons in each of these bands is $[N/2 \pm n/2]$. The total energy of each of these sub-bands is obtained by multiplying the average energy of one electron in the sub-band by the number of electrons in that sub-band. We find

3.2.6. $$E^{\pm}_{K.E.} \propto [N/2 \pm n/2]^{5/3}$$

The total K.E. of the system is the sum of the K.E. of the two sub-bands comprising the system, and is given by

3.2.7. $$E_{\text{total K.E.}} \propto [N/2 + n/2]^{5/3} + (N/2 - n/2)^{5/3}]$$

or, expressing it in terms of the relative magnetization, $\xi_o = n/N$,

3.2.8. $$E_{\text{total K.E.}} \propto E_o\ [\ (1 + \xi_o)^{5/3} + (1 - \xi_o)^{5/3}]$$

where E_o is the original Fermi energy.

The exchange energy, which is proportional to the total number of parallel spin pairs, can be expressed similarly as

3.2.9. $$E_{exch} \propto -k_b\theta' \left[(1 + \xi_o)^2 + (1 - \xi_o)^2\right]$$

and the total energy is the sum of these two contributions. Adding these two contributions and expanding the results in a Taylor series in ξ_o, one finds

3.2.10 $$E(\xi_o) \propto \left(\frac{2}{3} E_f - k_b\theta'\right) \xi_o^2 + 2/81\, E_f\, \xi_o^4 + \mathcal{O}\, \xi_o^6 + \ldots$$

For $k_b\theta' = 2/3E_f$, the first term in the expansion is zero. To second order in ξ_o it cost no energy to increase the magnetization of the system from zero. For $k_b\theta'$ just slightly greater than $2/3\, E_f$, it costs a negative amount of energy for the magnetization to begin to increase, and electrons begin to switch sub-bands, i.e., the gain in exchange energy slightly more than offsets the needed K.E. to raise the electrons to the higher k-states. However, as ξ_o (or equivalently, n) gets larger, the density of states in the region from which the electrons are being supplied gets smaller. Thus the K.E. required to raise these electrons becomes progressively larger (the ξ_o^4 and higher terms in our expansion), until a point is reached where further increase in ξ_o no longer reduces the total energy of the system; that is, ξ_o continues to increase until $E(\xi_o)$ reaches a minimum.

For the parabolic band shape assumed, Stoner showed that the position of the minimum in energy with respect to variations is related to $k_b\theta'/E_f$ by the closed relation

3.2.11. $$k_b\theta'/E_f = 1/2\xi_o \left[(1+\xi_o)^{2/3} - (1 - \xi_o)^{2/3}\right]$$

A Taylor expansion of the right hand side of this equation leads to the approximate relation between ξ_o and $k_b\theta'/E_f$:

3.2.12. $$k_b\theta'/E_f = 2/3 + 4/81\, \xi_o^2 + \mathcal{O}\, \xi_o^4 + \ldots$$

On measuring the saturation magnetization of Ni and Cu-Ni alloys as a function of temperature in the ferromagnetic region, and attempting to fit this data to the values predicted by Stoner's calculations, it was discovered that the Stoner model did not describe the shape of these curves very well.[31]

Hunt[32] attempted to explain this by including higher order terms in the exchange interaction:

3.2.13. $$E_{exch}(\xi) \approx -1/2\, k_b\theta'\, \xi^2 - \frac{1}{4} A\, k\theta'\, \xi^4 + \ldots$$

The presence of the higher order terms is given the understandable justification: In the molecular field approximation, we assumed implicitely that the exchange interaction between all pairs of electrons in the magnetic band was the same, independent of the k- states of the two electrons involved. Physically, this is not the case. There is some k-dependence in the exchange interaction. For a screened Coulomb interaction, for example, we showed

3.2.14. $$J(\vec{k},\vec{k}') \sim \frac{4\pi e^2}{V} \frac{1}{|\vec{k} - \vec{k}'|^2 + K_s^2}$$

where K_s is the screening parameter.

Thus, as we transfer electrons, and thus increase ξ, we change the distribution among the various k-states, and therefore, change the average exchange interaction. By symmetry, this effect must be the same for plus and minus ξ, i.e., it must be an even power series of ξ. A Taylor expansion of the exchange energy then leads to the form proposed by Hunt.

Hunt then found that the formula relating the value of ξ_o which minimizes the total energy, as one varies $k_b\theta'/E_o$, is modified from equation 3.2.11 and now takes the form

3.2.15 $$k_b\theta'/E_o\,(1 + A\,\xi_o^{\,2}) = 1/2\xi_o\,[(1 + \xi_o)^{2/3} - (1 - \xi_o)^{2/3}]$$

By making the appropriate modifications to the values of M(T) found by Stoner, he found he could obtain excellent agreement between the theoretical and experimental values by assuming A = .10 for pure Ni, decreasing continuously woth increasing Cu content to A = 0 for 20% copper.

Taylor expansion of Hunt's relation (equation 3.2.15) leads to the approximate relation between ξ_o and $k_b\theta'/E_o$.

3.2.16. $$k_b\theta'/E_o = \frac{2}{3} + (\frac{4}{81} - \frac{2}{3})\,\xi_0^{\,2} + \sigma\,\xi_0^{\,4} + \ldots$$

This relation is plotted in figure 6 for A = 0 (Stoner limit), and for A = .10. Also plotted on the same figure is the relative Curie temperature k_bT_c/E_o as a function of $k_b\theta'/E_o$ in the Stoner limit.

For $A > A_{critical} = 2/27 \approx .074$ the coefficient of $\xi_o^{\,2}$ in expression 3.2.16 becomes negative. The two values of ξ_o for values of $k_b\theta'/E_o$ slightly less than 2/3 corresponding to stationary values of $E(\xi_o)$ correspond to first a maximum then a minimum in the energy as a function of ξ_o. This can be seen from a Taylor expansion of the energy

3.2.17 $$\frac{E\,(\xi_o)}{E_o} \approx (-\frac{k_b\theta'}{E_b} + \frac{2}{3})\,\xi_o^{\,2} + (4/81 - A\,k_b\theta'/E_o)\,\xi_o^{\,4} + \ldots$$

This case leads to metamagnetism, whereby the application of a sufficiently strong magnetic field, and the subsequent removal, will leave the material in a magnetized state. Such a proposal was made in an article by Wohlfarth and Rhodes.[33]

Another remarkable feature of this model, which should be apparent from our discussion, is that in the limit of weak ferromagnetism, since neither sub-band is saturated, and since application of an external field will cause the parallel sub-band to become lower in energy and the anti-parallel sub-band to become higher in energy, additional electrons will

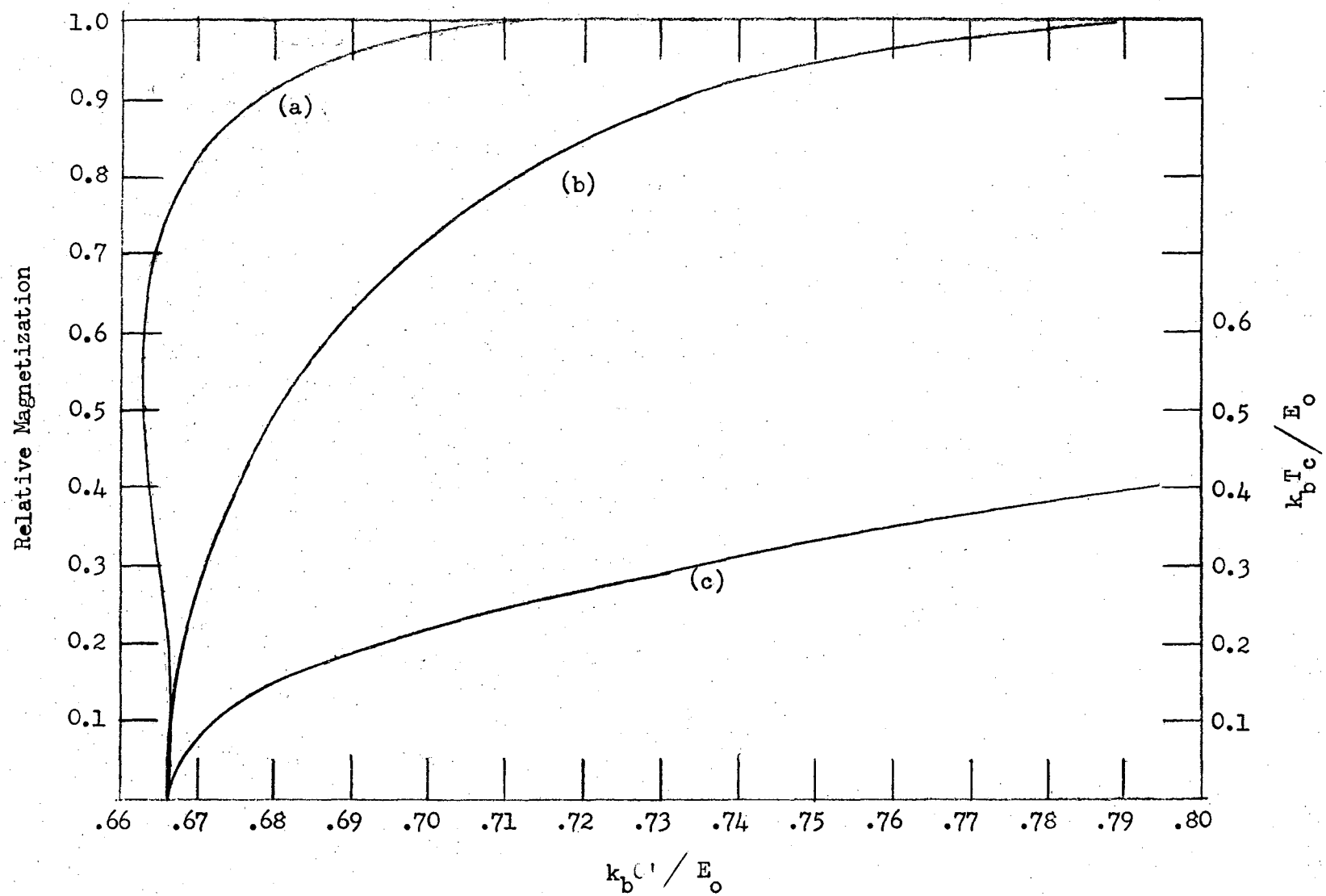
Relative Magnetization
1.0
0.9
0.8
0.7
0.6
0.5
0.4
0.3
0.2
0.1
(a)
(b)
(c)
.66
.67
.68
.69
.70
.71
.72
.73
.74
.75
.76
.77
.78
.79
.80
$k_b C' / E_o$
0.6
0.5
0.4
0.3
0.2
0.1
$k_b T_c / E_o$

Fig. 6

switch sub-bands, further increasing the magnetization. This leads to a finite value of the susceptibility in the ferromagnetic state, even at T=0.

Indeed, this high field differential susceptibility has already been noted in Ni-Rh[6] as well as in other weakly ferromagnetic substances. For example, it has been measured in the weakly ferromagnetic intermetallic compound $ZrZn_2$.[34] The fact that this high field susceptibility may be due to a canted ferromagnetic spin arrangement, (which would then be modified by application of a strong external field, leading to increase net magnetization) was ruled out by neutron diffraction measurements on this substance.[35] In fact, these measurements indicate that the magnetization of this substance is distributed throughout the lattice, with appreciable density between lattice sites (as opposed to being localized at the actual lattice sites themselves) lending further credence to the suggestion that $ZrZn_2$ is an itinerant ferromagnet. It has been suggested[36] that the ferromagnetism of this substance is due to ferromagnetic impurities (probably iron) introduced during preparation, (or contained in the raw zirconium used to prepare the specimen) but more recent studies[37] in which the impurities were controlled at very low levels, indicate that this material is indeed intrinsically a weak ferromagnet.

In $ZrZn_2$, the high field susceptibility remains essentially constant up to the highest field attainable, which in the case of the measurements of Foner et al.[36] was 150 koe. This high field differential susceptibility has been treated quantitatively by Wohlfarth.[38,39]

It should be apparent to the reader that the effects we have been discussing depend critically on the band structure of the magnetic electrons. Until now, we have considered only a parabolic band, where the density of states varied as $E^{1/2}$. We expanded the energy of repopulation of the elec-

trons among the two spin sub-bands in a Taylor series, around the unperturbed Fermi surface. Obviously, the coefficients of the various powers of ξ_o depend explicitely on the density of states function in the neighborhood of the Fermi surface, so our results will be modified accordingly. For example, the critical value of $k_b\theta'/E_o$ leading to ferromagnetism can be modified from its value of 2/3. The quantitative relationship between $k_b\theta'/E_o$ and ξ_o will also be modified by including the actual band shapes as well as will other relationships (dependence of Curie temperature on $k_b\theta'$ and E_o). We shall return to this point later. However, it is felt that the qualitative features of this model remain intact, i.e., the decreasing relative magnetization and Curie temperature as the exchange interaction parameter $k_b\theta'/E_o$ is reduced.

Thus, we should be able to explain the decreasing magnetization of our alloys with increasing Rh concentration, which, from the data in the region of dilute Rh content, indicates that the addition of Rh actually <u>increases</u> the number of magnetic carriers.

<u>Stoner Theory - Paramagnetism</u>

Continuing with our discussion of the Stoner theory, Stoner also calculated the magnetization as a function of applied field in the paramagnetic temperature range (and hence the paramagnetic susceptibility).

Wohlfarth[41] interpolated Stoner's results, and graphed what he calls the normalized inverse susceptibility, $(\xi_o/\xi)\ (\mu_b H/k_b T_c)$ as a function of T/T_c for various values of ξ_o, (or equivalently, $k_b\theta'/E_o$, since the two are related by Stoner's relationship, equation 3.2.15). One can show this normalized inverse susceptibility is simply

3.2.18. $$\frac{\xi_o}{\xi}\ \frac{\mu_b H}{k_b T_c} = \frac{\mu_b M_o}{k_b T_c}\ \frac{1}{X}$$

where M_o is the saturation magnetization and χ is the usual susceptibility, M/H. This equation then defines the susceptibility in terms of Stoner's calculated quantities. He showed that this susceptibility obeys roughly a Curie-Weiss susceptibility law, but with the Curie constant becoming a slowly varying function of temperature.

One uses equation 3.2.18 to determine the susceptibility from the theoretical values determined by Stoner's calculation. One then writes this susceptibility in the Curie-Weiss form

3.2.19 $$\chi = \frac{C}{T-T_c}$$

where $C = N\,\mu_{eff}/3\,k_b$ and μ_{eff} is the effective Curie magneton number. One then finds the Stoner expression can be written in the form

3.2.20 $$\frac{\mu_b\,H}{k_b\,T_c}\,\frac{\xi_o}{\xi} = \left(\frac{T-T_c}{T_c}\right)\frac{3n_{sat}}{(\mu^2_{eff}/\mu_b^2)} = \frac{T-T_c}{T_c}\,\frac{3\,n_{sat}}{q_c^2}$$

where n_{sat} is the number of Bohr magnetons per atom, determined from saturation magnetization, and q_c is the magnetic moment per atom in units of μ_b as determined from the Curie susceptibility constant. Then the slopes of Wohlfarths curves (i.e. equation 3.2.20) are just equal to the quantity $3n_{sat}/q_c^2$. This quantity, as we have mentioned, is somewhat temperature dependent. We plot $3n_{sat}/q_c^2$ versus ξ_o for two different temperatures, 1.5 T_c and 2 T_c in figure 7. We remind the reader, however, that these quantitative results are valid only in the Stoner approximation and will be modified by the inclusion of the correct band shapes.

We notice that in the limit of weak ferromagnetism, ($\xi_o < 1$) the ratio n_{sat}/q_c^2 gets small, or q_c/n_{sat} gets large. Thus, in this limit, the number of carriers per atom, determined by the susceptibility, will be much larger than that determined by the saturation magnetization. This was discussed by Rhodes and Wohlfarth,[40] and applied to a number of

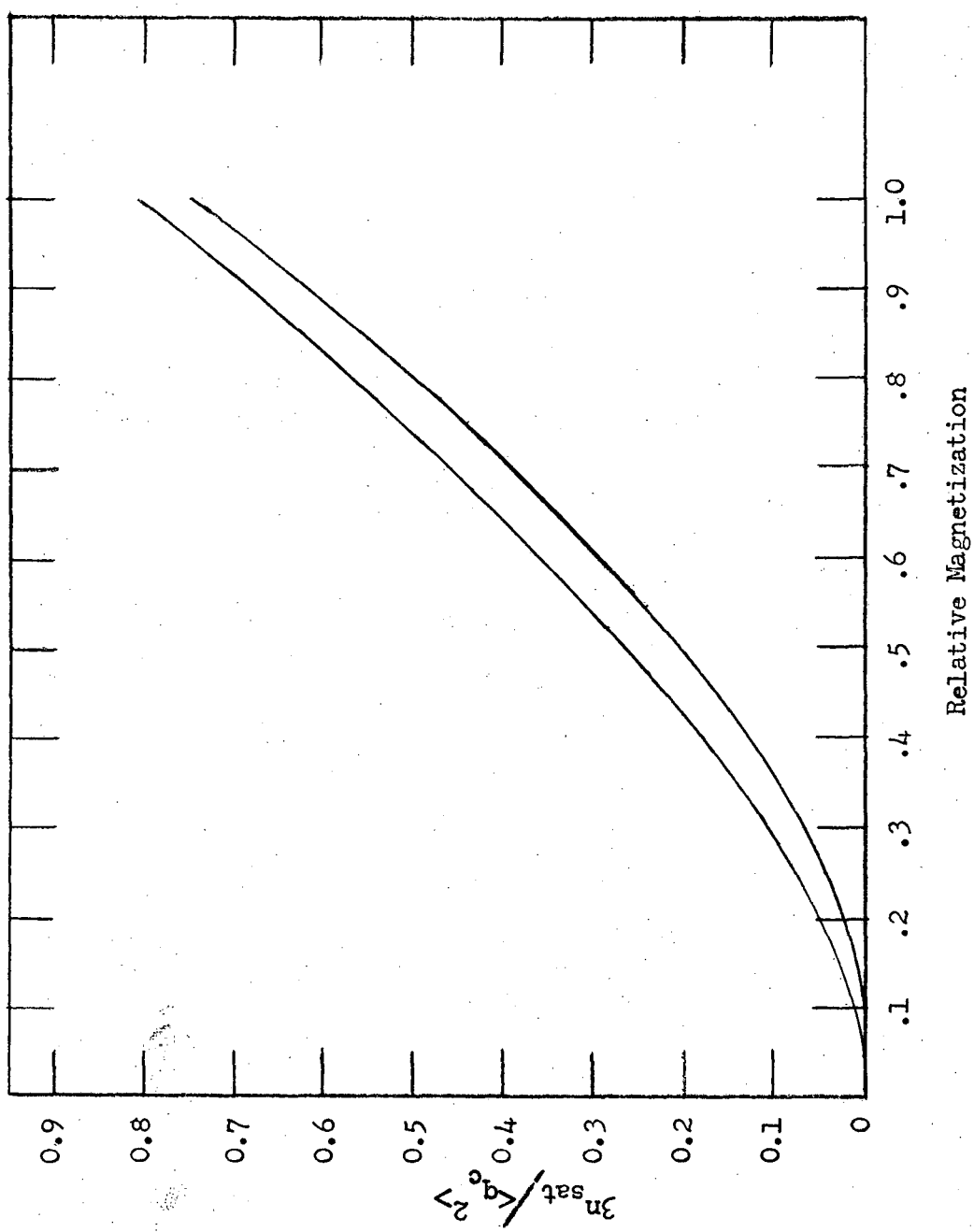
0.9
0.8
0.7
0.6
0.5
0.4
0.3
0.2
0.1
0
$3n_{sat}/\langle q_c^2 \rangle$
.1
.2
.3
.4
.5
.6
.7
.8
.9
1.0
Relative Magnetization

Fig. 7

weakly ferromagnetic materials. He found two classes of substances, one with q_c nearly equal to n_{sat}, which he ascribed as being due to the fact that these materials were dilute local moment ferromagnets, and a second type, where the ratio of q_c to n_{sat} when plotted against T_c, the transition temperature of the substance, increased smoothly with decreasing T_c. This is expected in a band magnet, (see figure 6). If E_o is taken to be relatively constant from substance to substance, and if we attribute the weakness of the ferromagnetism to the relative weakness of the exchange, we see that as ξ_o gets small, then $k_b T_c/E_o$ will get small, or equivalently, $k_b T_c$ will get small. Thus, these authors contend that the q_c/n_{sat} versus T_c curves (where T_c varies from substance to substance) are in a sense, equivalent to q_c/n_{sat} versus ξ_o curves. The observed form of his curves conform qualitatively to the behavior predicted by this theory.

In order to test the Stoner theory, Wohlfarth[41] attempted to explain the magnetostatic data obtained by previous workers for the Cu-Ni system. These alloys also exhibit continuously, almost linearly, decreasing saturation magnetization with increasing copper concentration. However, from a rigid band picture, this behavior is expected, primarily because each copper atom added to the alloy, containing one more electron than a nickel atom, adds one electron to the 3-d and 4-s bands. Since, from electronic specific heat measurements it is known that the density of states in the d-band at the fermi level is about ten times that of the 4-s band, of the electrons introduced by the copper, one-tenth go into the 4-s bands where the occupy equally spin up and spin down states, and nine-tenths go into the 3-d band, or equivalently, .9 holes are removed from this band. Then the number of holes in the d-band, with atomic concentration, c, of copper is

3.2.21 $$n_h = .54 - .9c$$

and the magnetic moment per atom, with g = 2.2 is, in units of Bohr magnetons, μ_b,

3.2.22 $$n_{sat} = 1.1\ (.54 - .9c) \approx .6 - c,$$ as observed.

Nevertheless, Wohlfarth argued that this effect is enhanced somewhat by the fact that the exchange interaction decreases with increasing copper concentration, causing the relative magnetization ξ_o to also decrease. Then the overall magnetization is simply the product of the number of hole-carriers in the d-band, multiplied by the relative magnetization factor, determined by the exchange parameter, $k_b\theta'/E_o$, which also varies with concentration.

Wohlfarth determined ξ_o as a function of concentration from two independent methods within the framework of the Stoner model.

First, using the rigid band approximation, and the fact that E_o varies as $(N)^{2/3}$ he inferred $E_o(c)$. He used the experimental values of T_c to determine T_c/E_o. Then, using Stoner's figure 6, he determined $\xi_o(c) = \xi_o(T_c/E_o)_c$.

The second method involved the ratio of magnetic carriers as determined by paramagnetic susceptibility, and by saturation magnetization. From Stoner's relations between ξ_o and this ratio, he obtained an independent determination of $\xi_o(c)$. He obtained excellent agreement between these two methods. However, since the decrease in saturation magnetization, M_{sat}, is due primarily to the filling of d-band vacancies, the effects of $k_b\theta'/E_o$ on the overall magnetization are masked. On the other hand, in the Ni-Rh system, where the addition of Rh increase the number of magnetic carriers, the decrease in M_{sat} is due entirely to decreasing ξ_o, so this system is even more desirable for such studies.

In addition to the work of Hunt, which we described, there have been additional refinements in the Stoner theory. Some of them are as follows.

Effect of overlapping bands. We suppose, as in the case of nickel the d-band with its high density of states, is overlapped by the s-band with a low density of states. We have just seen that such an overlapping band affects the number of electrons which go into the d-band upon alloying. There is yet another effect of overlapping bands. At high temperatures, the electrons are not only excited from one sub-band to the other, giving rise to redistribution among the two spin directions as described by equation 3.2.3. but some electrons are also excited from the d-band to the s-band. This serves to further influence the temperature dependence of the magnetization. These effects have been discussed by Band,[42] Lidiard[43] and Wohlfarth.[41]

Band shape effects. Open bands, closed bands, bands of different shapes, both overlapping and non-overlapping were discussed by Elcock, Rhodes, and Teviotdale.[44] They found that various susceptibility vs. temperature relations were possible, including some showing maximum in the susceptibility as a function of increasing temperature. They applied their results with some success to Pd and Pd:Ag.

Very weak magnetism limit. The theory of itinerant ferromagnets, in the limit of very weak ferromagnetism, has been worked out by a number of authors: D.M. Edwards and E. P. Wohlfarth,[45] E..P. Wohlfarth,[46] J. Mathon.[47]

In this limit, solution of the magnetization equations may be carried out in terms of the value of the density of states function and its derivatives, evaluated at the Fermi level. Thus, the knowledge of the entire band structure becomes unnecessary.

The first of these papers concerns itself primarily with the magnetic isotherms of such a system. However, the results of this theory are modified by the presence of spin waves at low temperature. We will return to this point in a later section.

The second paper also derives quantitative results for a very weak Stoner ferromagnet. Both papers apply these results quite successfully to the observed data for the weakly (itinerant) ferromagnetic intermetallic compound, $ZrZn_2$. They fit the observed isotherms for this material very well to those predicted by the theory, except at the very lowest temperatures, where spin wave contributions are expected to cause such deviations.

The third paper discusses some of the electrical and magnetic properties for a weakly ferromagnetic system of alloys, in the vicinity of the critical concentration. The author assumes that the density of states is a smoothly varying function of energy near the Fermi surface. He also assumes that the exchange and Fermi energy are smoothly varing functions of concentration. He assumes these parameters may be expressed as a Taylor expansion about the critical concentration:

3.2.23 $$k_b\theta'(c) = k_b\theta'_{critical} + A\,\Delta c + B(\Delta c)^2 + \ldots$$

3.2.24 $$E_o(c) = E_o|c_{critical} + R\,\Delta c + S(\Delta c)^2 + \ldots$$

where Δc is the deviation of composition from its critical value.

We will use the results of these authors when we discuss our magnetostatic measurements in the next section.

<u>Spin waves</u> It has been demonstrated by a number of authors that spin wave excitations can exist in a band ferromagnet, influencing the magneto-static properties. We will also discuss this at length in a later section.

C. Hurwitz-Van Vleck Description

For completeness sake, we should also describe briefly a slightly different approach to ferromagnetism, the so-called Hurwitz-Van Vleck, or minimum polarity model.

This model was described by Hurwitz,[48] Van Vleck,[49] and later reviewed by Van Vleck.[50]

We may think of this approach as a generalization of the localized moment (Heisenberg) description, to include the effects of the overlap of the neighboring d-wave function orbitals. This spatial overlap allows electrons to hop from one atomic site to another.

(This can be seen from a perturbational approach. One can calculate the transition probability, using the Golden Rule, of an electron making a transition from one localized atomic state to a neighboring one. This is related to the matrix element $\mathcal{H}_{AB}$ connecting these states, which, by definition is related to the overlap integral:

3.3.1. $$K_{AB} = \int \underset{\text{atom A}}{\phi(r')} \; \underset{\text{interaction}}{\mathcal{H}(r')} \; \underset{\text{atom B}}{\phi(r')} \; d\vec{r}'$$

where the $\underset{\text{atom i}}{\phi(r)}$ is the wave function localized at atomic site, i. This is non-zero if there exist some region of space where both atomic wave functions are non-zero simultaneously. This is just the condition of nearest neighbor overlap.)

The overlap also broadens the atomic d-states into bands of finite (but narrow) width. This picture is simply the tight binding approximation and is treated, for example, in Principles of the Theory of Solids.[51]

The result of this electron hopping is that the distribution of d-electrons throughout the lattice is changed from its value in the extreme localized (i.e., no overlap) case.

In the case of pure nickel, for example, we may think of the individual atomic sites as being in different states of ionization, or polarity; i.e., some atoms are in the d^{10} configuration, some in the d^9, d^8, etc. The fractional distribution of such states is subject to the auxilliary condition that the polarity averaged over the entire sample must correspond to the observed magnetic moment. For pure nickel, the average polarity is symbolically written $d^{9.46}$, to correspond to the observed value of .54 holes per atom. (Note: at the time these papers were published, the g.value for Ni was not known, and was assumed to be 2. Since it is now known to be 2.2, there are actually .54 holes per atoms, whereas Van Vlecks' description was based on .6. This correction makes no essential difference in the discussion.) Implicitly assumed in this model is that there is some mechanism to cause these moments to align parallel to each other at low temperature.

With this model, we are in a position to treat the effects of correlation. We do so by acknowledging the fact that it takes more energy to doubly ionize a site (d^8) than to singly ionize it (d^9). It is just the Coulomb (electron-electron) interaction which makes the energy of these higher polarity states of large. Therefore, by requiring the number of sites in states of high polarity to be small, we can describe the effects of correlation. We may then choose, as Van Vleck originally did, to rule out completely the states of high polarity. We then say that the system is in a state of minimum polarity. For nickel we would have 46 per cent of the sites in $3d^{10}$ and the remaining 54 per cent of the sites in the $3d^9$ configuration, yielding the average value of $3d^{9.46}$ as required.

On the other hand, we may choose not to rule out the high polarity states completely, but give them small but finite probabilities.

We do this because the minimum polarity approximation over-estimates the effects of correlation. In real metals, there is screening of the Coulomb interaction by other d-electrons, and by the s-electrons. Thus the energy of a d^8 state is not as much higher than a d^9 state in a metal as it is in a free atom. C. Herring[52] has suggested that the highly mobile 4-s electrons largely screen out the effects of the fluctuations in the polarity, making such fluctuations energetically more favorable than they would otherwise be.

By restricting ourselves to minimum polarity states only, we are in effect, restricting the electronic wave functions too severely, forcing them to be more localized in space than necessary, thereby increasing their kinetic energy. By allowing some small fraction of site to become ionized to d^8, or higher, we reduce the kinetic energy more than we increase the potential energy, and thereby reduce the total energy of the system.

We can also understand the presence of some high polarity states from the following argument: The various atomic d-states overlap with neighboring sites and with each other, so a particular atomic state is actually described by a linear combination of many atomic wave functions (which form a complete orthonormal set).

One can then calculate the probability of a particular polarity state at some given site by calculating the probability of vacancies in the appropriate number of atomic localized states at that site from the coefficients of the unperturbed atomic eigen-functions appearing in the linear combinations which describe the true wave functions.

The relative fraction of these higher polarity states were estimated by Van Vleck.[50]

The presence of these higher polarity states is attractive from a theoretical standpoint. It allows an additional contribution to the exchange, namely the Hund's rule type coupling, which tends to align electronic spins located on the same atomic site. In fact, it is felt by many authors that such a contribution to the exchange may be necessary in order to cause a band of electrons to become ferromagnetic.

Another consequence of this Hund's rule coupling, is that spin states (at least a few of them) are allowed to have spin quantum number $S = 1$ (or even higher), due to the coupling of individual $S = 1/2$ electrons at the same site. In the Stoner model (and in the minimum polarity model for pure nickel), all of the magnetic carriers have $S = 1/2$. The presence of these higher spin quantum number states lead to certain consequences. For example, it affects the angular dependence of the magnetocrystallineanisotropy (to be discussed in a later section).

This (narrow) band model has some of the features of other band models, e.g., large contribution to the specific heat from magnetic electrons, magnetization corresponding to non-integral Bohr magneton numbers, and spin waves. However, numberical results from this model are almost impossible to obtain. In order to make quantitative calculations in this model, one needs to know the ionization energies involved in the states of different polarity. Although these energies are known from spectrographic data for free ions, they are not known in the case of metals, where screening effects occur.

In any event we may state that while the Stoner approach neglects the effect of correlation (except in considering the screening in the long

range Coulomb interaction), this model overestimates these effects. The real description probably lies somewhere between the two limiting extremes of this model, and the Stoner model.

IV. MAGNETOSTATIC MEASUREMENTS IN NI-RH

A. Saturation Moment and Paramagnetic Susceptibility

As we mentioned in the introduction, the saturation moment and the Curie temperature have already been measured for a number of alloys in this system. Crangle and Parsons[7] measured these quantities for the Ni-Rh system (as well as for some related alloys). They attempted to analyze the magnetization data in the dilute region using the rigid band picture (and also a localized moments picture, with a magnetic moment associated with each atom, differing for the two species in the alloy). However, they did not have much success. In the Ni-Rh system, the addition of Rh was observed to contribute the magnetic moment equivalent to two holes per atom of Rh added, instead of one, as is expected by its atomic configuration. They also found similar discrepencies in the other systems they studied. For the Ni-Rh system, no explanation was offered for the continuous decrease in saturation moment which occured for increase in the Rh concentration over about five per cent.

We will attempt to provide an explanation of this using the Stoner model as a basis.

For our studies, the magnetization was measured as described in section II. The physical dimensions of the samples were accurately measured as was the weight. With these measurements, we accurately determined the average density of our samples. We determined the density of our alloys expected in the ideal case, using the lattice parameter versus concentration data determined by Luo and Duwez,[5] who determined these curves by X-ray diffraction measurements. We were then able to calculate the porosity of our samples, resulting from the preparation. With this information, we could express our observed values of magnetization in terms of Bohr magnetons per atomic unit.

In figure 8 we plot the magnetic moment per atom, extrapolated to $T=0$ as a function of alloy concentration. Included on this plot is the previous data of Crangle and Parsons. We note the agreement between these two sets of data.

Figure 9 shows the measured values of the Curie temperature for these alloys, again including the data of Crangle and Parsons. We determined T_c by extrapolating the high temperature inverse susceptibility versus temperature plot to the value of T giving $1/\chi = 0$. In the high temperature region, this plot was quite linear, and the extrapolated value was seen to be independent of the external magnetizing field. Again, agreement with Crangle and Parsons measurements was quite good.

We also display the saturation moment per atom as a function of the Curie temperature in figure 10.

In order to determine the relative magnetization, ξ_o, it is necessary to make some assumptions about the effects of alloying upon the number of d-carriers in the system.

We assert that each atom of Rh added to the alloy system has the effect of contributing some number of holes, $N_{holes\ added}$, to the common d-band, which we assume is between 1 and $1\frac{1}{2}$. (Since the d-band is expected to have a much higher density of states than the overlapping 4-s band, most of the holes added should, in fact, go into the d-band, with perhaps, one tenth of them going into the s-band.) We will see that the results we obtain are not critically dependent on the value we assign to $N_{holes\ added}$.

The justification for our assumption is described by Pauling.[53] He plotted the magnetic moment per atom for alloy of the 3-d transition ferromagnetic elements with other elements in the 3-d series, as a function

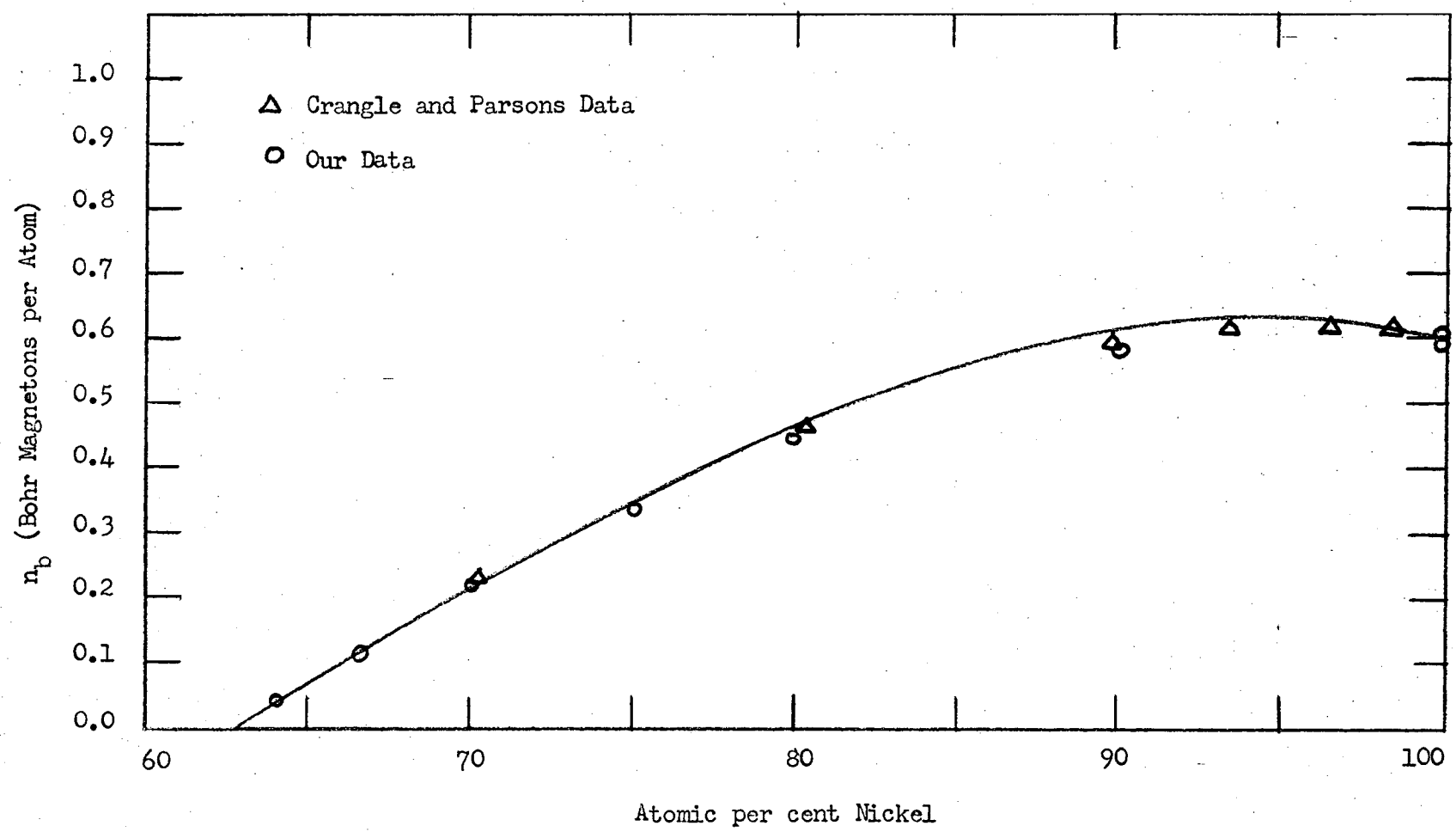
Crangle and Parsons Data
Our Data
n_b (Bohr Magnetons per Atom)
1.0
0.9
0.8
0.7
0.6
0.5
0.4
0.3
0.2
0.1
0.0
60
70
80
90
100
Atomic per cent Nickel

Fig. 8

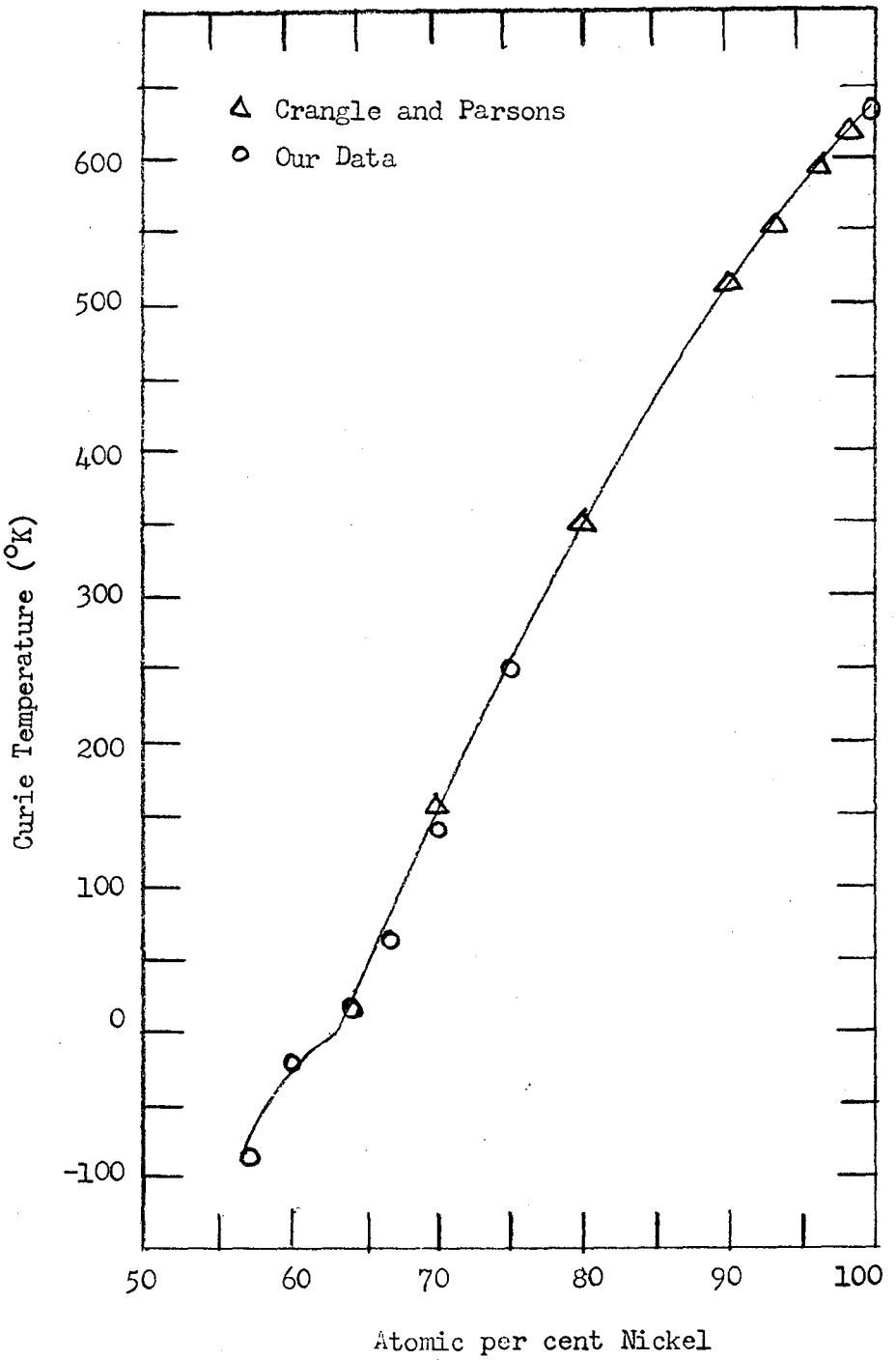
Crangle and Parsons
Our Data
600
500
400
300
200
100
0
-100
Curie Temperature (°K)
50
60
70
80
90
100
Atomic per cent Nickel

Fig. 9

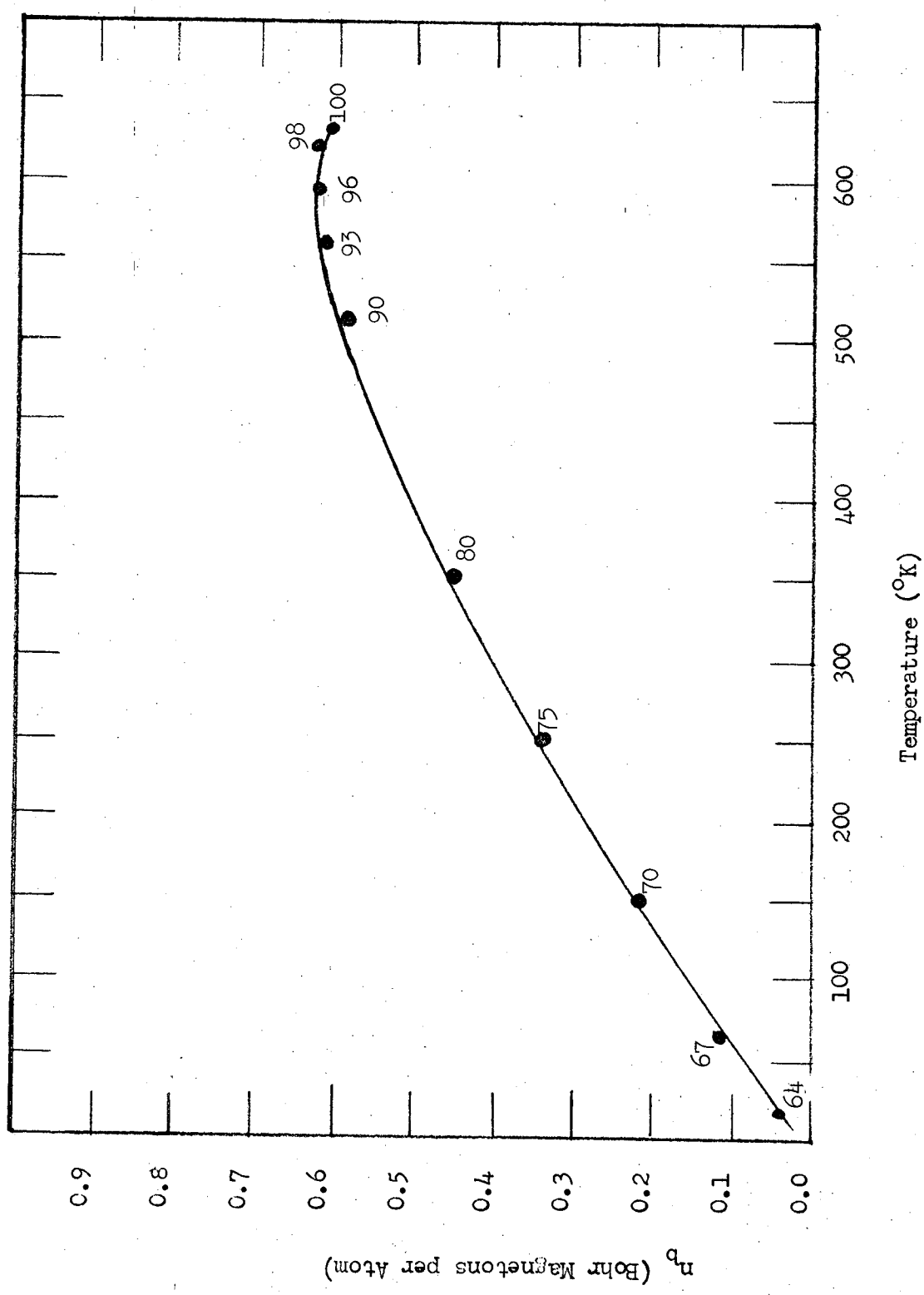
0.9
0.8
0.7
0.6
0.5
0.4
0.3
0.2
0.1
0.0
n_b (Bohr Magnetons per Atom)
100
200
300
400
500
600
Temperature (°K)
64
67
70
75
80
90
93
96
98
100

Fig. 10

of the average atomic number of the alloy, which is the weighted average of the atomic numbers of the two constituents. He found that in many cases, the net magnetic moment behaved just as if the addition of the solute contributed or removed carriers from the magnetic band, the number contributed or removed depending on the difference between the number of electrons in the solvent and solute. For example, we have seen the addition of Cu, with one more electron per atom than Ni, when added to nickel decreases the saturation moment by one Bohr magneton per copper atom added, since the electron contributed by the copper fills one vacancy in the spin down sub-band, removing one magnetic carrier. Similarly, Pauling found the addition of zinc to nickel, with two more electrons per atom, decreased the saturation moment twice as quickly as did copper. Cobalt, on the other hand, with one less electron per atom than nickel, increased the magnetic moment by about one Bohr magneton per added atom.

When palladium, with atomic configuration $4d^{10}$ is added to nickel ($3d^8\ 4s^2$ = 10 outer electrons), over a large range of concentration the magnetic moment remains constant.[54] Thus the addition of each Rh atom with one less electron than Pd, is expected to contribute about one hole.[7] However, we have noted that in the dilute region, the magnetization data has indicated that this number is about two holes per atom added. We attribute this to s-d mixing, which we will discuss later.

In the more concentrated Rh concentration region, we assume this number decreases somewhat, becoming closer to the expected value of 1. We then interpret our data using two separate sets of assumptions

4.1.1 case 1. $N_{holes\ added} = 1$

4.1.2 case 2. $N_{holes\ added} = 1.5$

We then calculate the effective number of magnetic carriers for these two cases.

4.1.3 case 1. $N_{holes\ total} = .6 + c$

4.1.4. case 2. $N_{holes\ total} = .6 + 1.5c$

where c is the concentration of Rh. We have implicitly included the fact that g = 2.2 over the range of interest, which is consistent with our magnetic resonance experiments.

The ratio between the number of magnetic carriers per atom inferred above, and the measured value of the low temperature saturation magnetization, can then be used to calculate the relative magnetization, ξ_o.

We plot ξ_o as a function of the rhodium concentration for our two sets of assumptions, in figures 11 and 12. We see that in both cases these relations are quite linear from the critical concentration to a concentration quite high in nickel. We will discuss this from the point of view of the Stoner theory in the next sub-section.

We also show ξ_o vs. T_c for the case $N_{holes\ added} = 1$. (The second case, $N_{holes\ added} = 1.5$, leads to qualitatively the same results, and is therefore not shown.) See figure 13.

Figure 14 shows the variation of the Curie constant describing the paramagnetic susceptibility of our alloys. This is expressed in terms of the effective Curie magneton number, q_c defined by the equations

4.1.5 $$\chi(T) = \frac{C}{T-T_c}$$

4.1.6 $$C = \frac{N(q_c\,\mu)^2}{3k_b} = \frac{N < q_c^{\,2} > \mu^2}{3k_b}$$

where N is the number of atoms per unit volume, μ the magnetic moment per carrier ($= \frac{1}{2} \cdot g\,\mu_b$), g is the spectroscopic splitting factor, μ_b

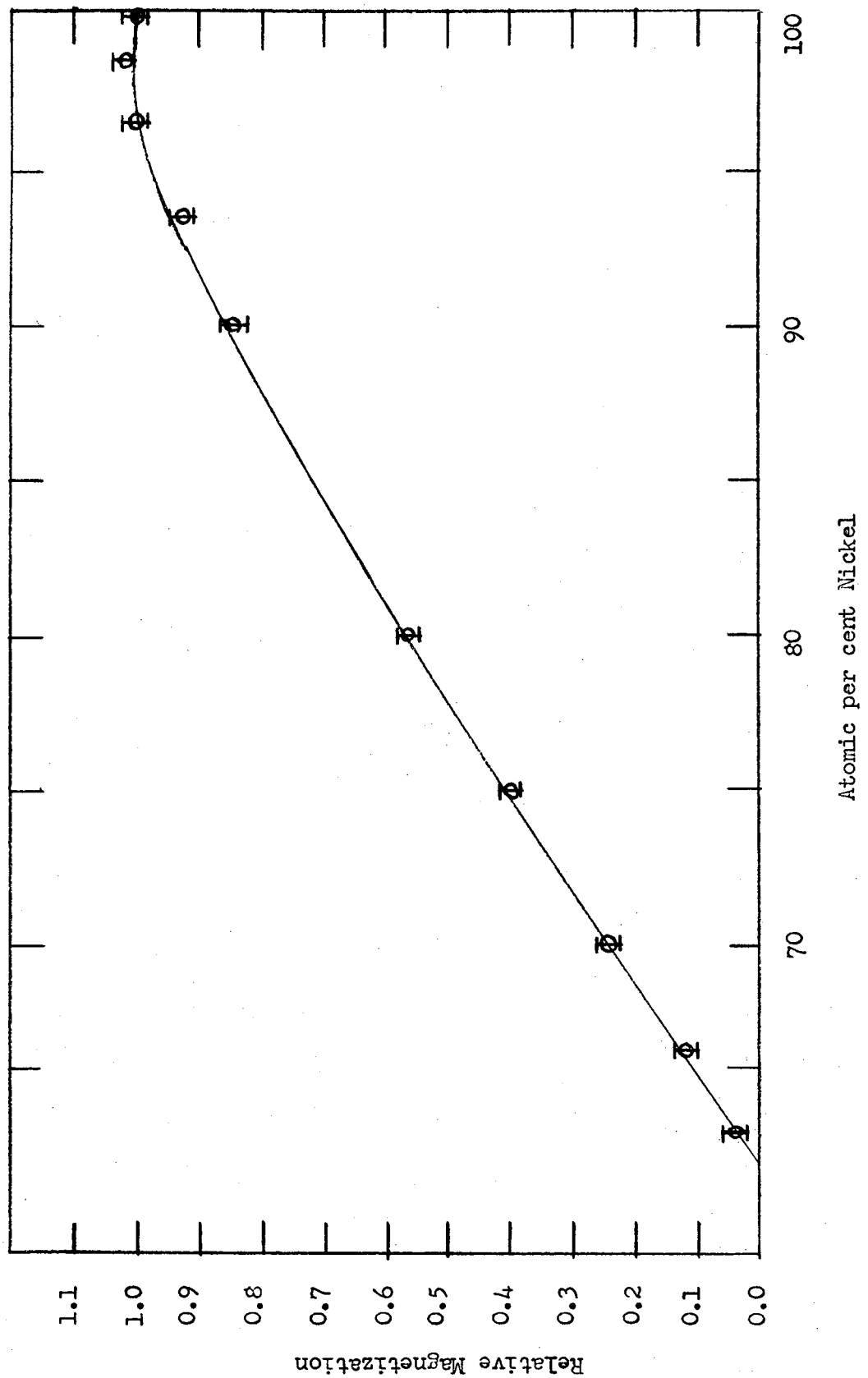
Relative Magnetization
1.1
1.0
0.9
0.8
0.7
0.6
0.5
0.4
0.3
0.2
0.1
0.0
70
80
90
100
Atomic per cent Nickel

Fig. 11

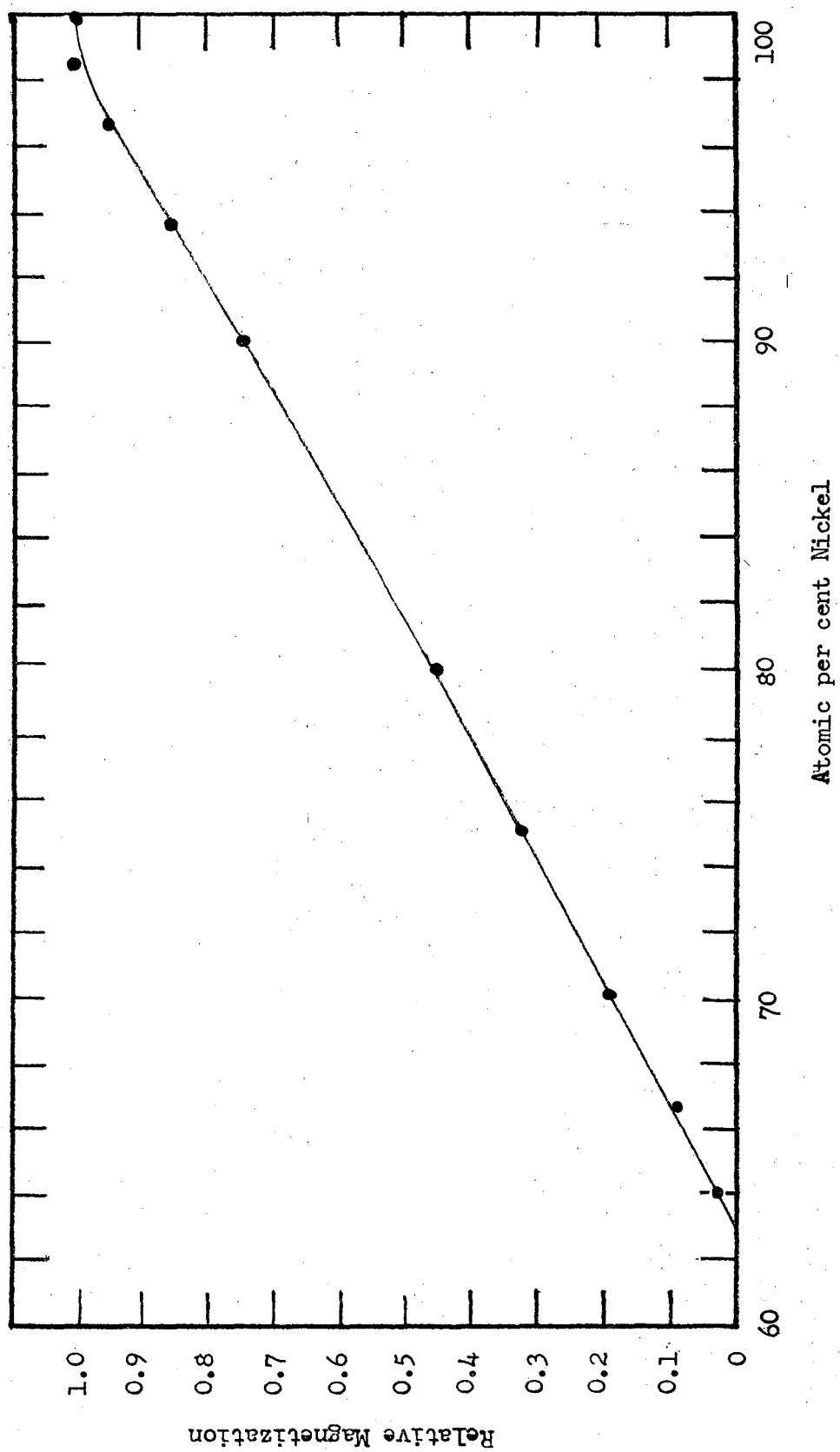
Relative Magnetization
1.0
0.9
0.8
0.7
0.6
0.5
0.4
0.3
0.2
0.1
0
60
70
80
90
100
Atomic per cent Nickel

Fig. 12

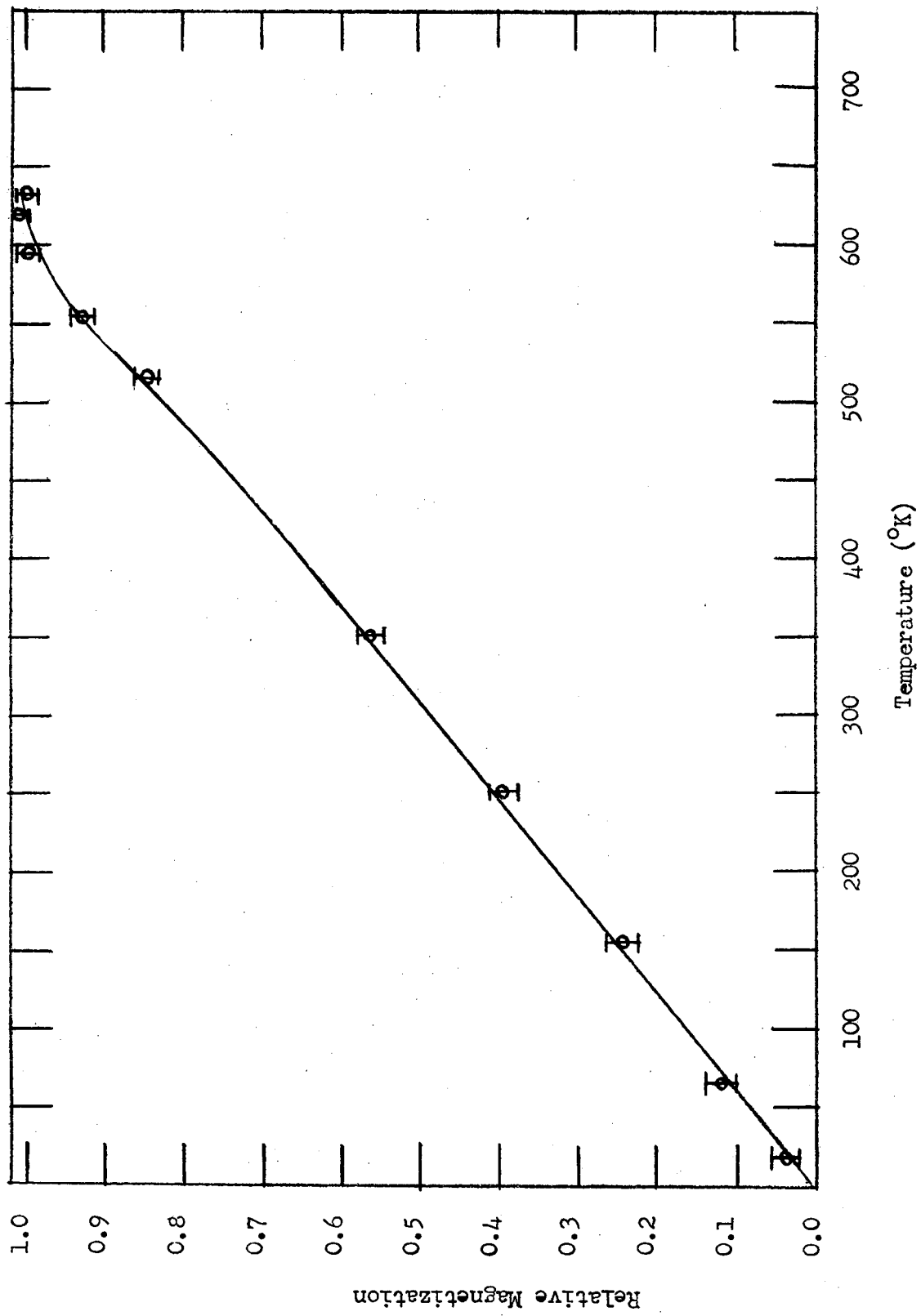
Relative Magnetization
1.0
0.9
0.8
0.7
0.6
0.5
0.4
0.3
0.2
0.1
0.0
100
200
300
400
500
600
700
Temperature (°K)

Fig. 13

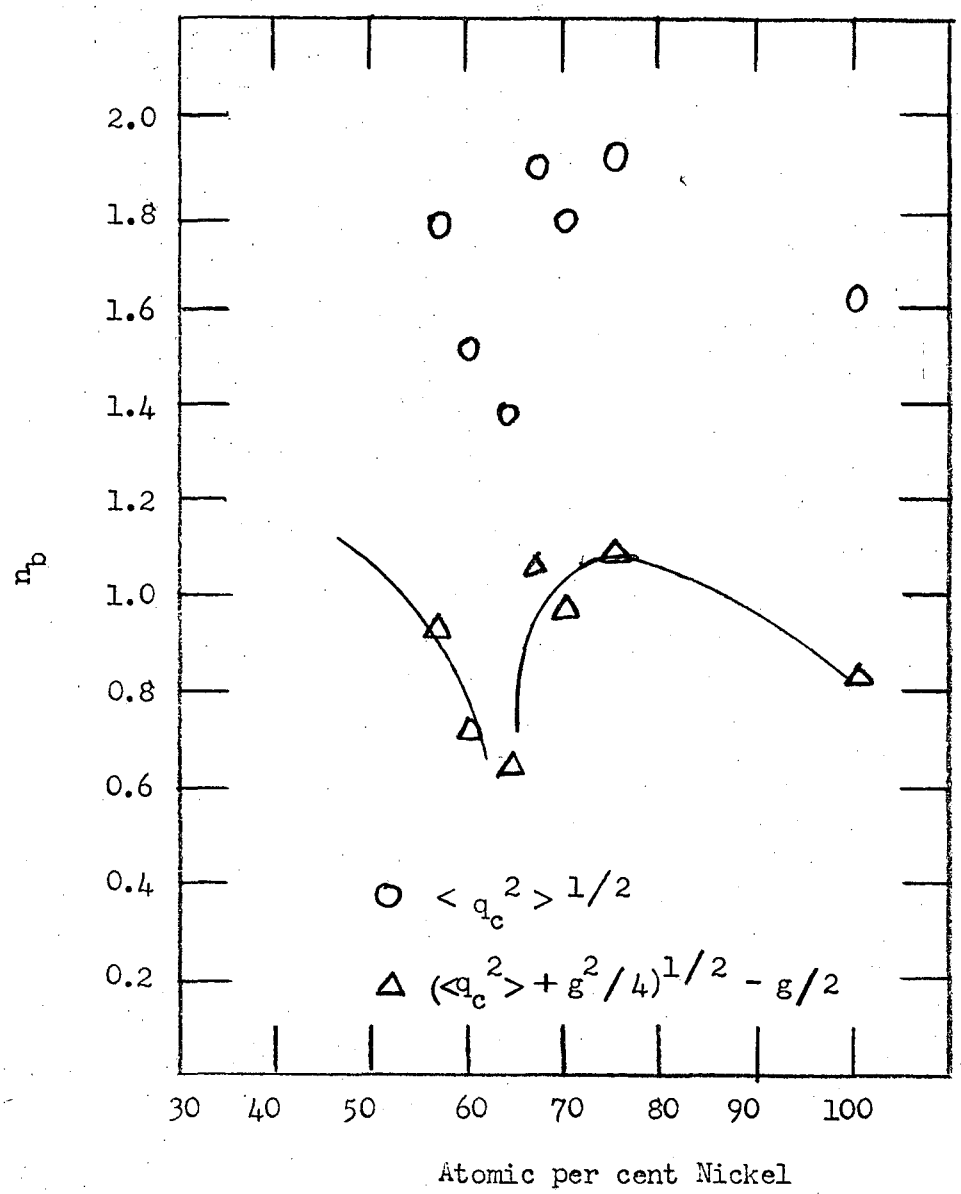
2.0
1.8
1.6
1.4
1.2
1.0
0.8
0.6
0.4
0.2
n_p
30
40
50
60
70
80
90
100
Atomic per cent Nickel
$\langle q_c^2 \rangle^{1/2}$
$(\langle q_c^2 \rangle + g^2/4)^{1/2} - g/2$

Fig. 14

is the Bohr magneton, and the spin, S, of the electron is 1/2. In determining q_c from $< q_c^2 >$, we must acknowledge the quantum mechanical nature of the electron spin.

Let us consider the following argument: We consider the magnetic moment of each carrier, in units of Bohr magnetons. Then the effective magneton number is defined from the equation

4.1.7 $$q_c = g \cdot S$$

However, in deriving the Curie-Weiss susceptibility law, it is the square of the magnetic moment which enters the problem. Quantum mechanically, this is given by

4.1.8 $$q_c^2 = g^2 \cdot S(S+1)$$

expanding, we find

4.1.9 $$g^2 S^2 + g^2 S - q_c^2 = 0$$

solving for S taking the positive root,

4.1.10 $$S = \frac{-g^2 + \sqrt{g^4 + 4g^2 q_c^2}}{2g^2}$$

and recalling equation 4.1.7, we find

4.1.11 $$q_c = (q_c^2 + g^2/4)^{1/2} - 1$$

for g = 2, this reduces to

4.1.12 $$q_c = (q_c^2 + 1)^{1/2} - 1$$

a form often used in the literature. We have plotted $< q_c^2 >^{1/2}$ and q_c as a function of c in figure 14. We see that as q_c remains fairly constant over the entire range (while n_{sat} goes to 0 at $c_{critical}$), with the exception of a slight dip near $c_{critical}$.

We will now attempt to relate our data to the predictions of the Stoner theory.

B. Comparison with Theory - Solution of Stoner Equations

It is apparent from equation 3.2.3 that the magnetic properties in general depend critically on the density of states function describing the band of magnetic electrons. However, in the limit of weak ferromagnestism, the bands shift only a small amount with respect to each other, hence, only those electrons near the Fermi level are involved. In this limit, one may express the solution of the Stoner equation in terms of the density of states function and its derivatives, evaluated at the (non-magnetic) Fermi level.

Equation 3.2.3 was solved in this limit by Edwards and Wohlfarth,[45] Wohlfarth,[46] and Thompson, Wohlfarth and Bryan.[55] They find that the fractional magnetization, ξ, is described by the equation.

4.2.0 $$(2/n)\, N(E_f)\, [k_b\theta'\xi + \mu H] = \xi\, [1 + \alpha\, (T/T_c)^2] + \gamma\, \xi^3 + Q\xi^5$$

where T_c is the transition temperature,

4.2.1 $$\alpha = \frac{1}{6}\pi^2\, (k_b T_c)^2\, (\upsilon_1^{\,2} - \upsilon_2)$$

and

4.2.2 $$\gamma = \frac{1}{8}\, \{\frac{n}{N(E_f)}\}^2\, (\upsilon_1^{\,2} - 1/3\, \upsilon_2)$$

and where

4.2.3 $$\upsilon_m \equiv \frac{d^m N(E)}{d\, E^m} \Big/ N(E) \Big|_{E=E_f}$$

$N(E_f) \equiv$ density of states at non-magnetic Fermi level per atom per spin direction

$n \equiv$ number of magnetic carriers per atom (= .54 for pure Ni).

Solving equation 4.2.0 in the limit of H = 0 and T = 0, and again defining $\xi_o = \xi|_{T=0}$ we find a relation between $k\theta'$ and ξ_o.

4.2.4. $$\frac{2}{n} N(E_f)\, k_b \theta' = 1 + \gamma\, \xi_o^{\,2}$$

Using equations 4.2.0 and 4.2.4 we find the relation between T_c/T_f and ξ_o (where $T_f \equiv E_f/k_b$):

4.2.5 $$\alpha = \gamma\, \xi_o^{\,2}$$

where T_c is defined in terms of α in equation 4.2.1.

These authors also show that one can write the expression describing the magnetic isotherms in the form

4.2.6 $$\left[\frac{M\,(H,T)}{M\,(0,0)}\right]^3 - \frac{M\,(H,T)}{M\,(0,0)} \left[1 - \frac{T}{T_c}^{\,2}\right] = \frac{2\,\chi_o\, H}{M\,(0,0)}$$

where M (H,T) = magnetization at field H and temperature T, and where

4.2.7 $$\chi_o = N \cdot N\,(E_f)\, \mu^2/\gamma\, \xi_o^{\,2}$$

where N is the number of atomic sites per unit volume and μ is the magnetic moment per electron, $= \frac{1}{2}\, g \cdot \mu_b$.

In order to make use of these equations, we must find an expression for the terms involving the υ_m. For a parabolic band, we recall:

4.2.8 $$N(E) = \frac{3n}{4\, E_f^{\,3/2}}\, E^{1/2} = A\, E^{1/2}$$

In this case, the terms involving the υ_m can be evaluted as follows:

4.2.9 $$\upsilon_1 = \frac{1}{2}\, E_f^{\,-1}$$

4.2.10 $$\upsilon_2 = -\frac{1}{4}\, E_f^{\,-2}$$

Therefore

4.2.11 $$[\upsilon_1^{\,2} - \upsilon_2] = \frac{1}{2}\, E_f^{\,-2}$$

and

4.2.12 $$[\upsilon_1^{\,2} - 1/3\, \upsilon_2] = \frac{1}{3}\, E_f^{\,-2}$$

We then generalize 4.2.8, 4.2.11 and 4.2.12 to non-parabolic bands, by defining the functions g_o, g_1, g_2:

4.2.13 $$N(E_f) \equiv \frac{3n}{4\,E_f}\; g_o\,(E_f)$$

4.2.14 $$(v_1^{\,2} - v_2) \equiv g_1(E_f) \cdot \frac{1}{2}\, E_f^{\,-2}$$

4.2.15 $$(v_1^{\,2} - 1/3\, v_2) \equiv g_2(E_f) \cdot \frac{1}{3}\, E_f^{\,-2}$$

In the limit of parabolic bands, these functions all approach the value 1.

In terms of these functions, the parameters α and γ can be evaluated. We find, using equation 4.2.1, 4.2.2, 4.2.13, 14, and 15,

4.2.16 $$\alpha = \frac{\pi^2}{12}\;\frac{T_c^{\,2}}{T_f^{\,2}}\; g_1(E_f)$$

and

4.2.17 $$\gamma = \frac{2}{27}\;\frac{g_2\,(E_f)}{g_o^{\,2}\,(E_f)}$$

Then equation 4.2.4 becomes

4.2.18 $$\frac{k_b\theta'}{E_f}\; g_o(E_f) = 2/3 + 4/81\;\frac{g_2\,(E_f)}{g_o^{\,2}(E_f)}\;\xi_o^{\,2}$$

This is a generalization of equation 3.2.12. $g_o(E_f) > 1$ implies a large density of states at the Fermi surface. We see that a large density of states can lead to ferromagnetism with relatively weaker exchange interactions than in the case of low density of states. This is just a restatement of equations 3.1.25 and 3.1.28; i.e., that the Stoner condition for ferromagnetism is $J \cdot N(E_f) > 1$. Equation 4.2.5 can then be written

4.2.19 $$T_c/T_f = \frac{2\sqrt{2}}{3\pi}\sqrt{\frac{g_2\,(E_f)}{g_o^{\,2}\,(E_f)\;g_1(E_f)}}\;\xi_o$$

4.2.19a $$T_c/T_f \equiv .30\sqrt{\frac{g_2\,(E_f)}{g_o^{\,2}\,(E_f)\;g_1\,(E_f)}}\;\xi_o$$

We may eliminate ξ_o from equations 4.2.18 and 4.2.19, to relate T_c/T_f directly to $k_b\theta'/E_f$. We then find

4.2.20 $$k_b\theta' g_o(E_f) \approx 2/3 + (4/81)(1/.09)g_1(E_f) \quad (T_c/T_f)^2$$

We may similarly evaluate the susceptibility parameter χ_o. From equations 4.2.7 and 4.2.17 we find

4.2.21 $$\chi_o = 81/8 \left[\frac{n\,N\,\mu^2}{kT_f}\right] \frac{g_o^3(E_f)}{g_2(E_f)} \quad 1/\xi_o^2$$

or using equation 4.2.19

4.2.22 $$\chi_o \approx .09 \left[\frac{81}{8} \frac{n\,N\,\mu^2}{k_b\,T_f}\right] \frac{g_o(E_f)}{g_1(E_f)} \quad \frac{T_f^2}{T_c^2}$$

We also solve the magnetic isotherm equation (equation 4.2.6) for several limiting cases.

<u>Low temperature, valid to high fields</u>

In the limit of T = 0, defining $\epsilon \equiv \dfrac{\Delta M(H, T=0)}{M(0,0)}$

we find, using equation 4.2.6

$$[1 + \epsilon]^3 - [1 + \epsilon] \approx \frac{2\chi_o H}{M(0,0)}$$

therefore, $$2\epsilon \equiv \frac{2\Delta M(H,T=0)}{M(0,0)} \approx \frac{2\chi_o H}{M(0,0)}$$

Therefore, the low temperature (high field) differential susceptibility is given by

4.2.23 $$\chi_{difn} = \chi_o$$

provided $$\chi_o H = \Delta M \ll M(0,0)$$

<u>Low field susceptibility</u>

By defining $\chi = \Delta M/\Delta H$ and using equation 4.2.6, one finds[46]

4.2.24 $$\chi(T) = \chi_o\,[1 - (T/T_c)^2]^{-1} \quad T < T_c$$

4.2.25 $$\chi(T) = 2\chi_o[(T/T_c)^2 - 1]^{-1} \quad T_f \gg T > T_c$$

Be defining the paramagnetic Curie magneton number from equation 3.2.19, ff. and using equations 4.2.22, and 4.2.25, we find

4.2.26 $$\langle q_c^{\,2}\rangle \approx 5.46\; n\,\frac{T_f}{T+T_c}\;\frac{g_o\,(E_f)}{g_1\,(E_f)}$$

If we evaluate this at $T = 2\,T_c$, we find

4.2.27 $$\langle q_c^{\,2}\rangle = 1.82\; n\,\frac{T_f}{T_c}\;\frac{g_o\,(E_f)}{g_1\,(E_f)}$$

or using equation 4.2.19 to eliminate T_f/T_c

4.2.28 $$\langle q_c^{\,2}\rangle = 6.06\; n\,\frac{g_o^{\,2}\,(E_f)}{\sqrt{g_1\,(E_f)\;g_2\,(E_f)}}\;1/\xi_o$$

In order to put this into a form often used in the literature, we use $n_{sat} = n\,\xi_o$ to write 4.2.28 in the following way

4.2.29 $$\frac{\langle q_c^{\,2}\rangle}{n_{sat}} = 6.06\,\frac{g_o^{\,2}\,(E_f)}{\sqrt{g_1\,(E_f)\;g_2\,(E_f)}}\;1/\xi_o^{\,2}$$

or

4.2.30 $$\frac{3n_{sat}}{\langle q_c^{\,2}\rangle} = .495\,\frac{\sqrt{g_1\,(E_f)\;g_2\,(E_f)}}{g_o^{\,2}\,(E_f)}\;\xi_o^{\,2}$$

This equation is the analytic form of the graph of figure 7, valid for small ξ_o.

In order to compare our data with the predictions of the Stoner theory we calculate the dependence of these magnetic parameters on the concentration, in the vicinity of the critical concentration. We begin our discussion by stating that there is nothing special about $k_b\theta'$ and E_f

near the critical concentration, other than the fact that they happen to form the ratio 2/3. In the foregoing solutions, it was assumed that the density of states function N(E) was a smooth function of E. If we adopt a rigid band model, we see that the addition of Rh to the alloy changes the number of carriers in the d-band, thereby shifting the Fermi level according to the equation

4.2.31 $$n(c) = \int_0^{E_f} N(E')\, dE'$$

where n is the number of d-carriers at alloy concentration c, and N(E') is the rigid band density of states function. Thus E_f will vary smoothly with the concentration c. Even if the band does change shape, and if we allow the s-band to change its position with respect to the d-band, we still expect E_f to be a continuous function of concentration. We should expect it to be expressible as a Taylor series in the concentration, expanded about some arbitrary (but non-singular) value of c, which we conveniently pick as the critical concentration. We should then be able to express the Fermi energy in the form

4.2.32 $$E_f(c) = E_f(c_{crit}) + \epsilon_1 \Delta c + \epsilon_2 (\Delta c)^2 + \ldots$$

where Δc is the deviation of the Rh concentration from its critical value.

Similar discussions pertain to the dependence of the exchange parameter with concentration. Then

4.2.33 $$k_b\theta'(c) = k_b\theta'_{critical} + \delta_1 \Delta c + \delta_2 (\Delta c)^2 + \ldots$$

We then take the ratio of these two quantities.

4.2.34 $$\left.\frac{k_b\theta'}{E_f}\right|_{c = c_{crit} + \Delta c} = \frac{k_b\theta'_{crit} + \delta_1 \Delta c + \delta_2 (\Delta c)^2 + \ldots}{E_f^{crit} + \epsilon_1 \Delta c + \epsilon_2 (\Delta c)^2 + \ldots}$$

We can rewrite this as

4.2.35 $$\left.\frac{k_b\theta'}{E_f}\right|_c \approx \frac{k_b\theta'_{crit}}{E_f^{crit}} \left\{1 + (\delta_1/k_b\theta'_{crit} - \epsilon_1/E_f^{crit})\,\Delta c + \ldots\right\}$$

which can be put in the form

4.2.36 $$\left.\frac{k\,\theta'}{E_f}\right|_c \approx \frac{k_b\theta'_{crit}}{E_f^{crit}} \left(1 + \beta_1\,\Delta c + \beta_2(\Delta c)^2 + \ldots\right)$$

There is no a priori reason to expect $\beta_1 = (\delta_1/k_b\theta'_{crit} - \epsilon_1/E_f^{crit})$ to be zero. Thus we expect $k_b\theta'/E_f$ (c) to vary as the <u>first power</u> of deviations in the concentration from its critical value.

With this assumption, we can calculate how we expect the magnetic parameters to vary with concentration.

We define

4.2.38 $$\eta \equiv \frac{k_b\theta'}{E_f}$$

using equation 4.2.18, η_o, the critical value for ferromagnetism is

4.2.39 $$\eta_o = \frac{2}{3}\,\frac{1}{g_o\,(E_f^{crit})}$$

then

4.2.40 $$\eta\,(\Delta c) = \eta + \eta_1 \cdot \Delta + \ldots$$

where $$\eta_1 = \beta_1\,\eta_o$$

We first discuss the high field susceptibility near the critical concentration. Combining equations 4.2.21 and 4.2.18, we find

4.2.41 $$\chi_{difn} = \frac{n\,N\,\mu^2}{k\,T_f}\,\frac{1}{g_o(E_f)\;k_b\theta'/E_f - 2/3}$$

which is valid in the ferromagnetic region.

In the paramagnetic region, generalizing our discussion of the molecular field theory (c.f. eqn. 3.1.25)

4.2.42
$$\chi = \chi_{pauli} \times S$$
$$= \frac{n N \mu^2}{k_b T_f} \frac{1}{k_b \theta' N(E_f) - 2/3}$$

which we re-write as

4.2.43
$$\chi^{para} = \frac{n N \mu^2}{k_b T_f} \frac{1}{g_o(E_f) \cdot k_b \theta'/E_f - 2/3}$$

We may then write the low temperature susceptibility, valid for both ferromagnetic and paramagnetic regions as

4.2.44
$$\chi = \frac{n N \mu^2}{k_b T_f} \frac{1}{g_o(E_f) k_b \theta'/E_f - 2/3}$$

By using equations 4.2.38, 39, and 40, we find:

4.2.45
$$\chi(c) = \frac{n N \mu^2}{k_b T_f} \frac{1}{\eta_1 \Delta c}$$

We therefore expect the low temperature susceptibility to diverge as $1/(\Delta c)$ as we approach the critical concentration, in agreement with the dependence reported by Bucher, et al.[6] From equation 4.2.19, we expect T_c/T_f to vary linearly with ξ_o. Since T_f should vary only by a small amount as we vary the concentration a small amount from the critical value, we expect T_c to vary linearly with ξ_o, as observed. (See figure 13).

To discuss the variation of ξ_o with concentration, we combine equations 4.2.38, 39 and with 4.2.18. We then find that

4.2.46
$$\xi_o(c) = 9/2 \frac{g_o(E_f)}{\sqrt{g_2(E_f)}} (\eta_1)^{1/2} (\Delta c)^{1/2}$$

and $\xi_o(c)$ is expected to vary as $(\Delta c)^{1/2}$. Again, by using equation 4.2.18, one can show

4.2.47
$$T_c \approx 1.35 \sqrt{\frac{1}{g_1(E_f)\, g_2(E_f)}} (\eta_1)^{1/2} \cdot (\Delta c)^{1/2} \cdot T_f$$

and the Curie temperature is also expected to vary as $(\Delta c)^{1/2}$. We note that our experimental values disagree with this prediction, displaying a remarkably linear relationship in both cases (See figures 9,11, and 12).

In our discussion, we are assuming the density of states function is smooth enough, so that small changes in the concentration, which shift the Fermi level, do not cause the functions $g_1(E_f)$ to vary too drastically from their value at the critical concentration. This assumption should be valid if there is no singularity at the critical concentration.

We also find disagreement between theory and experiment when we plot the Curie magneton number versus concentration.

From equation 4.2.28, we expect $\langle q_c^2 \rangle$ to diverge as $1/\xi_o$ or, using equation 4.2.46 we expect this quantity to diverge as $1/(\Delta c)^{1/2}$.

However, we see in figure 14, that there is no such tendency; but q_c remains fairly constant, with a small dip near the critical concentration.

Discussion of results

We see that our data disagrees with the predictions of the Stoner theory. We offer some possible explanations.

1. The behavior predicted by the Stoner theory may be valid only over a very narrow region of concentration. This region may be too narrow to be observed in our measurements. However, this does not seem very likely unless the density of states near the Fermi level corresponding to the critical concentration, or the variation of the band shape with concentration in this region, varies very rapidly.

2. Our assumptions leading to equations 4.2.32, ff. may not be valid. The density of state function at the value corresponding to E_f^{crit} may be singular. Then E_f would no longer be expressible as

$$E_f(c) = E_f^{crit} + \epsilon_1 \cdot \Delta c + \ldots$$

but for example, might also include a term in the sum going like $\epsilon_{1/2}(\Delta c)^{1/2}$. Such a singularity (for example, of the Van Hove form) could also lead to a strong concentration dependence of the normalized derivative functions $g_1(E_f(c))$ and $g_2(E_f(c))$, causing them to vary as $(\Delta c)^{1/2}$ instead of the expected form

$$g_i\ (E_f(c)) \sim \text{const.}_o + \text{const.}_1 \cdot \Delta c + \ldots$$

However, band calculations in pure nickel[56,57] do not predict such violent discontinuities in the density of states function (or its derivatives), although they do show a broad peak near the top of the band, containing about .8 - 1 electrons per spin direction separated from the rest of the band by a smooth (and not very shallow) minimum. In fact, this minimum may be responsible for $(k_b\theta'/E_f)\ g_o(E_f)$ reaching its critical value where it does, but unless the density of states varies quite sharply here, the Stoner predictions should still apply. That this minimum is not very shallow is supported by the electronic specific heat data of Bucher et al.[6] in the vicinity of the critical concentration.

3. The s-d interaction may modify our results somewhat. It is well known that the s and d bands overlap. Thus, there is ad-mixing of s and d states, resulting in the formation of a d-like band with high density of states, and an s-like band with low density of states. As we vary the alloy concentration, we may vary this interaction causing a shift in the position and shape of these two bands, so that equation 4.1.4 is not strictly valid. As we increase the Rh concentration, many of the holes introduced might go into the s-band. Then the number of magnetic carriers might vary in some complicated way as a function of c, so the value of $\xi_o(c)$ we inferred are incorrect, and the $(\Delta c)^{1/2}$ depen-

dence is masked. Although such an effect may explain the initial rapid increase in $n_{sat}(c)|_{c\approx 0}$, only under very special circumstances could we expect this tendency to mask the $(\Delta c)^{1/2}$ dependency which is expected, and cause it to appear linear.

Again, this seems highly unlikely.

C. Low Temperature Variation of Magnetization Elementary Excitations in Band Ferromagnets

According to the Stoner model, which we have been discussing thus far, the effects of finite temperature on the magnetization of the system can be treated by solving equation 3.2.3 as a function of temperature. One assumes the distribution of single particle (hole) states are described by applying Germi statistics to the energy states available (which are described by the density of states function for the band). The effects of increasing T are to decrease the magnetization, M, because the higher temperatures tend to excite particles from their lowest energy states to higher energy states, bringing about a redistribution of the electrons among the two spin sub-bands. These excitations are usually termed single particle or Stoner excitations. Under most conditions, more spins are excited from the majority spin sub-band to the minority spin sub-band than vice versa, thus causing M to decrease with increasing T.

Depending upon the strength of the exchange interaction, i.e., whether or not the magnetization is complete, the temperature dependence of this contribution to the low temperature saturation magnetization follows one of two forms.

In the case of strong ferromagnet, (see figure 15a) there exists an energy gap, Δ, between the top of the full band and the Fermi level of the partially filled sub-band. This leads to an exponential approach to saturation at low temperatures, of the form[55]

$$4.3.1 \qquad \frac{\Delta M_{sp}(T)}{M(0,0)} = \frac{2\,I(T)}{n} \exp\left(-\Delta / k_b T\right)$$

where n is the number of carriers, $I(T) = \int_0^\infty N(E) \exp(-E/k_b T)\, dE$, and ΔM_{sp} is the deviation of magnetization from the value at T=0 due to

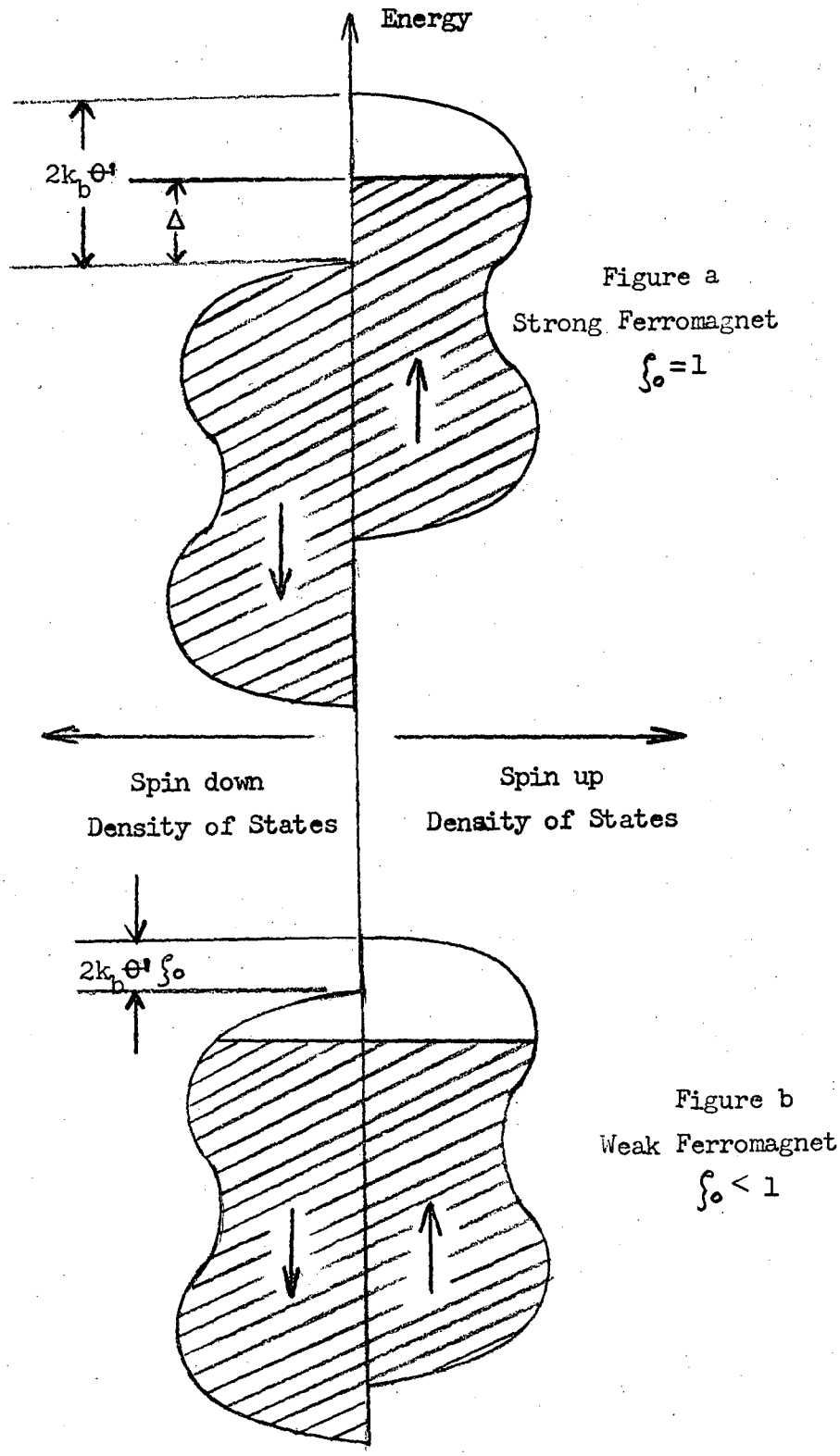
Energy
$2k_b\theta'$
Δ
Figure a
Strong Ferromagnet
$\zeta_0 = 1$
Spin down
Density of States
Spin up
Density of States
$2k_b\theta'\zeta_0$
Figure b
Weak Ferromagnet
$\zeta_0 < 1$

Fig. 15

these single particle excitations. In the limit of weak ferromagnets, there is no such gap (see figure 15b). Then from equation 4.2.6, with $H=0$ and $T < T_c$ we obtain

4.3.2 $$\left[\frac{M_{sp}(T)}{M(0)}\right]^2 = \left[1 - (T/T_c)^2\right]$$

which can be expanded for $T \ll T_c$

4.3.3 $$\frac{\Delta M_{sp}(T)}{M(0)} \approx (1/2)(T^2/T_c^{\,2})$$

However, it is known that there is still another type of excitations in a band of interacting electrons, which also can change the magnetization. There are collective excitations, brought about by many-body correlation effects, and can be thought of as spin waves.

Herring and Kittel[58] demonstrated the possibility of such excitations in a continuous ferromagnetic medium, from the assumption that there is a contribution to the energy of the system varying as[95]

4.3.4 $$E = A\,|\vec{\nabla}\cdot\vec{M}|^2/M^2$$

They justified the form of this term, which arises from the exchange interaction among the electrons. Since this interaction tends to align the electrons parallel to each other, and local deviations from this state, are described by the magnitude of $|\vec{\nabla}\cdot\vec{M}|$, according to these authors, this lead to an energy contribution of the form shown.

This tendency for the magnetism to remain uniform in direction throughout the sample is termed exchange stiffness, and the coefficient of the $|\vec{\nabla}\cdot\vec{M}|$ term in the energy, A, is termed the exchange stiffness constant. It is this term, for example (in conjunction with the magnetocrystalline anisotropy), which determines the thickness and energy density of the transition region between magnetic domains, the so-called Bloch walls.

These authors then showed that the energy of these collective excitations vary as

4.3.5 $$E_{\vec{q}} \sim (2 A \Omega/S) q^2 \sim Dq^2$$

where Ω is the atomic volume, S is the spin of the carrier, $\vec{q}$ the wave vector of excitation and q is equal to $|\vec{q}|$. This result is valid, at least, for small q.

They then pointed out that this dispersion relation leads to the familiar Bloch $T^{3/2}$ law in the low temperature saturation magnetization.

They also suggested that these two types of excitations which we have mentioned, especially at low temperatures, can be treated as acting independently. Thus, the contributions to the specific heat and to the deviation of the saturation magnetization at low temperatures can expressed as the sum of these two contributions. Then for weak ferromagnets, the low temperature magnetization is expected to vary as

4.3.6 $$\frac{M(T)}{M(0)} \sim 1 - A T^{3/2} - B T^2 - \ldots$$

where the coefficient of the $T^{3/2}$ term is related to the exchange stiffness.

Herring[59] did a many body calculation of the exchange stiffness coefficient using a perturbational approach and the random phase approximation, to calculate the energy of sinusoidal disturbances in the system described by wave vector $\vec{q}$. He also found that the energy of these disturbances varied as q^2.

This work was extended by a number of authors. Particular attention was paid in explaining the neutron diffraction phenomena in the 3-d transition ferromagnets.

Elliott and Marshall[60] had explained the previously measured neutron diffraction data quite successfully, using a localized moments approach.

Included in their discussion were inelastically scattered Laue spots (corresponding to collisions of neutrons with magnons) at low temperature, critical scattering below and above T_c, and paramagnetic scattering.

Kubo et al[61] and Izuyama et al.[62] discussed these effects from the standpoint of the band picture of magnetism. They showed the neutron scattering cross section is related to the dynamic susceptibility function $\chi(\vec{q}, \omega)$, describing the system (which is essentially the response function of the system to a perturbation at frequency ω and wave vector $\vec{q}$), using the fluctuation-dissipation theorem.[63] They proceeded to do a many-body calculation of the dynamic susceptibility within the random phase approximation, making certain simplifying assumptions about the electron (quasi-particle) energies, and their interactions. They found that in addition to the expected single particle excitations leading to poles (which according to Elliott[64] lead to rather weak poles in the neutron scattering cross section, i.e., weak Bragg spots), there are also poles for values of $(\vec{q}, \omega(\vec{q}))$, corresponding to collective excitations, where the dispersion relation for these excitations followed a form $\omega(\vec{q}) \sim D q^2$.

Other authors also calculated the exchange stiffness coefficient using varying approaches, most based upon the RPA, and include Thompson,[65] Edwards,[66] Mattis,[67] Edwards.[68]

In the second of these papers the author demonstrated the separability of the two types of excitations. In the fourth of these papers, Edwards shows that the presence of single particle excitations sets an upper limit on the allowed wave vectors (and hence on the number of allowable independent modes) of the collective excitations. This limit occurs at the intersection of the dispersion relations of the two types of excitations. Above this threshold, the collective excitations are

critically damped by the single particle excitations.

Edwards and Wohlfarth[45] stated that a good estimate of this maximum wave vector for the spin waves is given by

4.3.7. $$q_{max} = (8\pi^3 nN/A_f)\,\xi_o$$

where N is the number of atoms per unit volume, n is the number of magnetic carriers per atom and A_f is the surface area of paramagnetic Fermi surface. This critical wave vector is just the average value of the difference of the radii of the spin up and spin down Fermi surfaces. When collective excitations have a wave vector larger than this value they can then excite single particles from one sub-band to the other.

The change in magnetization at finite temperatures due to the spin wave contribution is determined by calculating the number of such excitations as a function of temperature, and noting that each spin wave reduces the net magnetization by one Bohr magneton. Then the expression for the reduction in magnetization is, according to Edwards and Wohlfarth[45]

4.3.8 $$\Delta M_{sw}(T) = \frac{\mu_b}{4\pi^3} \int \frac{d\vec{q}}{\exp(\hbar\omega_{\vec{q}}/k_b T) - 1}$$

where the integral is carried out over the allowed values of q.

These authors evaluated this integral, using the dispersion relation

4.3.9 $$\hbar\omega_{\vec{q}} = D\,q^2$$

and obtain

4.3.10 $$\Delta M_{sw}(T) = \frac{\mu_b}{\pi^2}\; T/T_c\; \frac{q_{max}\,k_b\,T_c}{D}$$

in the limit $D\,q^2_{max}/k_bT \ll 1$, which holds for very weak ferromagnets at reasonable low temperatures.

Expressions for D have been worked out by Izuyama and Kubo,[69] Doniach and Wohlfarth,[70] and Edwards.[71] In the limit of weak ferro-

magnetism, they showed that this parameter can be expressed as

4.3.11 $$D = \{n \times (k_b\theta')^2 R^2/36\} \; [N(E_f) + E_f N'(E_f)] \; \xi_o$$

where n is the number of carriers per atom, R the nearest neighbor distance, and $N(E_f)$ the density of states per atom. For a parabolic band, this generalizes to

4.3.12 $$D \approx \frac{n^2}{36} \frac{(k_b\theta')}{E_f} \xi_o R^2$$

(where we can generalize this expression to other band shapes by using equations 4.2.13, 14, 15)

Using this expression for D, the expression for q_{max} (4.3.7), and our expression relating ξ_o to $k_b\theta'/E_f$ (section 4.2), we find after, a little algebra

4.3.13 $$\frac{\Delta M_{sw}(T)}{M(0)} \sim \left(\text{numerical factor depending on band structure}\right) \left(\text{slowly varying function of composition}\right) \frac{T}{T_c}^{*}$$

valid in the limit $1 \gg T/T_c \gg \xi_o^2$.

In the extreme low temperature limit, $T/T_c \ll \xi_o^2$, the temperature is so low that the exponential factor in the integral automatically rules out spin waves with wave vector approaching q_{max}, and the intergral can be carried out over all of q-space. In this case, the maximum in the allowable value of q does not affect the final result, and we obtain

---

* Numerical factor depending on band structure depends on factors like $A_f R^2$ and dimensionless ratios between ξ_o and $k_b\theta'/E_f$ depending on the $g_i(E_f)$, as well as numerical constants on the order of unity. These are modified by changes in alloy composition through $A_f R^2$, n, $E_f/k_b\theta'$, and $g_i(E_f)$.

4.3.14 $$\frac{\Delta M_{sw}(T)}{M(0)} \sim \begin{pmatrix}\text{numerical}\\ \text{factor}\end{pmatrix} \begin{pmatrix}\text{slowly varying}\\ \text{function of}\\ \text{composition}\end{pmatrix} \frac{1}{\xi_o} (T/T_c)^{3/2}$$

These two forms join continuously in the region $T/T_c \approx \xi_o^2$.

Thus, at very low temperatures, the spin wave contribution varying as $T^{3/2}$ should dominate the single particle contribution varying as $(T/T_c)^2$, while at higher temperatures, where the single particle excitations damp large wave vector spin waves, the single particle contribution, still varying as T^2 should now dominate the spin wave term which is linear in T in this region.

Of course, the exact value of the coefficient of the spin wave term depends explicitly on the band structure, and thus varies from one system to another, so the temperature where the single particle contribution becomes dominant depends on the band structure.

For example, the magnetic isotherms for the weak itinerant ferromagnet $ZrZn_2$ were measured experimentally by Ogawa and Sakamoto,[72] and were analyzed by Edwards and Wohlfarth.[45] They found that at all but the very lowest temperatures, the saturation moment was described very well by the expression,

4.2.15 $$\left[\frac{M(T)}{M(0,0)}\right]^2 = (1 - T^2/T_c^2)$$

i.e., single particle excitation form.

In figure 16a-f, we present our low temperature magnetization data for several of our samples plotted both as

$$\left[\frac{M(H_o,T)}{M_o}\right]^2 \text{ vs. } (T/T_c)^2 \quad \text{to display Stoner excitations}$$

and

$$\frac{M(H_o,T)}{M_o} \text{ vs. } (T/T_c)^{3/2} \quad \text{to display spin waves}$$

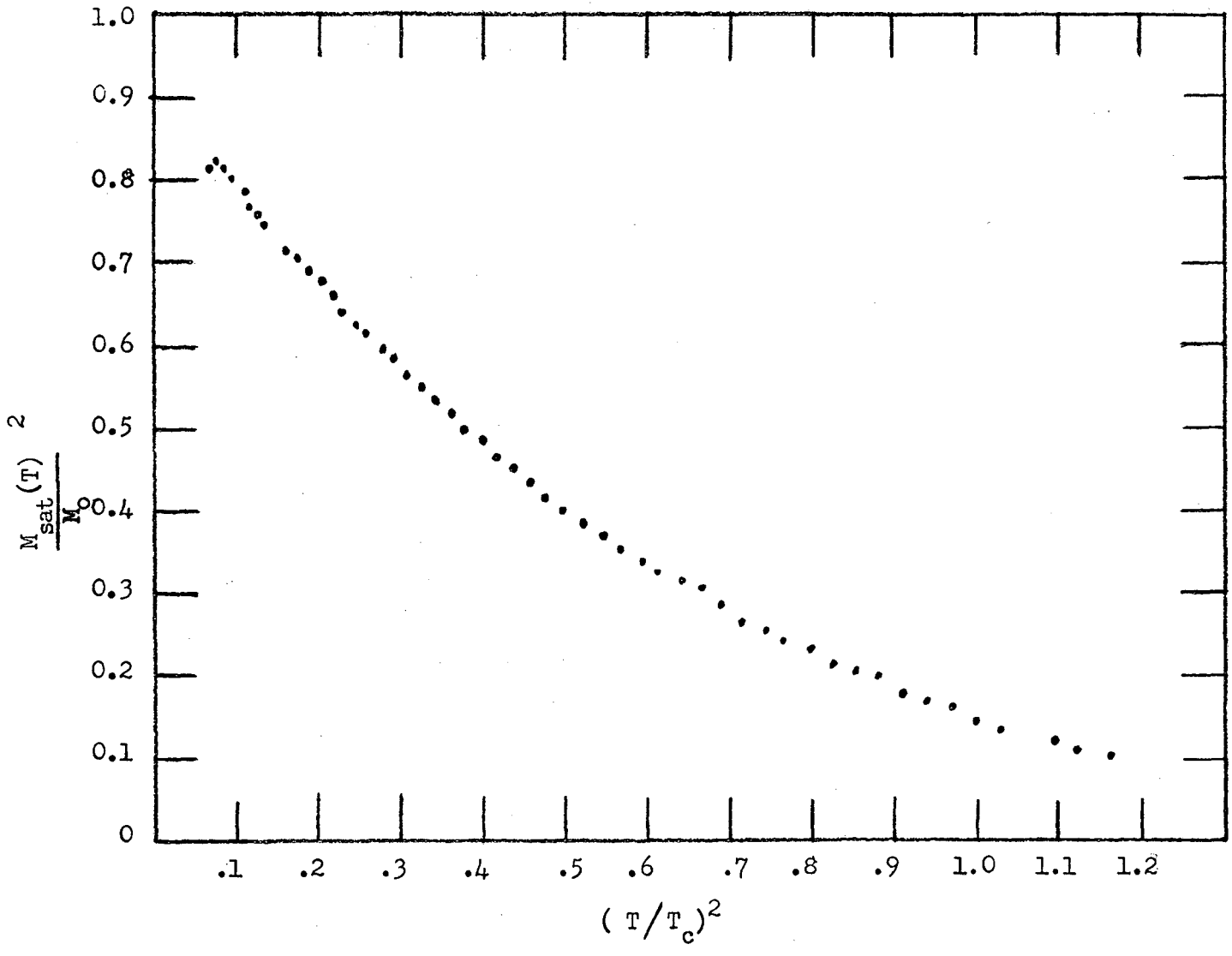
1.0
0.9
0.8
0.7
0.6
0.5
0.4
0.3
0.2
0.1
0
$\frac{M_{sat}(T)}{M_o}^2$
.1
.2
.3
.4
.5
.6
.7
.8
.9
1.0
1.1
1.2
$(T/T_c)^2$

Fig. 16a

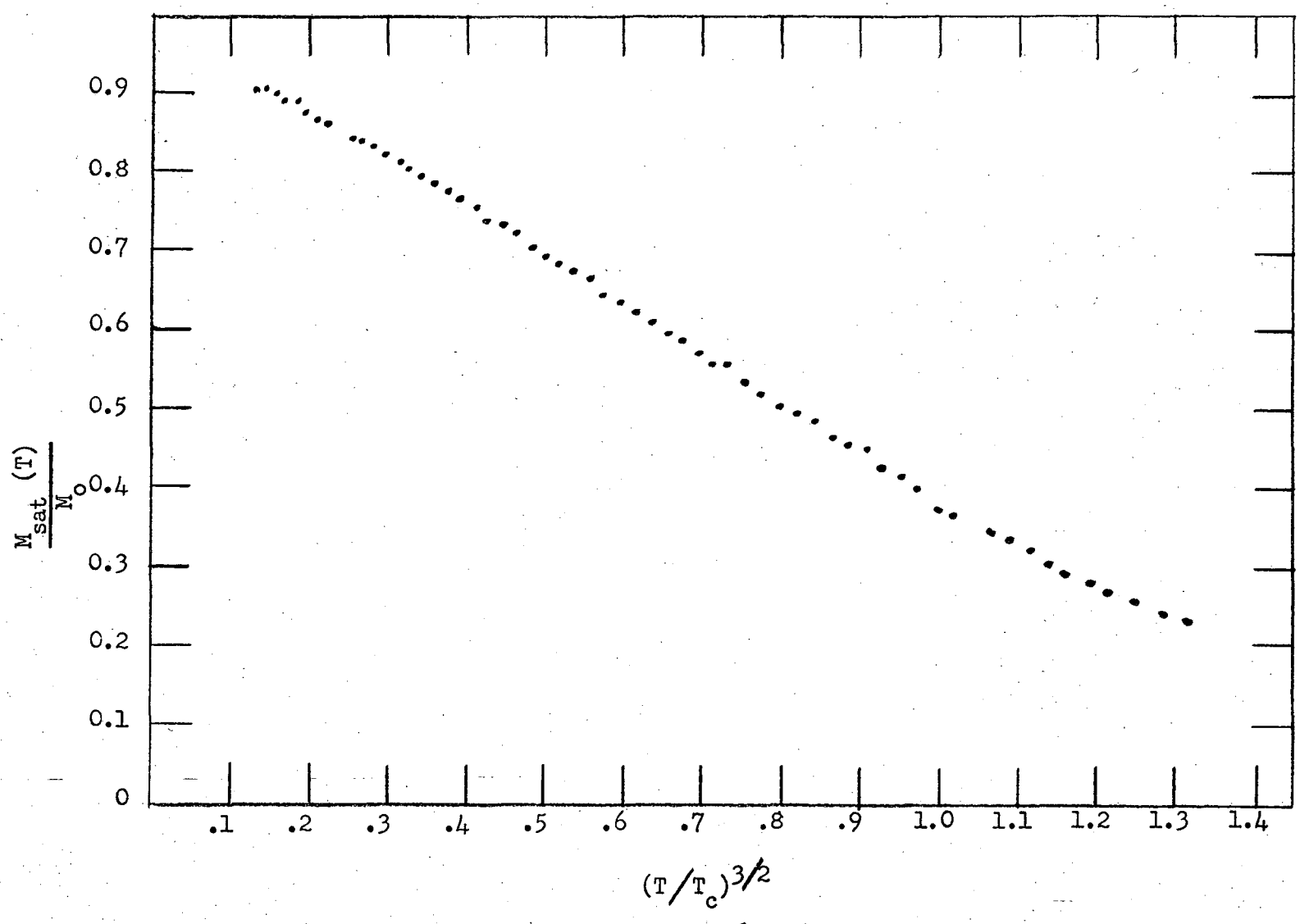
0.9
0.8
0.7
0.6
0.5
0.4
0.3
0.2
0.1
0
$\frac{M_{sat}(T)}{M_o}$
.1
.2
.3
.4
.5
.6
.7
.8
.9
1.0
1.1
1.2
1.3
1.4
$(T/T_c)^{3/2}$

Fig. 16b

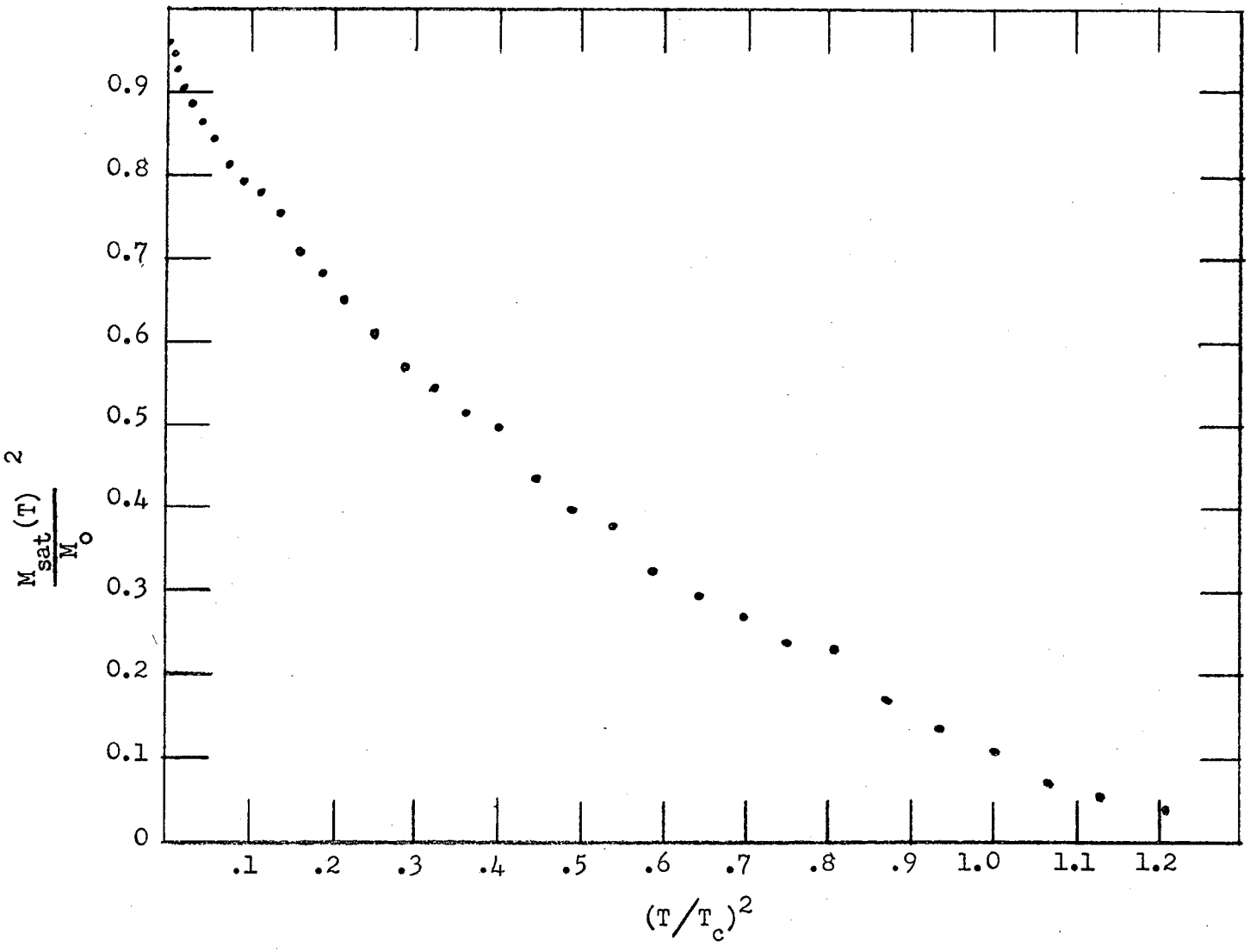
0.9
0.8
0.7
0.6
0.5
0.4
0.3
0.2
0.1
0
$\left(\frac{M_{sat}(T)}{M_o}\right)^2$
.1
.2
.3
.4
.5
.6
.7
.8
.9
1.0
1.1
1.2
$(T/T_c)^2$

Fig. 16c

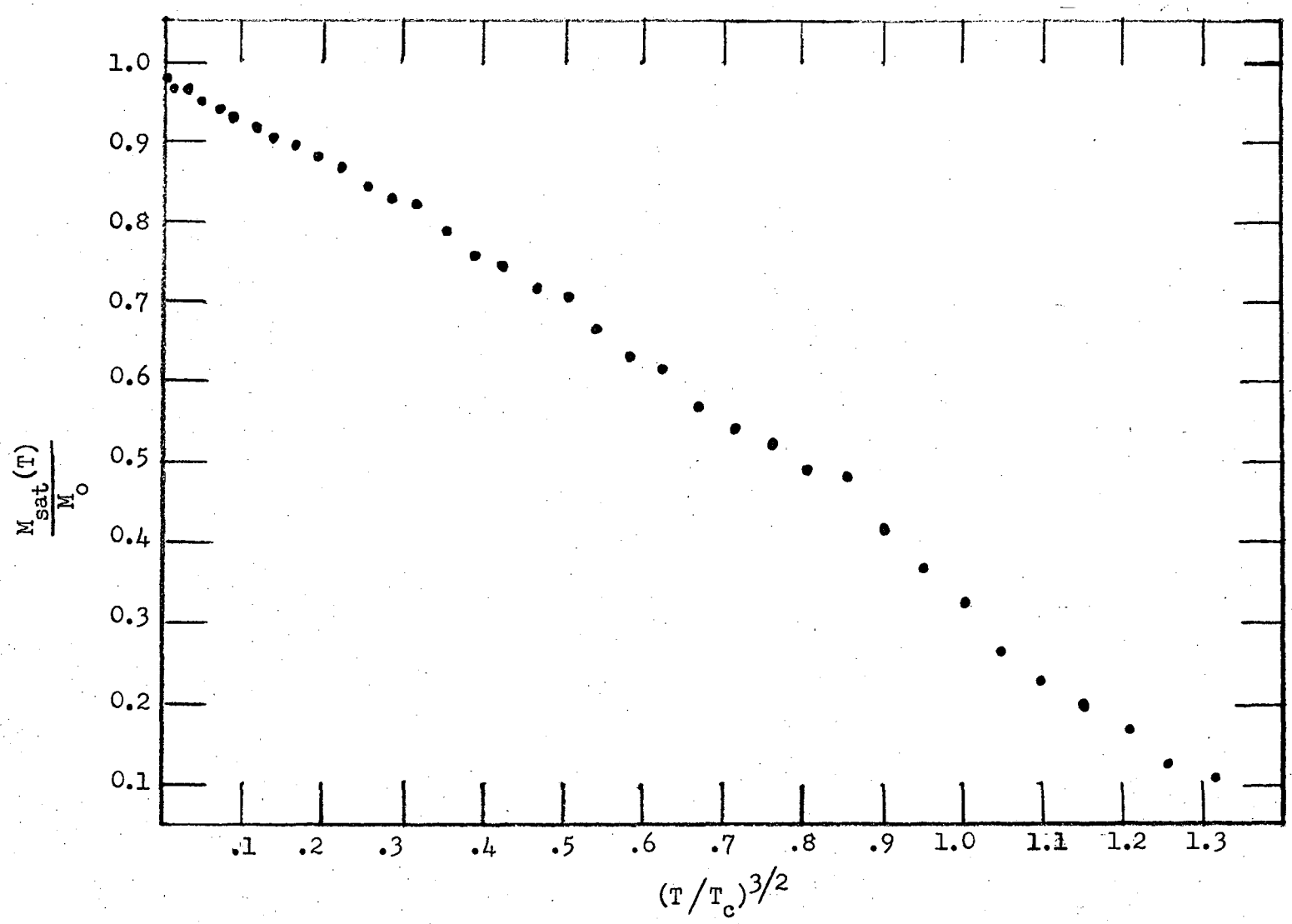
1.0
0.9
0.8
0.7
0.6
0.5
0.4
0.3
0.2
0.1
$\frac{M_{sat}(T)}{M_o}$
.1
.2
.3
.4
.5
.6
.7
.8
.9
1.0
1.1
1.2
1.3
$(T/T_c)^{3/2}$

Fig. 16d

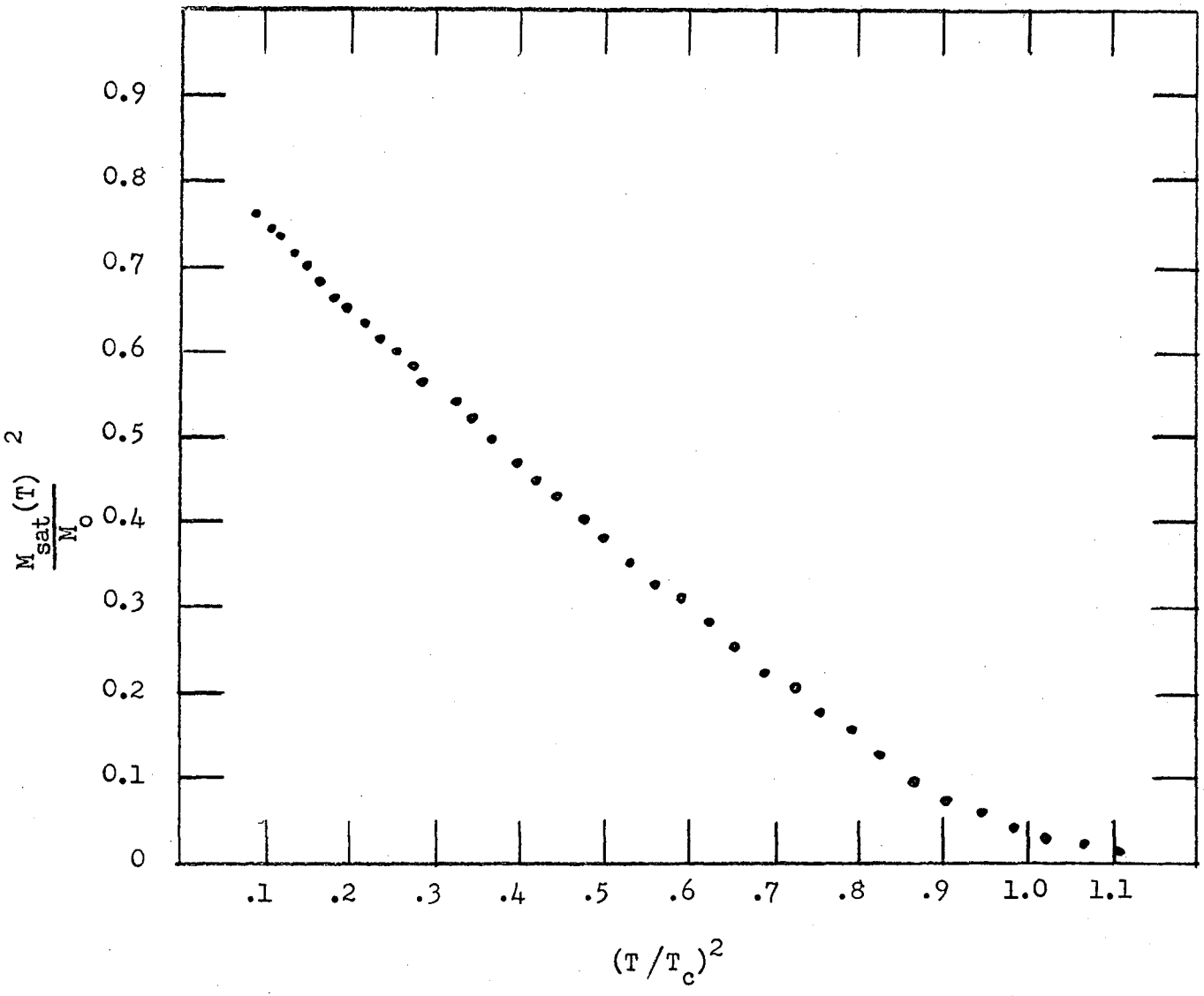

Fig. 16e

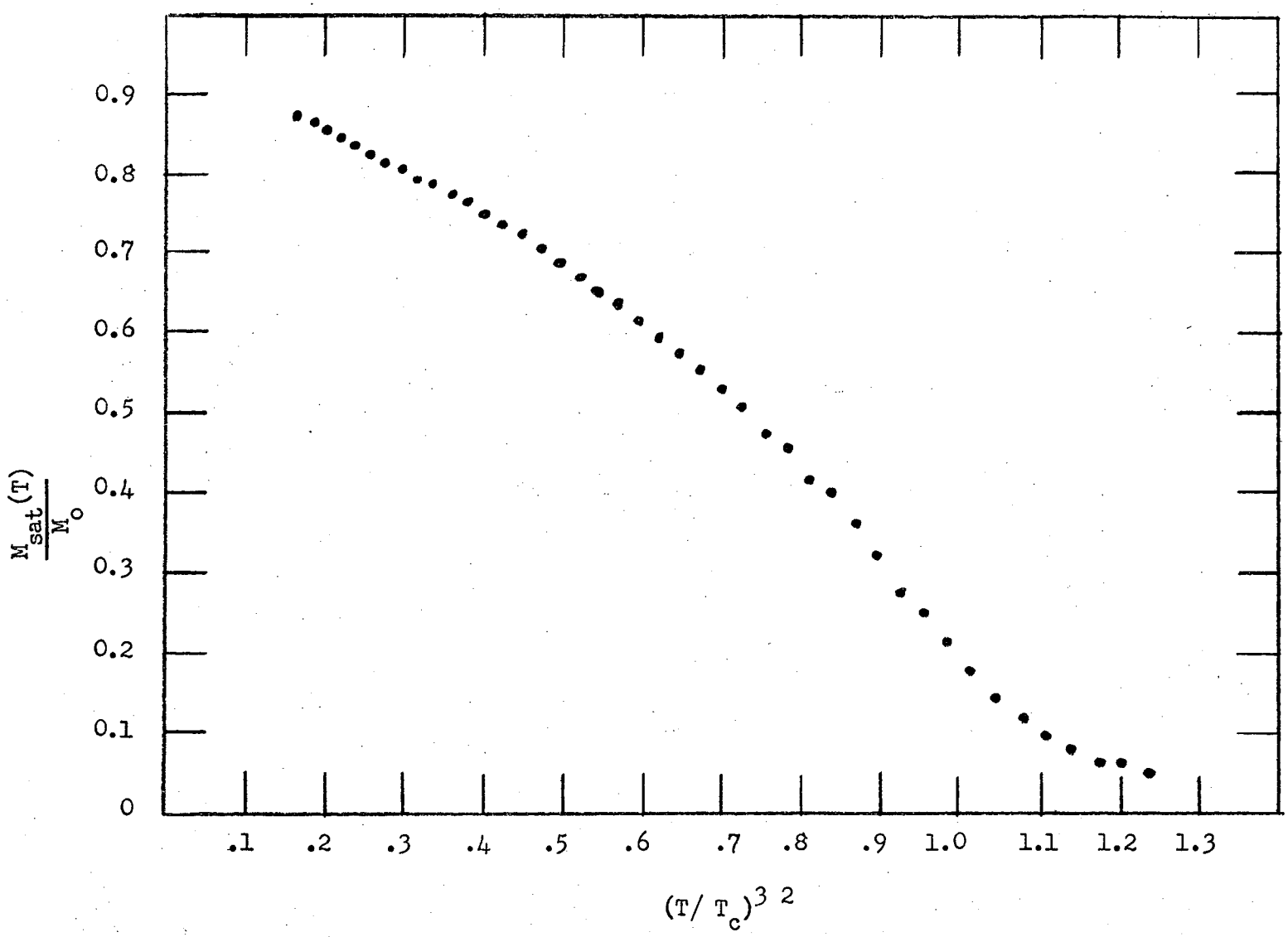
0.9
0.8
0.7
0.6
0.5
0.4
0.3
0.2
0.1
0
$\frac{M_{sat}(T)}{M_o}$
.1
.2
.3
.4
.5
.6
.7
.8
.9
1.0
1.1
1.2
1.3
$(T/T_c)^{3/2}$

Fig. 16f

with H_o the externally applied field, and M_o is some normalizing value of M chosen for convenience, near M(0,0).

Discussion

Although there is some experimental scatter in our data points, the M^2 vs. T^2 (Stoner) plots seem to be quite linear up to a value of $(T/T_c)^2 \approx .4$, (or $(T/T_c) \approx .6$). Then these plots become concave upward, due to the effects of the externally applied (saturating) magnetic field, which increases the magnetization to a value larger than that which would occur in its absence. However, this field is necessary to ensure macroscopic saturation of the magnetization, which is brought about by rotating the magnetic domains along some preferred (i.e., the external field) direction.

Not only does this linearity of this plot agree with the predictions of the Stoner theory, but the slope of these plots is also close to the value predicted by the theory. From equation 4.3.2 we see that a plot of $M(T)^2$ vs T^2 should be linear, and should intersect the M^2 axis at $T^2 = T_c^2$.

Our curves intersect at $(T/T_c)^2$ between .8 and .9, corresponding to (T/T_c) between .9 and .95, in good agreement with theory.

We also see on the $Ni_{.70}Rh_{.30}$ plot, that the curve is concave upward at very low temperatures, but on the $T^{3/2}$ plot, this region is quite linear.

It should again be pointed out at this point that similar plots of the magnetization of $ZrZn_2$[45,46] also showed excellent agreement with the Stoner theory, except at the very lowest temperatures, where the spin wave contribution, varying at $T^{3/2}$ is expected to dominate the single particle contribution, varying at T^2.

D. Magnetic Isotherms - Magnetocrystalline Anisotropy

Measurements of the magnetization as a function of the externally applied field, H_o, for various values of temperature were made, as explained in section II.

For a strong, or localized moment ferromagnet, the description of these curves are fairly well understood. A comprehensive survey can be found in Ferromagnetism.[73] For weak ferromagnets, the description will be altered somewhat.

In the very low applied field region, the permeability (and hence the susceptibility) is very large. For samples with definable demagnetizing factors, which are not unusually small (ruling out long needle-shaped samples and toroids), the magnetic field inside the sample (i.e, the internal field) will be the sum of the externally applied field and the demagnetizing field

4.4.1 $$H_{demag} = -NM$$

where N is the demagnetizing factor in direction of field. Due to the high susceptibility in this region, the magnetization will assume a value which will maintain the internal field at a very small value. This can be seen by the following derivation:

4.4.2 $$H_{int} = H_o - NM$$

also, from the definition of the susceptibility, χ, we have

4.4.3 $$M = \chi H_{int}$$

therefore

4.4.4 $$M = \chi(H_o - NM)$$

solving

4.4.5 $$M (1/\chi + N) = H_o$$

but $1/\chi$ is very small and assumed to be negligible in comparison to N, therefore

4.4.6 $$M \approx \frac{1}{N} H_o$$

and

4.4.7 $$H_{int} = H_o - N M \approx 0$$

(actually, to first order in $1/\chi$

4.4.7a $$H_{int} \approx \frac{1}{\chi N} H_o \ll H_o)$$

Equation 4.4.6 provides us with a very useful relationship. It states that the initial slope of the M vs. H_o curves are determined solely by the demagnetizing factor. The values we calculated from our measured slopes corresponded quite well to the values expected from our sample dimensions. The demangetizing factor for right circular cylinders as a function of length to diameter ratio is graphed in Bozorth.[16] The value obtained by our slope method was about 2.4 Oersted per gauss magnetization, varying somewhat from sample to sample, due to porosity and slight differences in the sample dimensions. Knowledge of these demagnetizing factors was quite useful, for we could then determine the internal field at all the values of H_o, given H_o and $M(H_o)$. This knowledge was necessary to determine the anisotropy of our samples.

The variation of the observed susceptibility with applied field is described by the domain theory of magnetism (see Magnetism,[73] also Introduction to Solid State Physics.[4]) The domain theory also applies to band ferromagnets.

According to this theory, the large initial (i.e., low field) susceptibility is due to domain wall displacement, which changes the relative volumes of magnetic domains magnetized parallel and anti-parallel to the direction of the applied field.

For slightly larger values of the field, the susceptibility, $X = M/H$, is determined by domain rotation. The magnetization (which is relatively constant in magnitude) within each domain is rotated into the direction of the applied magnetic field. In the case of a weak ferromagnet, the magnitude of M within a domain also increases (but usually quite slowly) with the applied field. This term does not dominate until virtually all of the domains are lined up along the field direction (which usually does not occur until H_o reaches several kilo-oersteds. For fields larger than this, the magnetization is observed to increase linearly. From this slope, we can calculate the rate of increase of the intrinsic, or domain, magnetization. We can extrapolate this slope backwards, into the region of domain rotation, to estimate the intrinsic magnetization in this region also).

Then, for intermediate values of H_o, the approach to saturation of the macroscopic magnetization is determined by domain rotations. For polycrystalline samples such as we have, in the absence of external fields, the magnetization direction within individual domains is determined by magnetocrystalline anisotropy (for a discussion of this, see Bozorth, op. cit). This anisotropy causes the energy density within a domain to depend on the angle between the magnetization direction and the various crystallographic directions. For a cubic system, the anisotropy energy (as we shall see) has the form

4.4.8 $$E_{anis} = K_1 (\alpha_1^2 \alpha_2^2 + \alpha_2^2 \alpha_3^2 + \alpha_3^3 \alpha_1^2) + K_2 (\alpha_1^2 \alpha_2^2 \alpha_3^2)$$

where the α_1 are the direction cosines of M along the three crystallographic axes; while the interaction with the externally applied field has the form

4.4.9 $$E_H = M H_o \cos \phi$$

where ϕ is the angle between H_o and M. The overall magnetization within a domain assumes the value minimizing the sum of these two contributions. Thus, the effect of large external fields is to rotate the magnetization within a domain away from the crystallographic directions of easy magnetization, and into the direction of applied field.

Bozorth writes an approximate expression, due to Becker and Boring,[74] which describes the approach to saturation of a sample composed of a randomly distributed collection of polycrystals. The result, to lowest order in 1/H is

4.4.10 $$\frac{M(H)}{M_\infty} = 1 - \frac{8 K_1^2}{105 H^2 M_\infty^2} - (\text{terms involving } K_2, 1/H^3, \ldots)$$

where H is now the field acting on the domains (i.e., the internal field), M_∞ is the assymptotic value of the observed magnetization, equal to the intrinsic (domain) magnetization, and K_1 is the anisotropy constant defined in equation 4.4.8, which in general, varies quite rapidly with temperature.

As we have stated, for weak ferromagnets the domain magnetization is itself a function of the external field. However, it can be written in the form

4.4.11 $$M(H) = M_o + \chi_{difn} \cdot H$$

so in equation 4.4.10 we simply replace M_∞ by the value appropriate to the applied field. For all of our samples where K_1 could be determined, this was a small effect.

Our observed isotherms were then corrected for the demagnetizing factor and the differential susceptibility, and fit to a function of the form of equation 4.4.10, thereby determining K_1.

In this way we were able to determine the anisotropy constant as a function of alloy composition, at various temperatures. These results are shown in figure 17.

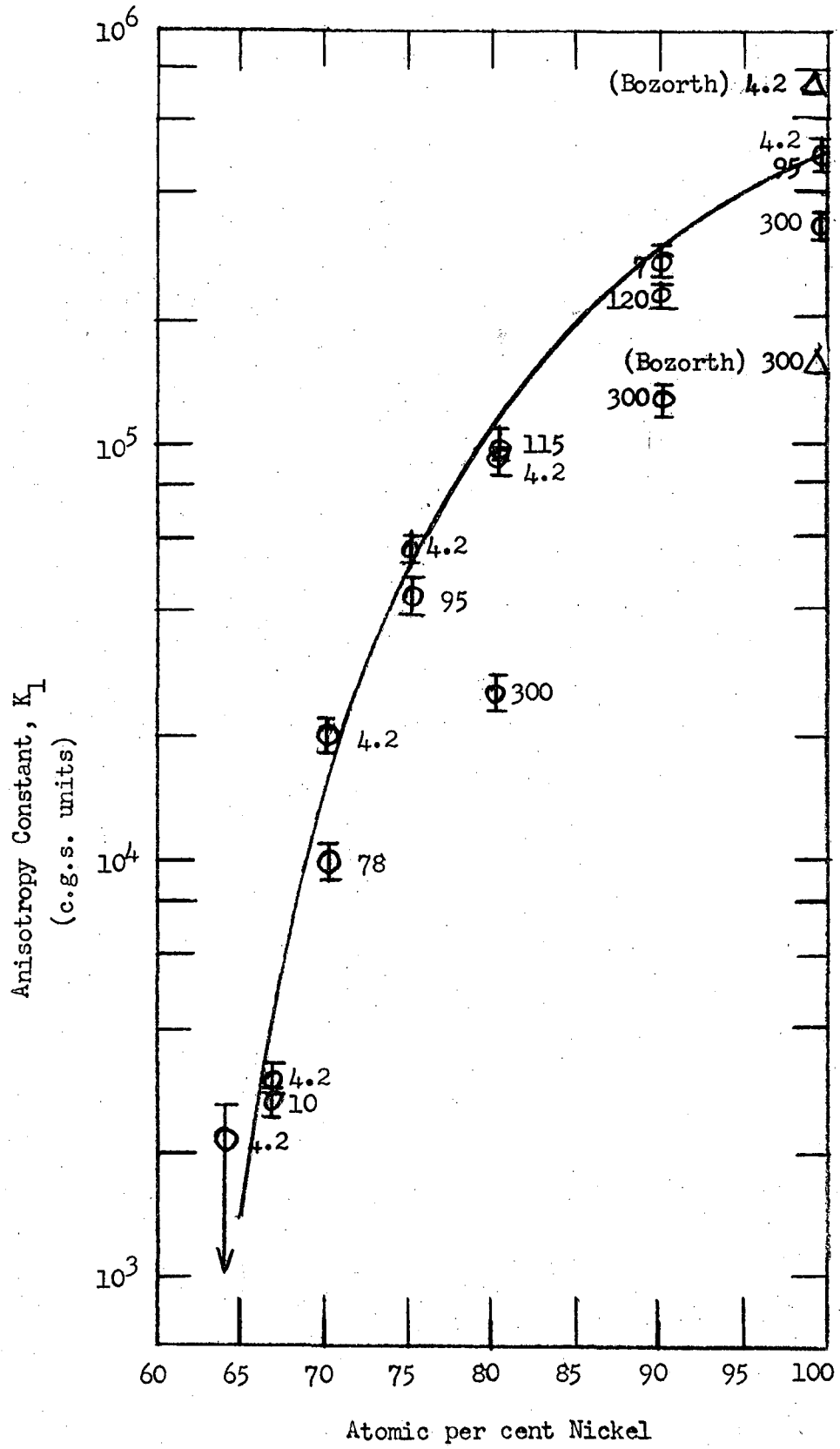
10^6
10^5
10^4
10^3
Anisotropy Constant, K_1
(c.g.s. units)
(Bozorth) 4.2
4.2
95
300
7
120
(Bozorth) 300
300
115
4.2
4.2
95
300
4.2
78
4.2
10
4.2
60
65
70
75
80
85
90
95
100
Atomic per cent Nickel

Fig. 17

The error bars shown on this figure indicate only the distribution in K_1 found by calculating it for various values of H along the curves of the approach to saturation.

Also shown on this graph is the anisotropy for Ni, which is listed in Bozorth, and which was determined by more accurate (single crystal) measurements. We see that this value comes fairly close to our value.

The observed deviation probably stems from the following: We have implicitly ignored the contribution from the K_2 term, and our measurement probably represents a kind of weighted average of these two constants. Secondly, as Bozorth points out, the approach to saturation is critically dependent on strains and heat treatment, and this could also affect our results quantitatively.

However, these errors should probably vary in the same way for all of our samples, and the relative shape of this curve is probably fairly accurate.

We see the anisotropy decreases with increasing temperature as expected. We also show the results of the measurements at the lowest temperature we attained in our experiment (4.2°K) as a function of composition in figure 18. In figure 19, we show the low temperature anisotropy versus the square of the observed saturation magnetization (expressed in Bohr magnetons per atom of alloy) for our samples. This graph appears to be linear in the region near the critical concentration, and extending up to at least 80 per cent nickel.

Discussion

In order to discuss the anisotropy measurements, we will first outline briefly the theory of anisotropy in cubic crystals.

As our model of a magnetic material, we suppose we have a cubic array of magnetic dipoles forming a lattice. We further suppose for the time

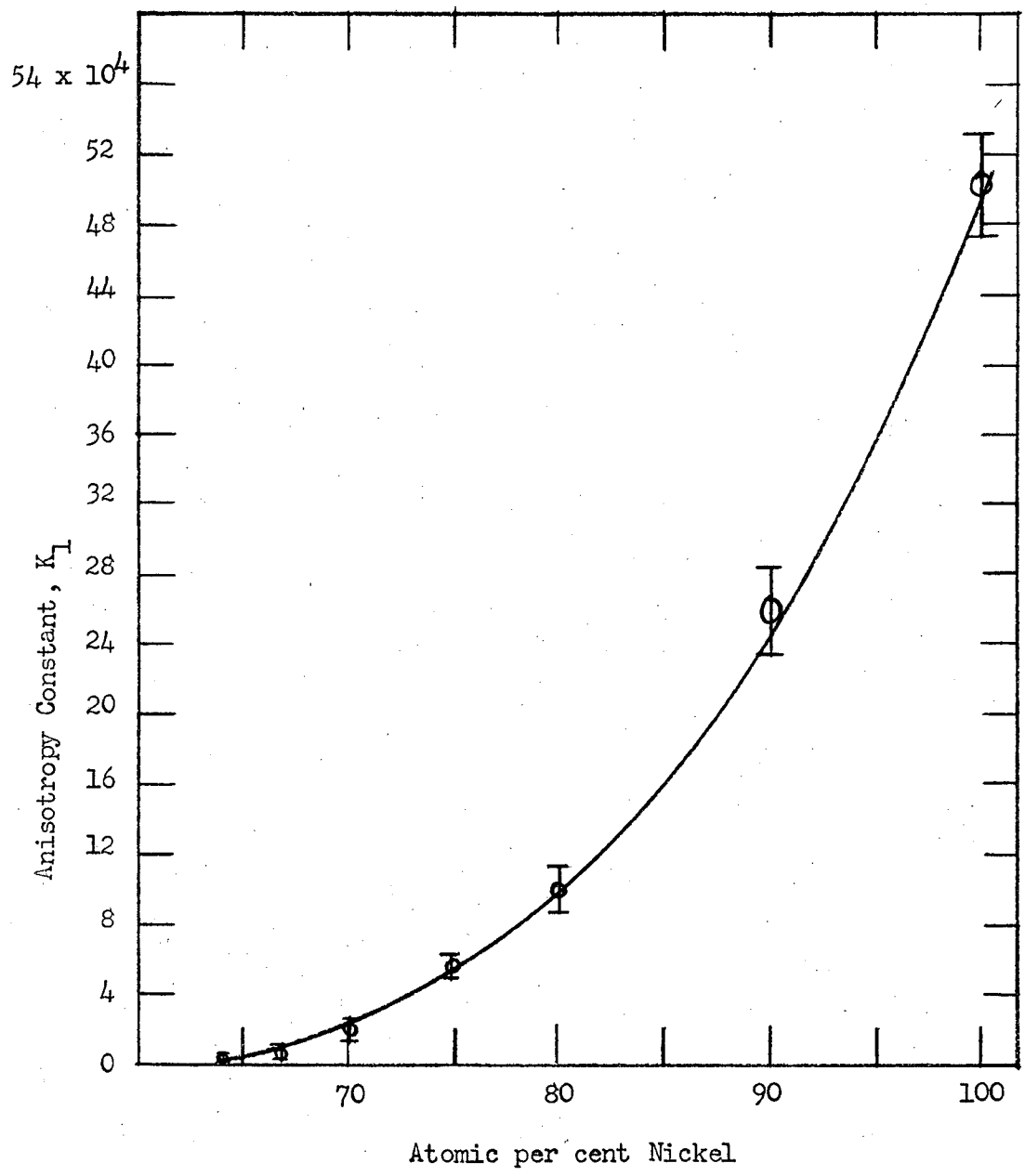
54 x 10^4
52
48
44
40
36
32
28
24
20
16
12
8
4
0
Anisotropy Constant, K1
70
80
90
100
Atomic per cent Nickel

Fig. 18

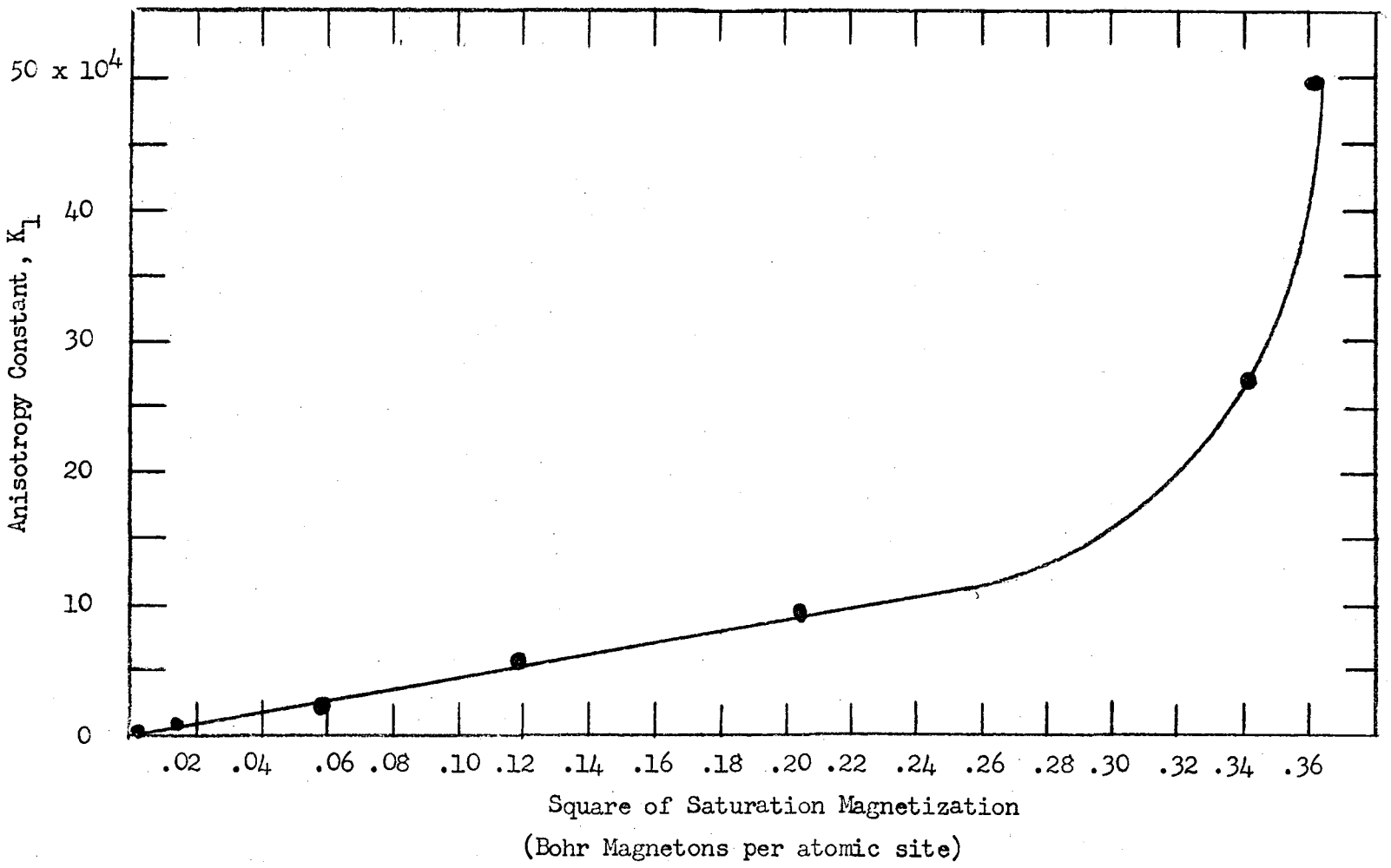
50 x 10^4
40
30
20
10
0
Anisotropy Constant, K1
.02 .04 .06 .08 .10 .12 .14 .16 .18 .20 .22 .24 .26 .28 .30 .32 .34 .36
Square of Saturation Magnetization
(Bohr Magnetons per atomic site)

Fig. 19

being, that at absolute zero they are all parallel to the macroscopic magnetization direction, and hence, to each other. Such a description should apply equally well to localized moment magnets and band magnets. In the case of the band magnets, suppose the d-wave functions are of the tight binding type. Then the electronic charge density (and hence, the spin density) should peak at the atomic sites. Even if the wave functions are not of the tight binding type, they at least retain the symmetry of the ionic lattice. In any event, we should be able to associate an identical dipole moment to each atomic site, although this moment may be spread out through the atomic cell in the lattice. In the band case, however, the dipole moment per atom is $n \cdot (g\,\mu_b\,S) \cdot \xi_o$ where n is the number of carriers per atom. This corresponds to $n/2\,(1 + \xi_o)\,\mu\uparrow$ and $n/2\,(1 - \xi_o)\,\mu\downarrow$ at each lattice site.

Thus, even though the individual electrons, each with spin 1/2, are in rapid motion, the moment per atomic site is the time average of the contributions of all the electrons, yielding

4.4.12 $$\langle n \rangle_{net} = n\,\xi_o$$

or

$$\langle \vec{S} \rangle = \xi_o\,\vec{S}$$

where $\langle\ \rangle$ denotes the quantum mechanical expectation value.

It is an experimental fact that the total energy of a magnet depends on the relative orientation between the magnetization and the crystallographic axes. For cubic systems, the lowest order expression is of the form

4.4.13 $$E_{anis} = K_1\,(\alpha_1^{\,2}\alpha_2^{\,2} + \alpha_2^{\,2}\,\alpha_3^{\,2} + \alpha_3^{\,2}\,\alpha_1) + K_2(\alpha_1^{\,2}\alpha_2^{\,2}\,\alpha_3^{\,2}) + \ldots$$

where α_i is the direction cosine of M along the ith crystallographic axis.

One might expect even a lower order term varying as

4.4.14 $$K_o\,(\alpha_1^{\,2} + \alpha_2^{\,2} + \alpha_3^{\,2})$$

but for a cubic system

4.4.15 $$\alpha_1^{\,2} + \alpha_2^{\,2} + \alpha_3^{\,2} \equiv 1$$

so this term reduces to a trivial constant.

We then ask, what interactions can contribute such a term to the overall energy of our system, i.e., what interaction will change the energy of a lattice of parallel dipoles as they are all rotated through the same angle, thereby remaining parallel to each other, but changing their orientation with respect to the crystal axes, and hence to the vectors directed between them.

The strongest interaction between our dipoles is the exchange interaction, the interaction responsbile for keeping the dipoles parallel to each other in the first place. This interaction is of the form $J\,\vec{S}_1\cdot\vec{S}_2$, and depends only on the relative orientation between two dipoles, so cannot contribute to the anisotropy.

Next, we consider the magnetic dipole-dipole interaction. The interaction between two dipoles is given by the well known expression[75]

4.4.16 $$E_{dip\text{-}dip} = \frac{\vec{\mu}_1\cdot\vec{\mu}_2}{r^3} - 3\,\frac{(\vec{\mu}_1\cdot\vec{r})\,(\vec{\mu}_2\cdot\vec{r})}{r^5}$$

where $\vec{\mu}_1$ and $\vec{\mu}_2$ are the two dipole moments and $\vec{r}$ is the radius vector directed between them.

For free electrons, the dipole moment is related to the spin $\vec{S}$ by

4.4.17 $$\vec{\mu} = g\,\mu_b\,\vec{S}$$

and the interaction takes the form

4.4.18 $$E_{dip-dip} = C\,(r_o/r)^3 \left\{ \vec{S}_1 \cdot \vec{S}_2 - \frac{3\,(\vec{S}_1 \cdot \vec{r})\,(\vec{S}_2 \cdot \vec{r})}{r^2} \right\}$$

where

4.4.19 $$C = g^2\,\mu_b^{\,2}/r_o^{\,3}$$

and r_o is the nearest neighbor distance.

This energy is anisotropic, depending not only on the relative orientation between two given spins, $(\vec{S}_1 \cdot \vec{S}_2)$, but also on their orientation with respect to the radius vector directed between them, through the $(\vec{S}_1 \cdot \vec{r})\,(\vec{S}_2 \cdot \vec{r})$ part of the interaction.

However, in a cubic system when these interactions are summed over all pairs of dipoles, this term also reduces to a trivial constant. That is to say, a system of <u>parallel</u> magnetic dipoles on a cubic lattice displays no anisotropy.

As Van Vleck[76] pointed out, in order to achieve anisotropy from a system of parallel magnetic dipoles, one must ascribe a quadrupole moment to these sites. Then, from the quadrupole-quadrupole interaction, one obtains a term in the interaction energy varying as[76]

4.4.20 $$E_{int} \sim \gamma\,(r_o/r)^{10}\,(\vec{S}_1 \cdot \vec{r})^2\,(\vec{S}_2 \cdot \vec{r})^2$$

which <u>does</u> yield anisotropy in a cubic system.

However, it is well known that $\gamma=0$ for S less than 1. Quantum mechanically, S = 1/2 spins have no quadrupole moment. For S=1 or greater, however, we can get a contribution to the K_1 term in the anisotropy.

However, for pure nickel, as well as our alloys, it would be hard to justify the presence of such a contribution. In a tight binding model, following the discussion of the Hurwitz Van Vleck approach to correlation, most of the tight binding states can be described by a d^{10} or d^9 configuration, i.e., 0 or 1 holes at any atomic site. It is only

in a rare number of cases that an atomic site will be in a d^8, d^7, etc. state, because of the relatively high polarity energy of such states; i.e. correlation keeps more than one hole from a site at a time. For multiple holes at an atomic site, we would have carriers with S=1 or higher, due to Hund's rule coupling, which couples S=1/2 holes together into a state of the highest multiplicity allowed by the exclusion principle. This could lead then, to quadrupolar coupling, but the fraction of such sites is expected to be small, hence the contribution to the anisotropy weak.

It has been pointed out, however, that the dipolar interaction <u>is</u> able to yield anisotropy, but only in second order. The dipolar interaction does not commute with the exchange interaction, but acts a a perturbation. A system of parallel dipoles can lower its energy slightly if the dipoles tilt slightly with respect to each other. These tilted dipoles then precess around their original (i.e., the macroscopic magnetization) directed with a conical half angle, whose order of magnitude is C/J. This leads to an effective contribution to the Hamiltonian of the form

4.4.21 $$\mathcal{H}_{pert} \sim C^2/J\ (r_o/r)^{10}\ (\vec{S}_1 \cdot \vec{r})^2\ (\vec{S}_2 \cdot \vec{r})^2$$

in the limit $C \ll J$.

Thus one obtains an anisotropy from the dipolar interaction when this interaction is carried out to second order. This interaction leads to a value of $K_1 \approx C^2/J$, where K_1 is defined in equation 4.4.13. This can be demonstrated by calculating the expectation value of $\mathcal{H}_{pert}$ for a given site, assuming all of the S are aligned along some direction with direction cosines α_i, i = 1, 2, 3, along the three crystal axes. We sum this interaction over all the allowed dipole pairs, by direction $\vec{r}$

from our central site to all the other sites in the lattice. Owing to $1/r^6$ dependence of the interaction, the sum converges rapidly, and can be approximated by a sum over the nearest neighbor sites only. The $(\vec{S}_1 \cdot \vec{r})^2 (\vec{S}_2 \cdot \vec{r})^2$ part of the interaction, when summed over these neighboring cubic sites, yield the angular dependence found in equation 4.4.13, while the coefficient of this expression becomes C^2/J. Included in deriving this angular dependence is expansion of the identity $(\alpha_1^2 + \alpha_2^2 + \alpha_3^2)^2 \equiv 1^2$, which transforms the quartic dependence of the direction cosines in equation 4.4.21 to the biquadratic dependence of equation 4.4.13.

The results one obtains in this way are about a factor of 50 too small, when compared with the experimental values of K_1 in 3-d ferromagnets, for example, pure Ni.[76]

In order to explain the observed anisotropy, one needs an interaction of the diplar or quadrupolar type, but much stronger than that arising from the purely magnetic interaction. Such an interaction was shown to exist by Van Vleck.[76] It results from spin-orbit coupling.

The orbital magnetic states are quenched by the crystal potential. From atomic physics, one knows that there exists a spin-orbit interaction[99]

$$4.4.22 \qquad \mathcal{H}_{\text{spin-orbit}} = \left[\frac{\hbar^2}{2\, m_e^2 c^2} \frac{1}{r} \frac{dV(r)}{dr} \right] \vec{L}.\vec{S}. = A\, \vec{L} \cdot \vec{S}$$

between the electron spin and the orbital motion of the electron in the atomic potential. Here, $\vec{L}$ is the orbital angular momentum operator, A is the expectation value of the bracketed quantity for the states involved and V(r) is the (spherically symmetric) atomic potential. This interaction acts like a perturbation on the orbital states, tending to unquench the angular momentum and thereby perturbs the oribtal state. Thus a spin at a given site perturbs the orbital wave function associated with this site. This orbital wave function overlaps neighboring wave functions, and perturbs

them, which in turn, interact with the spins on these sites. It is in this way that there exists an effective coupling between electron spins, similar to the couplings we have been discussing, but with a much stronger coupling coefficient, which we call D. Thus the S=1/2 spins can couple with a strong dipole-like, or pseudo-dipolar interaction, S=1 spins, with a pseudo-quadrupolar interaction, etc.

One might suspect that in the presence of these spin-orbital effects, the electron spins could couple directly to the orbital states, which convey the cubic symmetry, and thus feel the anisotropic forces directly, rather than having to interact with each other through this indirect (and fourth order in spin-orbit coupling parameter) process. In other words, we might expect presence of a term

4.4.23 $$\mathcal{H}_{anis} \sim B \left\{ (S^{\alpha})^4 + (S^{\beta})^4 + (S^{\gamma})^4 \right\}$$

where α, β and γ refer to the cubic directions. However, the presence of such a term is impossible, quantum mechanically, for S less than 2; therefore, such a contribution to the anisotropy is very unlikely.

Thus, for a system of localized spins, with S=1/2, we obtain an anisotropy constant

4.4.24 $$K_1 = D^2/J$$

where D is now the pseudo-dipolar coupling constant. However, this result is modified by the fact that in the case of band ferromagnets, the average moment associated with each site is reduced. However, this reduction in the magnetic moment $\langle\vec{\mu}\rangle$, or equivalently, the expectation value of the local spin, $\langle\vec{S}\rangle$, does not affect the magnitude of the spin-orbit coupling parameter very seriously.[77] Then the magnitude of D itself remains unchanged as we decrease ξ_o. Generalizing equations 4.4.16, 18 and 21 we have

4.4.25 $$\mathcal{H}_{pert} \sim D^2/J \left\{ (\langle \vec{S}_1 \rangle \cdot \vec{r})^2 \; (\langle \vec{S}_2 \rangle \cdot \vec{r})^2 \right\}$$

where $\langle \vec{S}_i \rangle = \xi_o \vec{S}_i$ and $|\vec{S}_i| = 1/2$. Thus this interaction is reduced by a factor of ξ_o^4, due to the diminishing of the moment by a factor of ξ_o.

The factor of J in the denominator is the exchange stiffness between two sites, tending to keep them parallel. It results from the exchange interaction, which we still suppose is describable by a molecular field approximation. Then

4.4.26 $$H_{mol\ field} \sim k_b \theta' \xi_o$$

$k_b \theta'$ is assumed to be relatively constant as we vary composition, causing ξ_o to vary. The energy difference between a moment in the direction parallel and anti-parallel to M is

4.4.27 $$E_{ex} \sim \langle \vec{\mu} \rangle \cdot \vec{H}_{eff}$$

4.4.28 $$\sim g \mu_b \xi_o \cdot k_b \theta' \xi_o$$

4.4.29 $$\sim J_o \xi_o^2$$

where J_o is the value of J which appears in equation 4.4.24 for $\xi_o = 1$. Then the anisotropy constant is determined by calculating the expectation value of this interaction as a function of the direction cosines describing how the $\langle \vec{S}_i \rangle$ are aligned with respect to the crystal axes. Combining these results we see that K_1 should vary as

4.4.30 $$K_1 (0) = (D^2/J) \xi_o^2$$

where we have allowed K_1 to be a function of temperature, $K_1(T)$, but our present discussion is restricted to T=0. Indeed this is just what we observed near the critical concentration.

Williams and Bozorth[78] measured the anisotropy for Cu-Ni alloys, and when their values of K_1 were plotted against the saturation magnetization

of the alloy, they also found a quadratic dependence.

Actually, the theoretical justification for this quadratic dependence can be made stronger than the crude argument we presented.

Brooks[79] published a paper dealing with the anisotropy of itinerant ferromagnets. He assumed wave functions of the tight binding form. For the atomic functions he uses the cubic triplet Γ_5.

4.4.31

$$\phi_1 = yzf(r)$$
$$\phi_2 = zxf(r)$$
$$\phi_3 = xyf(r)$$

From these, he constructs three bands

4.4.31a $$\psi_n(\vec{k}) = N^{-1/2} \sum_{\ell} \exp(i\,\vec{\ell}\cdot\vec{k})\,\phi_n(\vec{r}-\vec{\ell})$$

(where $\vec{\ell}$ denotes the lattice sites, N is the total number of atoms), and assumed the nearest neighbor wave functions overlap. Thus the Hamiltonian matrix must be re-diagonalized, since this overlap perturbs the local states. He then included the spin-orbit interaction, whose strength he describes by a parameter, A. He set up the secular equation for the energy eigenvalues, including the contribution from the molecular field. He then solved the secular equation, obtaining a general expression for the contribution to the anisotropy constant from electrons in various k-states (his equation 23).

For low relative magnetization, his expression can be expanded in a power series in ξ_o (related to his parameter δ). The resulting expression is proportional to A^4 and is a polynomial in ξ_o, whose lowest order terms are linear in ξ_o, varying as ξ_o/ϵ_1^4, and ξ_o/ϵ_2^4, where ϵ_1 and ϵ_2 are the energy differences for the states of the same wave vector but in the

two bands higher than the lowest band. Also included are terms of higher order in ξ_o, ϵ_1 and ϵ_2. To calculate the total contribution to K_1, these terms must be summed over all the singly occupied k-states i.e., the states contributing to the observed magnetization. For low ξ_o, this contributes another factor of ξ_o, causing K_1 to vary as ξ_o^2, to lowest order in ξ_o, as observed.

Of course, this result is sensitive to band structure, and contains terms of higher order in ξ_o, a fact which can account for the deviation from this quadratic relationship which is observed at the higher nickel concentrations.

Thus, our observed anisotropy data seems to follow the predictions of the band theory. In developing this theory, we did not use the Stoner model of ferromagnetism explicitly, but simply assumed that within a band picture, one is able to distribute the magnetization throughout the lattice in such a way that each lattice site has an identical small moment associated with it.

V. MAGNETIC RESONANCE STUDIES

A. Background

For interpretation of our magnetic resonance data, we will follow the approach taken by Salamon.[10] He studied the Electron Paramagnetic Resonance of pure nickel near the Curie temperature, using a bimodal cavity spectrometer.[80] Depending upon the type of unbalance created between the two modes of this cavity, the microwave losses of such a system can be made proportional to various linearly independent, linear combinations of $\chi_1(\omega)$ and $\chi_2(\omega)$. These are, respectively, the in-phase or inductive, and out-of-phase, or resistive, parts of the frequency dependent magnetic susceptibility of the sample placed in the cavity. He was thus able to extract χ_1 and χ_2 from his observed line shapes.

Our unimodal microwave reflection spectrometer also exhibits losses proportional to a linear combination of χ_1 and χ_2.[14,81]

If the transverse component of the magnetization (i.e., the component in the plane normal to the applied static field) relaxes to its thermal equilibrium value (of zero) according to

5.1.1 $$dM_T/dt = -M_T/T_2$$

(where T_2 is a parameter having dimensions of time)
then one can show[10,82] that the resonant behavior of the susceptibility can be described by

5.1.2a $$\chi_1(\omega) \approx \chi_o/2 \quad \omega_o T_2 \frac{(\omega_o - \omega) T_2}{1 + (\omega - \omega_o)^2 T_2^2}$$

5.1.2b $$\chi_2(\omega) \approx \chi_o/2 \quad \omega_o T_2 \frac{1}{1 + (\omega - \omega_o)^2 T_2^2}$$

where[14] χ_o is the static susceptibility, $= M_z/H_o$, ω_o is the resonant frequency stemming from the gyromagnetic nature of the electrons contributing to the magnetization. For our experimental field configuration (i.e, H_o parallel to the face of the sample,)

5.1.3 $$\omega_o = \gamma\,[(H + 4\pi M)\cdot(H)]^{1/2} \equiv \gamma\,(BH)^{1/2} +$$ small shift proportional to anisotropy which vanishes as T is increased to T_c

and

5.1.4 $$\gamma = g\,\mu_b/\hbar$$

The half-intensity width, or half-width of this resonance line is given by

5.1.5 $$(\Delta\,\omega_{1/2}) = 2/T_2$$

Since we sweep the applied field (causing ω_o to be swept) and hold ω fixed at the microwave frequency ω_{rf}, the half-width, in terms of the field is

5.1.6 $$(\Delta H_{1/2}) = 2/\gamma T_2$$

Our observed lines were fit on a computer to a general linear combination of χ_1 and χ_2 defined in equation 5.1.2. In most cases, the fit was very good, and we were thus able to determine T_2 and $g = \gamma\hbar/\mu_b$.

We would like to discuss these parameters from the standpoint of the microscopic model of our system.

The behavior in the ferromagnetic region is quite complicated, and not thoroughly understood quantitatively. In this region, the transverse magnetization relaxation rate is usually thought of as resulting from scattering of magnons whose components of wave vector are between 0 and $1/\delta$ (where δ is the R.F. skin depth) in the z direction (normal to the surface of the sample) and 0 in the transverse direction. (This is the so called uniform precession mode.) These relaxation processes are discussed,

for example, by Sparks,[83] and include interactions of magnons with other magnons, phonons, conduction electrons, surface and volume pits and imperfections, strains, impurities, and crystallographic grain boundaries. There is also a naturally occuring width in a polycrystalline sample due to the spread in resonance frequencies resulting from the various crystallite orientations. The width of the spread is of the order

5.1.7 $$\Delta H \approx K_1(T)/M(T)$$

These processes are quite dependent on sample quality. For very pure strain-free single crystals of nickel, ferromagnetic linewidths as narrow as 150 Oe. have been observed,[84] whereas our linewidths were at least 2000 Oe. We are therefore, unable to discuss the ferromagnetic linewidth quantitatively from the standpoint of the fundamental properties of the system.

However, the principle relaxation mechanism in the paramagnetic region is the spin-spin (dipolar) interaction.[85]

Following Salamon, the macroscopic (transverse) relaxation rate of M may be related to the microscopic relaxation rate, $1/T_2$, for the individual spins, and leads to the relation

5.1.8 $$\frac{1}{T_2 M} = \frac{C}{T} \cdot \frac{H}{M} \left[\frac{1}{T_2}\right]$$

where $1/T_2{}^M$ is the relaxation rate of M, and is proportional to the observed linewidth,

5.1.8a $$\Delta H = \frac{1}{\gamma} \frac{1}{T_2{}^M}$$

where $H/M = 1/\chi$ is the inverse magnetic susceptibility appropriate for the applied field H and temperature T. Also,

5.1.9 $$C = N \mu^2/3 k_b$$

where μ is the magnetic moment of the individual spins which are relaxing at the rate $1/T_2$ and N is the number of such spins per unit volume. We recognize C as the classical Curie constant for the system.

This temperature dependence, which causes a narrowing of the line as we approach T_c from above, follows from general thermodynamics arguments about irreversible processes. Salamon presented a simplified physical argument which demonstrates this relation. It has also been discussed by Kittel and Portis[86] as a general thermodynamic result (for the part of the relaxation rate stemming from the non-secular portion of the dipolar interaction at least). This result is also discussed for a magnetic system using a more general (quantum mechanical calculation of the auto-correlation function of the magnetization) approach by Mori and Kawasaki.[87] Their results takes the form

5.1.10 $$\frac{1}{T_2^M} = \frac{T-T_c}{T}\left[\frac{1}{T_2}\right]$$

but this reduces to equation 5.1.8 when the inverse susceptibility is expressed in the Curie-Weiss form.

We are then left with the problem of calculating the spin relaxation rate, $1/T_2$, in the paramagnetic region. The interaction responsible for this relaxation, as we have stated, is the (pseudo-) dipolar interaction between the individual spins, which is modified, as we shall see, by the exchange interaction.

Bloembergen, Purcell, and Pound[88] considered the effects of the dipolar interaction on the relaxation rates between nuclear moments in liquids, but the results are easily generalized to the effects of pseudo-dipolar interactions between electrons in a solid. They also considered the effects of the relative motion of these moments which provides a

random time variation (i.e., Markoffian modulation) of this interaction, which occurs over a time scale τ_c, called the correlation time. They showed that in the static case, the half-width is given by

5.1.11 $$(\Delta \omega_{1/2}) \approx \omega_D$$

where ω_D is the precession rate of a magnetic carrier due to its dipolar interaction with its nearest neighbors. Defining the dipolar interaction from equation 4.4.18 and again introducing the pseudo-dipolar interaction strength, D we find

5.1.12 $$\omega_D \approx D/\hbar$$

(c.f. also Principles of Magnetic Resonance, page 29 for a qualitative discussion of this precession rate). In the case of short correlation time, $1/\tau_c \gg \omega_D$, they showed the half width is reduced by a factor ω_D/τ_c, yielding

5.1.13 $$(\Delta \omega_{1/2}) = \omega_D^2 \tau_c \qquad \omega_D \ll 1/\tau_c$$

Van Vleck[89] considered the effects of exchange. He calculated the second and fourth moments of the dipole perturbed Zeeman levels. He found a second moment (expressed in frequency) given by

5.1.14 $$\langle \Delta\omega^2 \rangle \approx \omega_D^2$$

and a fourth moment

5.1.15a $$\langle \Delta\omega^4 \rangle \approx \omega_D^2 \omega_e^2 \qquad \omega_e > \omega_D$$

5.1.15b $$\langle \Delta\omega^4 \rangle \approx \omega_D^4 \qquad \omega_e < \omega_D$$

where

$$\omega_e = J/\hbar$$

He showed that this corresponds to a half-width

5.1.16a $$(\Delta\omega_{1/2}) = \omega_D^2/\omega_e \qquad \omega_e > \omega_D$$

5.1.16b $$(\Delta\omega_{1/2}) = \omega_D \qquad \omega_e < \omega_D$$

He thus showed that the exchange served to randomly modulate the dipolar interaction at a rate

5.1.17 $$\omega_e \equiv 1/\tau_e = J/\hbar$$

and ascribed some physical significance to this fact.

In the second paper[90] he considered (at least one of) the effects of the ferromagnetic transition. As the spin system orders (as it will for $T > T_c$ in the presence of an external field) the amount of randomness in the dipolar fields at the various sites decreases. He showed that this effectively reduces the second moment, and hence the half-width, according to the relation

5.1.18 $$\langle\Delta\omega^2\rangle = \{ \langle S_z^{i\,2}\rangle - \langle S_z^{i}\rangle^2\} \ \langle\Delta\omega_\infty^2\rangle$$

where $\langle g\,\mu_b\, S_z^i\rangle$ equals the average moment of some random spin site

equals 0 in the paramagnetic region

equals $g\,\mu_b\,|\vec{S}_z^{\,i}|$ at T=0

we can rewrite equation 5.1.18 as

5.1.19 $$\langle\Delta\omega^2\rangle = \{M^2(0) - M^2(T)\} \ \langle\Delta\omega_\infty^2\rangle$$

This result is in addition to the thermodynamic result we quoted previously in equation 5.1.8. It is simply a consequence of the fact that as the magnetic system orders, the amplitude of the random fluctuating dipolar fields decrease according to the above factor. Thus, at T=0, the dipolar width vanishes, according to our discussion so far. This is because all the spins are aligned parallel, so every spin sees an identical local magnetic field, so the local Zeeman levels are no longer broadened.

However, Keffer[91] demonstrated that the line-width at low temperature due to zero-point motion of the spins (purely a quantum mechanical effect) approaches a non-zero value. This value vanishes in the classical limit (i.e , as S gets large but the overall magnetization is held constant). This effect arises from the non-secular terms in the dipolar Hamiltonian, which can only contribute to the relaxation if the Zeeman levels are mixed, as in the case where $J \gg \frac{\bar{\gamma} H_o}{\hbar}$. This mixing is discussed by Anderson and Weiss[92] and also leads to the so-called 10/3 effect.

However, for our samples, M(T) was already down to about half of its values at T=0 for $T=T_c$, so that in the paramagnetic region, the loss of disorder in the dipole distribution, as T_c is approached from above is probably a small effect.

Thus, combining our results, we find

5.1.20 $$(\Delta H_{1/2}) = \gamma \frac{C}{T} \frac{H}{M} [1/T_2]$$

5.1.20a $$1/T_2 = \omega_D^2 \tau_c$$

where τ_c is the appropriate correlation time between random changes in the dipole distribution, $C=N \mu^2/3k_b$, and μ is the magnetic moment per carrier.

This relation is modified by yet another process as the Curie temperature is approached from above. The onset of short range order has been shown[10] to interfere with the exchange modulation process, slowing the random modulation rate down somewhat as the Curie temperature is reached. This becomes significant at a temperature about ten per cent above the Curie temperature. This number is a consequence of the number of nearest neighbors of each site. Thus, in order to extract the microscopic relaxation rate from the observed linewidth data, we must

apply equation 5.1.20 to data corresponding to temperatures higher than T_c by at least ten per cent.

We now consider the problem of calculating ω_D and τ_c for our band magnet. We recall the important features of the model we are using. We are considering a band of mobile electrons, which are in rapid motion. A fraction $(1 + \xi)/2$ of these electrons have spin up, and the remaining fraction $(1 - \xi)/2$ have spin down. At any particular lattice site, an electron resides for a time, τ, then hops to a neighboring site, and is replaced at the original site by another electron. Since there are more spin up electrons than spin down ones, the average magnetic moment at each site, when averaged over many hopping times is $g\,\mu_b\,\vec{S} \cdot \xi$. As the temperature is increased, the fraction of electrons with spin up decreases, so the average moment associated with each site decreases.

The origin of anisotropy in a ferromagnet is a static process. In section 4.4, we associated the quantum mechanical average value of the moment per site with each lattice site. We then calculated the quantum mechanical expectation value of the energy of orientation of the average moments.

The relaxation of the spins, however, is a dynamic process. We must therefore, treat our system as a collection of rapidly moving individual electrons when we attempt to calculate the relaxation rate.

One can show that the hopping time for such a system is given roughly by

5.1.21 $$\tau_{hop} = \hbar/E_o \equiv 1/\omega_{hop}$$

where E_o is the band width, or Fermi energy. The electrons also exhibit an exchange interaction with each other. The exchange interaction between two electrons near the same site is the full molecular field $k_b\theta'$, which

we call J to conform to the literature. These two electrons also experience the full pseudo-dipolar interaction strength, appropriate to S=1/2 electrons, D. Thus, the dipolar precession rate, ω_D, of these fast-moving electrons is still given by equation 5.1.12.

This dipolar field is interrupted by two random processes, the hopping rate

5.1.22 $$\omega_{hop} = E_o/\hbar$$

and the exchange rate

5.1.23 $$\omega_{ex} = J/\hbar$$

We mention at this point that for our weakly ferromagnetic system,

5.1.24 $$J \approx E_o$$

It is intuitively obvious that the modulation rates from independent processes are additive. That is, the net modulation rate is the sum of the two individual modulation rates. Then we generalize equation 5.1.16a and obtain

5.1.25 $$1/T_2 \approx \frac{\omega_D^{\ 2}}{\omega_{ex} + \omega_{hop}} \approx (1/2)\, \omega_D^{\ 2}\, \tau$$

where $\tau \approx \hbar/E_o \approx \hbar/J$.

This can be written, using our expressions for ω_D (5.1.12) and ω_{ex} (5.1.23)

5.1.26 $$1/T_2 \approx (1/2\hbar)\ D^2/J$$

In order to extract $1/T_2$ from the observed linewidth data, using equation 5.1.20 we must also calculate $C = N\mu^2/3\, k_b$. It is obvious from our present discussion that since we are dealing with the effects of rapidly moving individual electrons, the value of the moment, μ, we must use to evaluate C is the magnetic moment of an individual electon,

5.1.27 $$\mu = g\, \mu_b\, S$$

$$S = 1/2$$

thus

5.1.28 $$C = N(\tfrac{1}{2}\, g\, \mu_b)^2/3\, k_b$$

We recall that our expression for the anisotropy constant is given by an expression, equation 4.4.30,

$$K_1(0) \approx (D^2/J)\, \xi_o^{\,2}$$

We thus have a relation between T_2 (i.e., the linewidth) and $K_1(0)$ (the anisotropy constant at T (0).

5.1.29 $$1/T_2 \approx K_1(0)/\xi_o^{\,2}$$

This relation was discussed by Cooper and Keffer[85] for a localized magnet ($\xi = 1$). They showed that if the anisotropy does not arise from any (pseudo-) quadrupolar interaction terms (see our discussion of the anisotropy), that the linewidth and $K_1(0)$ should vary as D^2/J. However, they also pointed out that at finite temperatures, due to lattice expansion, that the coefficients D and J may become (slightly) temperature dependent. They estimate that the ratio D^2/J may change by as much as 50 per cent between T=0 and $T=T_c$. Then our relation, equation 5.1.29 should be modified:

5.1.30 $$\frac{1}{T_2} = \frac{K_1(0)}{\xi_o^{\,2}}\, f(T)$$

where f(T) probably lies in the range $1/2 < f(T) < 2$, for T only slightly higher than T_c.

B. Data and Discussion

In figures 20a-d, we show raw linewidth vs. temperature data for several of our samples.

The decrease in linewidth with increasing temperature for $Ni_{80}Rh_{20}$ is attributed to the decrease in anisotropy occurring as T_c is approached from below.

In figures 21a-c, we plot the individual spin relaxation rate, $1/T_2$ vs. temperature, using equation 5.1.8, 8a, 9, and using 5.1.27 for the value of C.

In figure 22 we plot the composition dependence of $1/T_2$ for the spins in the paramagnetic region by evaluating $1/T_2$ at $T = 1.1\ T_c$ or greater. Included on this plot is the value for pure Ni found by Salamon.

Also shown in figure 22 is $K_1(0)/\xi_o^2$ vs. concentration, multiplied by a factor to make these two quantities equal for pure nickel. According to equation 5.1.30, these two curves should follow roughly the same concentration dependence.

It is apparent from this plot that equation 5.1.30 simply does not describe our system with the values of $1/T_2$ determined according to our discussion.

In figure 23 we show a plot of $K_1(0)$ vs. concentration as well as $1/T_2$ vs. concentration, the K_1 plot again suitably normalized. In this case, we find excellent agreement between the two curves.

The fact that $K_1(0)$ and the values of $1/T_2$ observed by using equation 4.1.20 scale together as ξ_o decreases, strongly suggests several

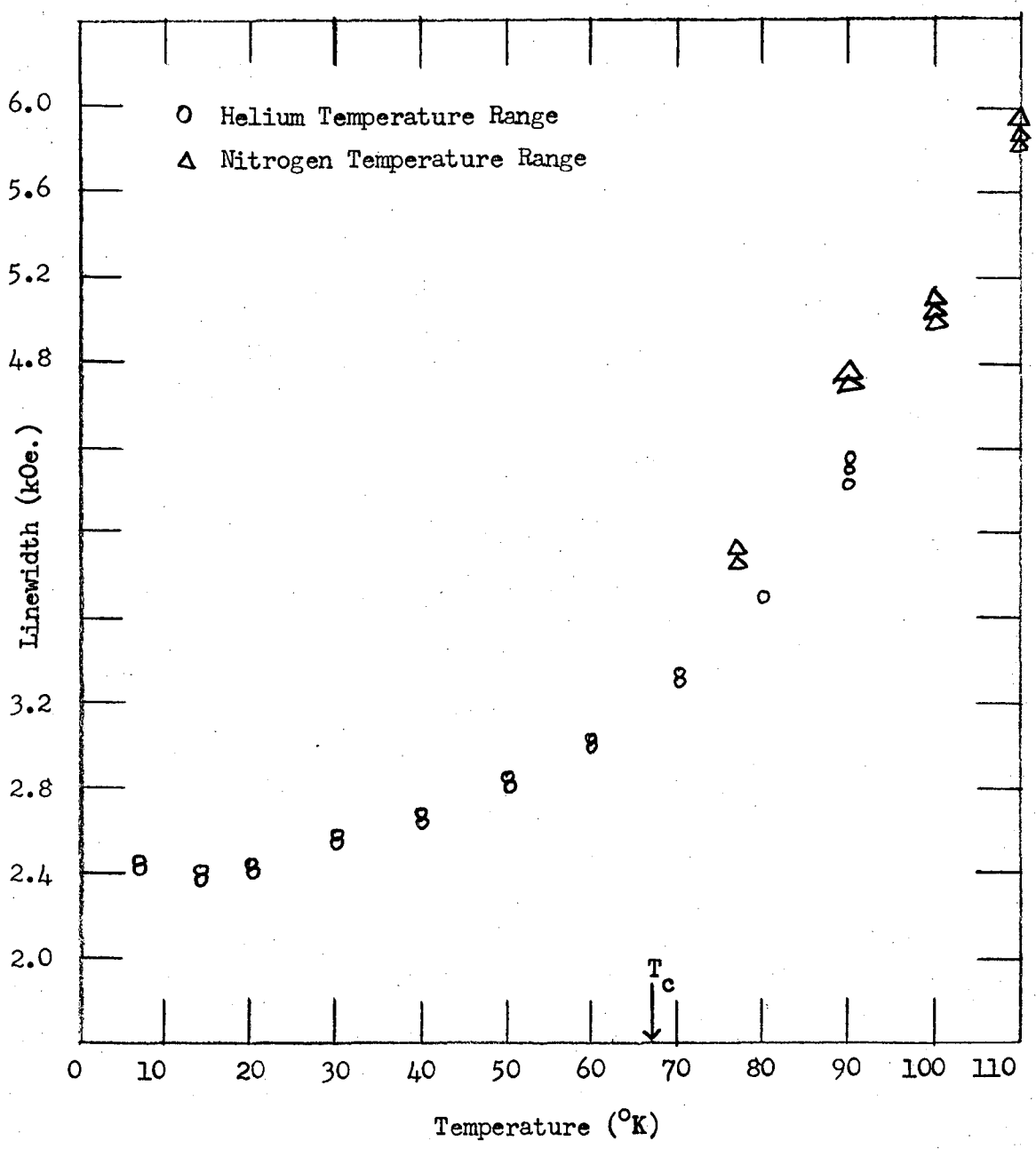
O Helium Temperature Range
Δ Nitrogen Temperature Range
6.0
5.6
5.2
4.8
3.2
2.8
2.4
2.0
Linewidth (kOe.)
T_c
0
10
20
30
40
50
60
70
80
90
100
110
Temperature (°K)

Fig. 20a

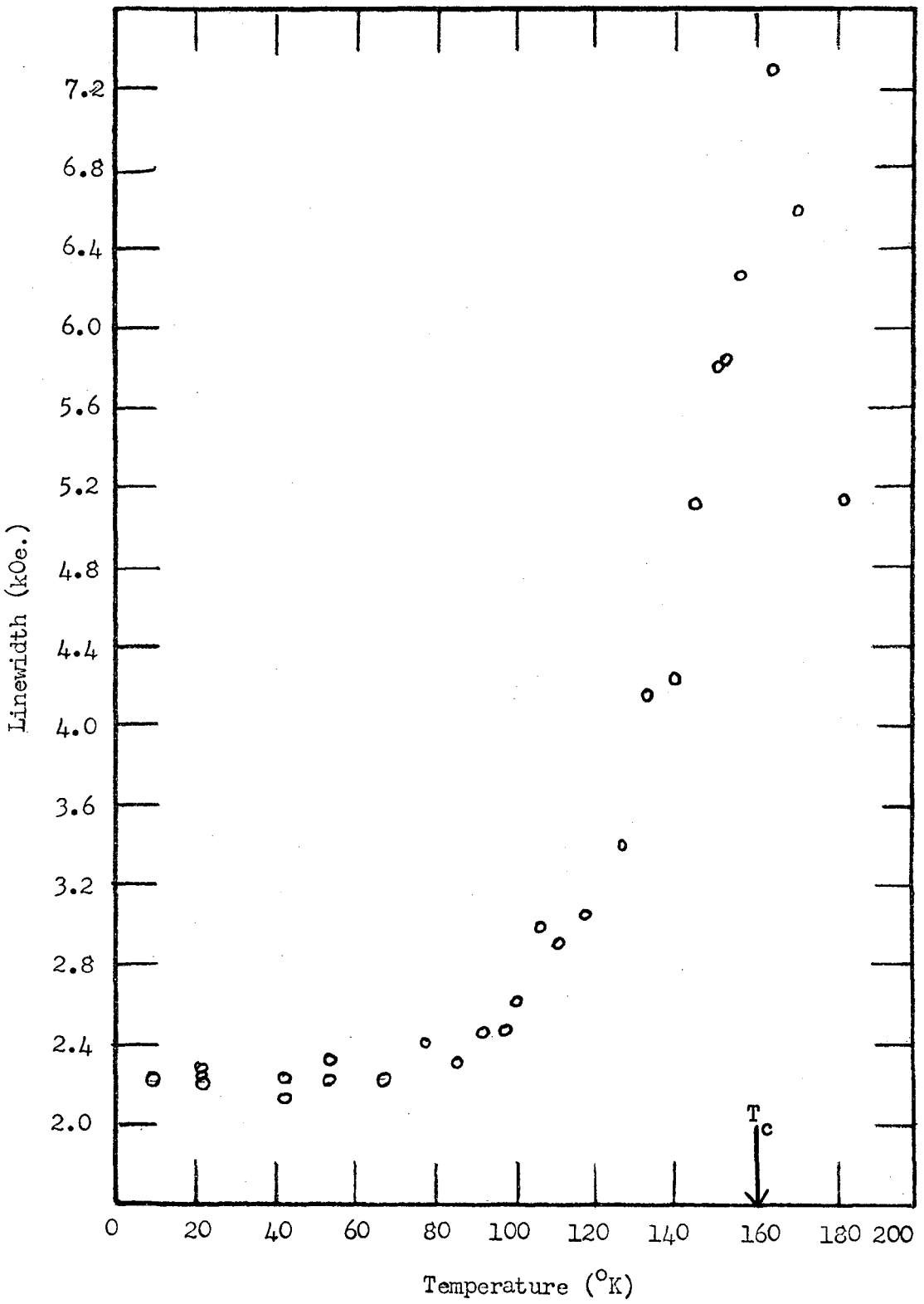
7.2
6.8
6.4
6.0
5.6
5.2
4.8
4.4
4.0
3.6
3.2
2.8
2.4
2.0
Linewidth (kOe.)
0
20
40
60
80
100
120
140
160
180
200
Temperature (°K)
T_c

Fig. 20b

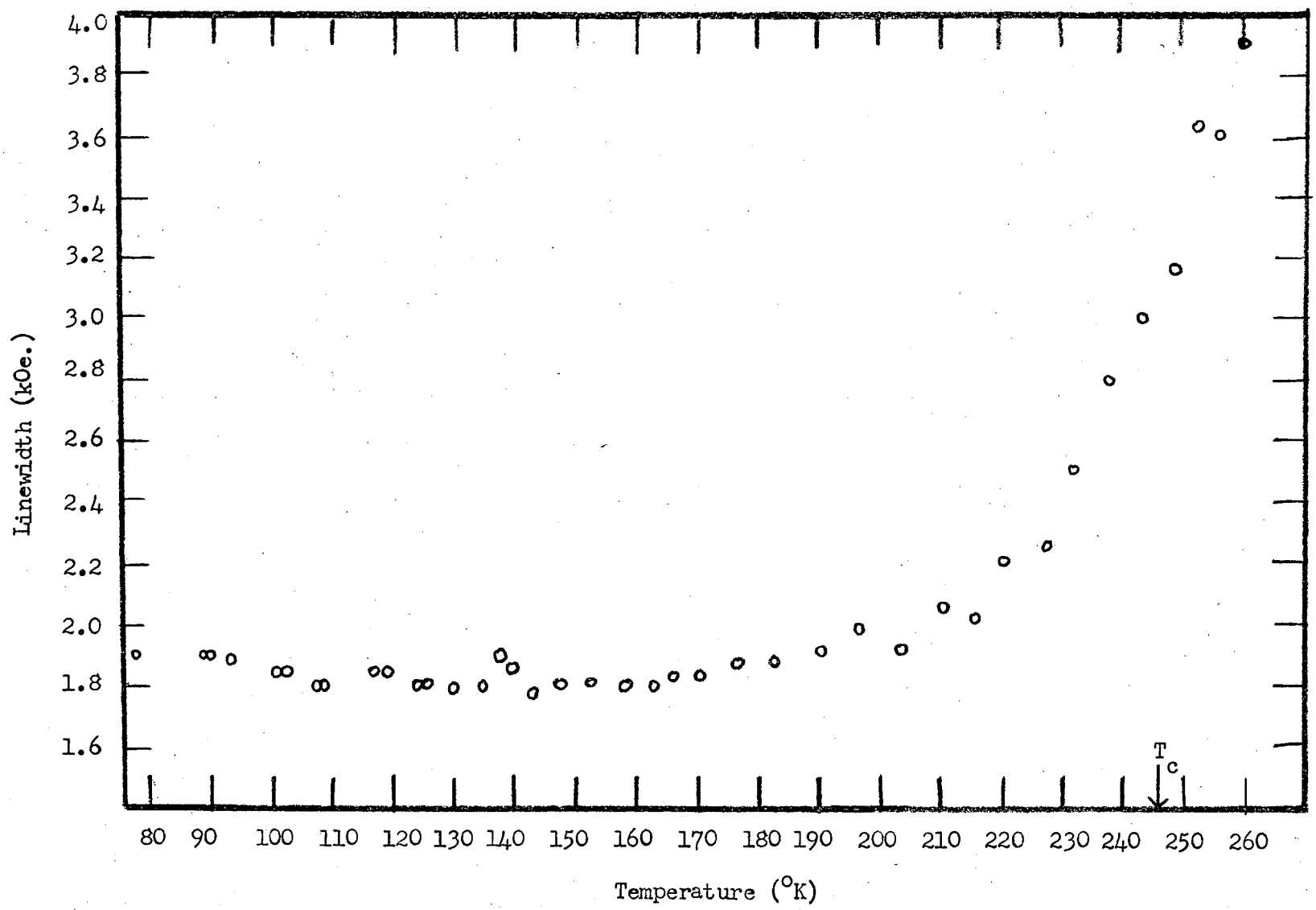
Linewidth (kOe.)
4.0
3.8
3.6
3.4
3.2
3.0
2.8
2.6
2.4
2.2
2.0
1.8
1.6
80 90 100 110 120 130 140 150 160 170 180 190 200 210 220 230 240 250 260
Temperature (°K)
T_c

Fig. 20c

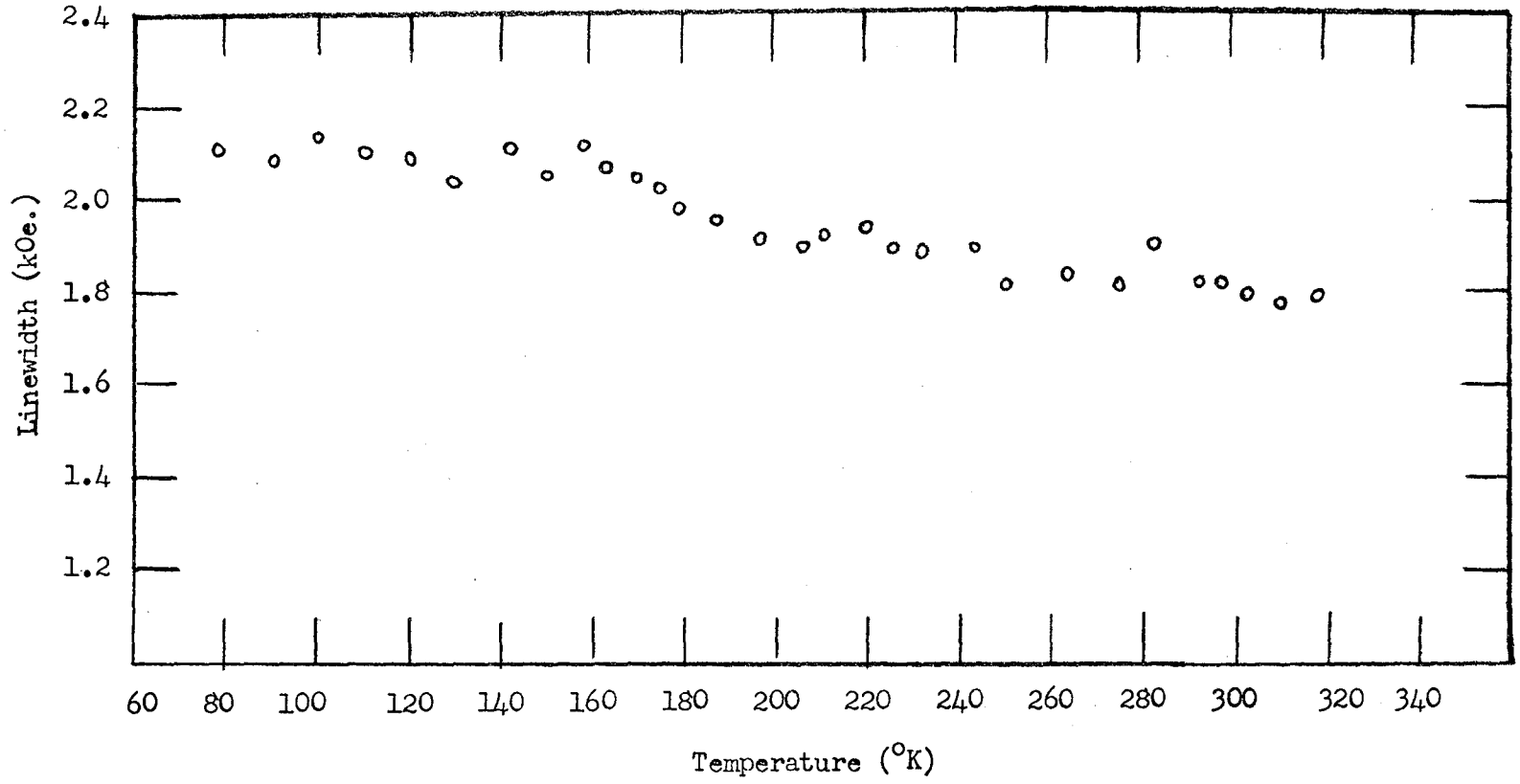
2.4
2.2
2.0
1.8
1.6
1.4
1.2
Linewidth (kOe.)
60
80
100
120
140
160
180
200
220
240
260
280
300
320
340
Temperature (°K)

Fig. 20d

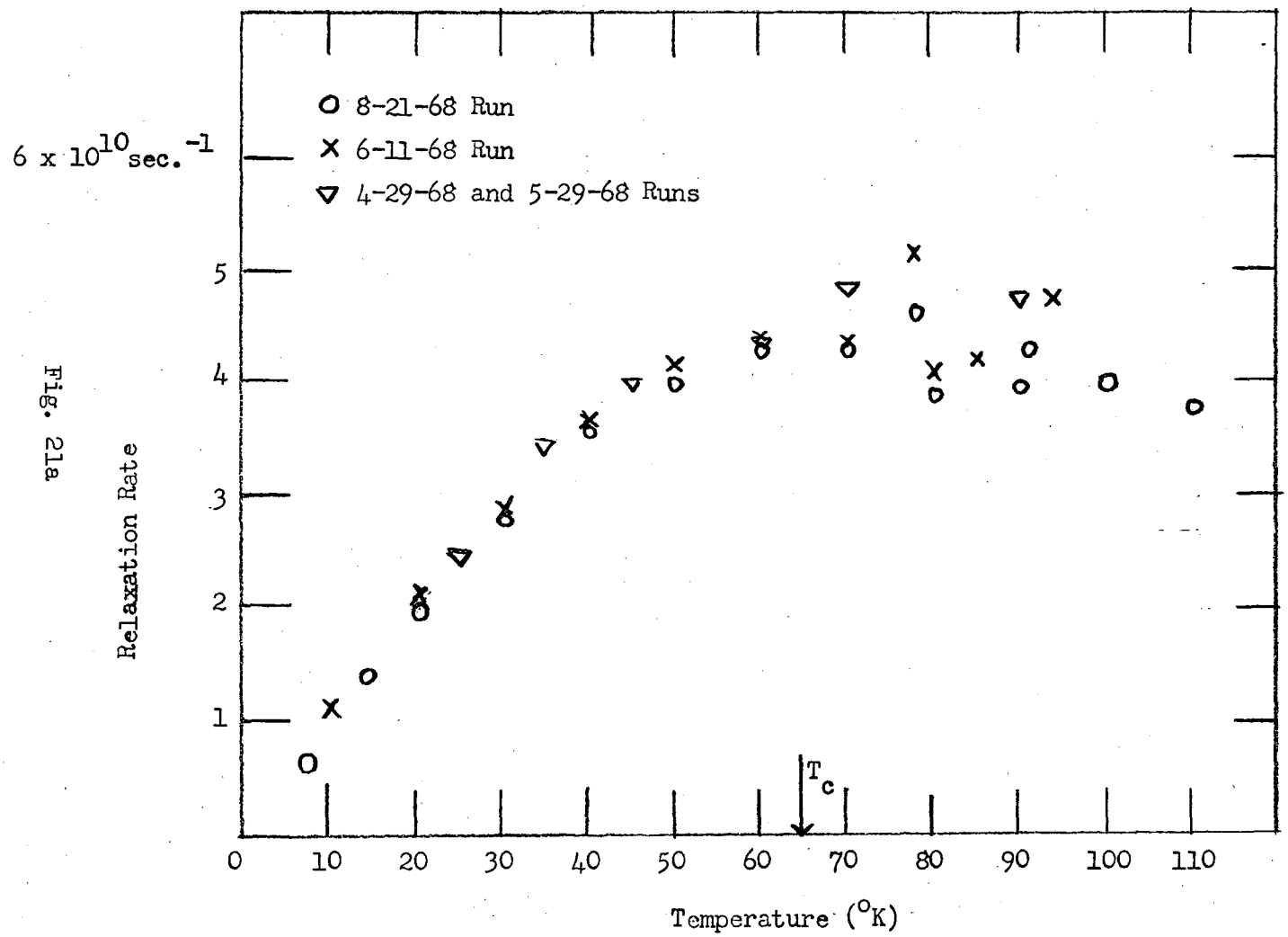
8-21-68 Run
6-11-68 Run
4-29-68 and 5-29-68 Runs
6 x 10^10 sec.^-1
5
4
3
2
1
Relaxation Rate
T_c
0
10
20
30
40
50
60
70
80
90
100
110
Temperature (°K)

Fig. 21a

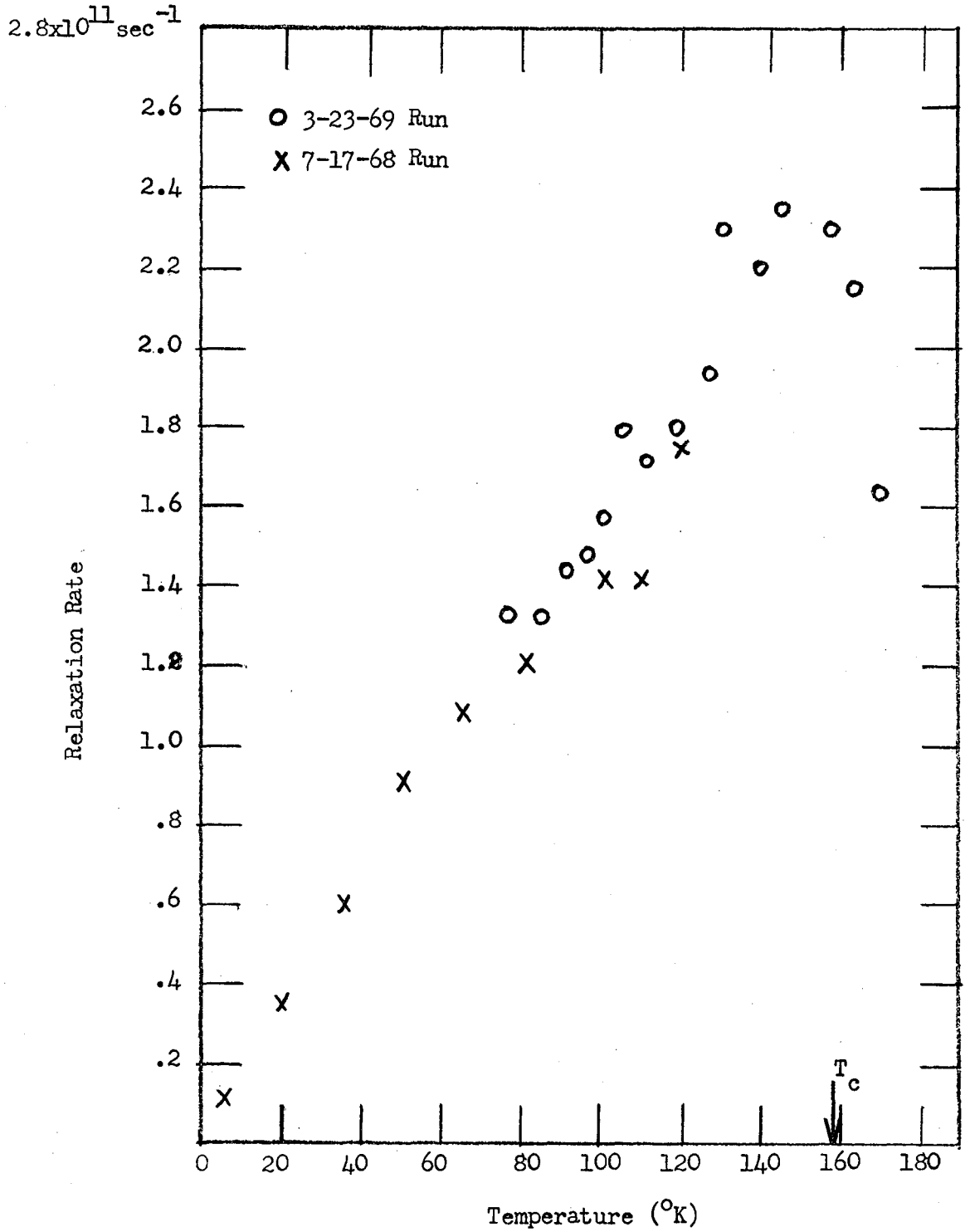
2.8x10^11 sec^-1
2.6
2.4
2.2
2.0
1.8
1.6
1.4
1.2
1.0
.8
.6
.4
.2
Relaxation Rate
O 3-23-69 Run
X 7-17-68 Run
T_c
0
20
40
60
80
100
120
140
160
180
Temperature (°K)

Fig. 21b

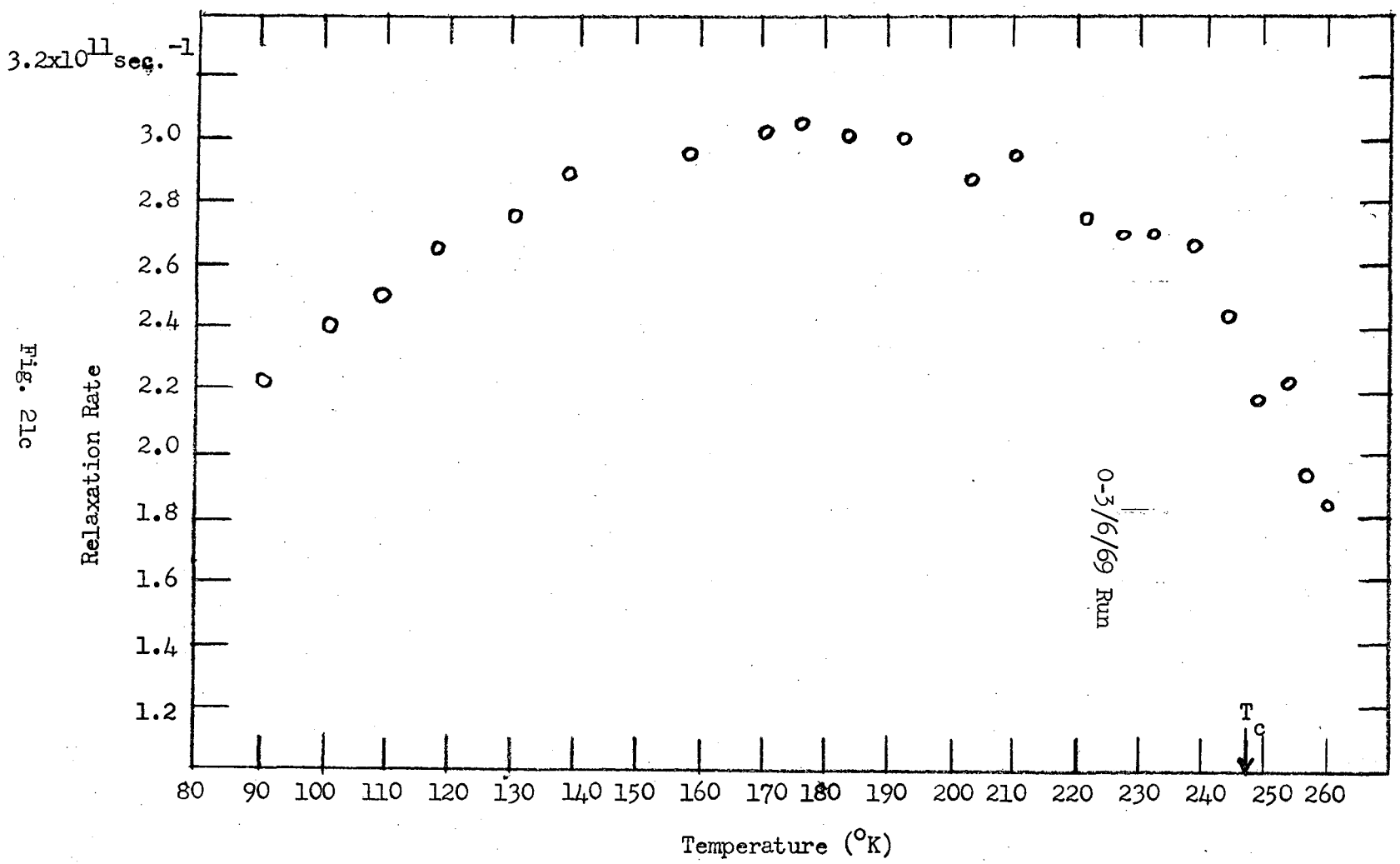
3.2x10^11 sec.^-1
3.0
2.8
2.6
2.4
2.2
2.0
1.8
1.6
1.4
1.2
Relaxation Rate
80 90 100 110 120 130 140 150 160 170 180 190 200 210 220 230 240 250 260
Temperature (°K)
T_c
0-3/6/69 Run

Fig. 21c

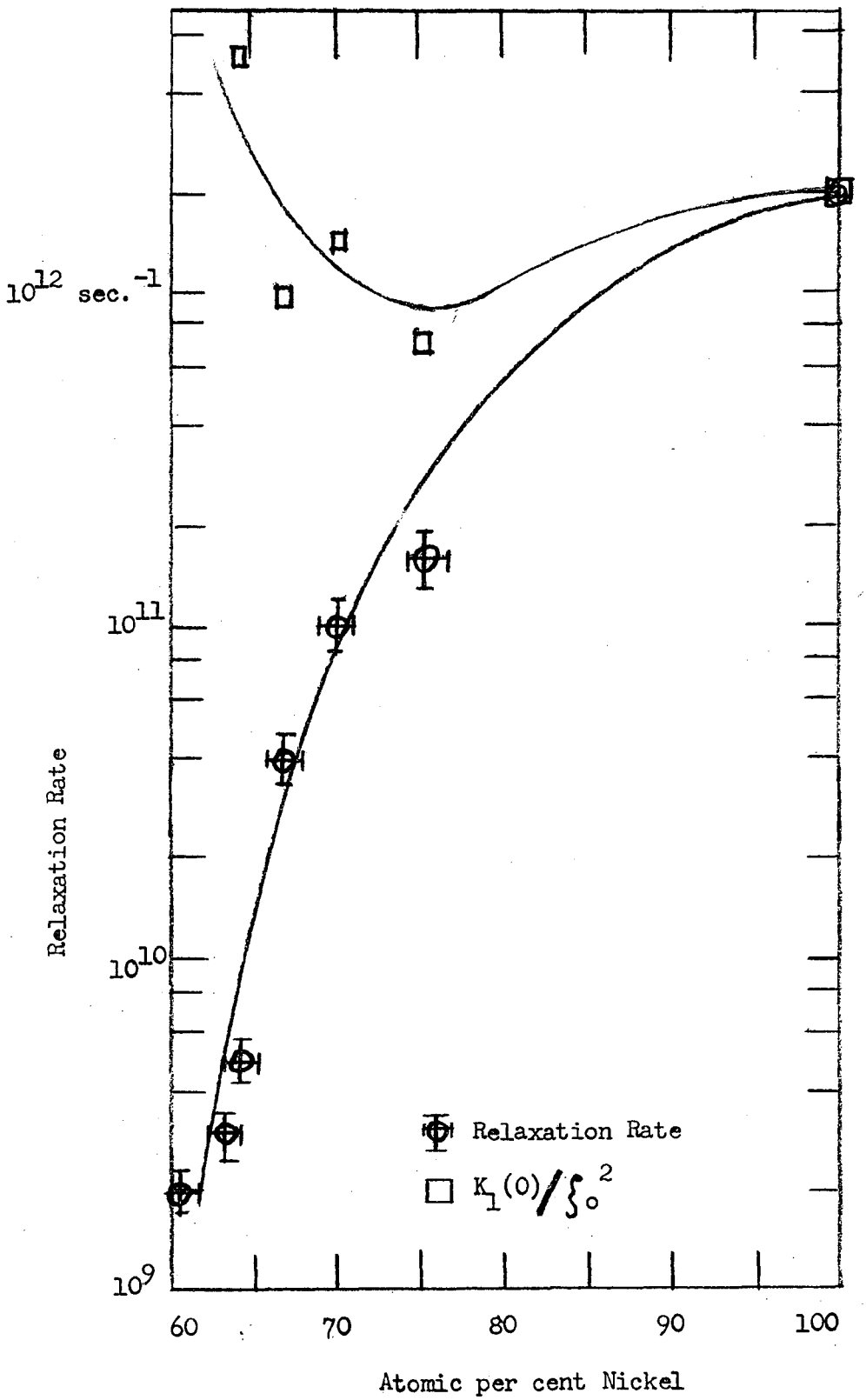
10^{12} sec.$^{-1}$
10^{11}
10^{10}
10^{9}
Relaxation Rate
60
70
80
90
100
Atomic per cent Nickel
Relaxation Rate
$K_1(0)/\zeta_0^2$

Fig. 22

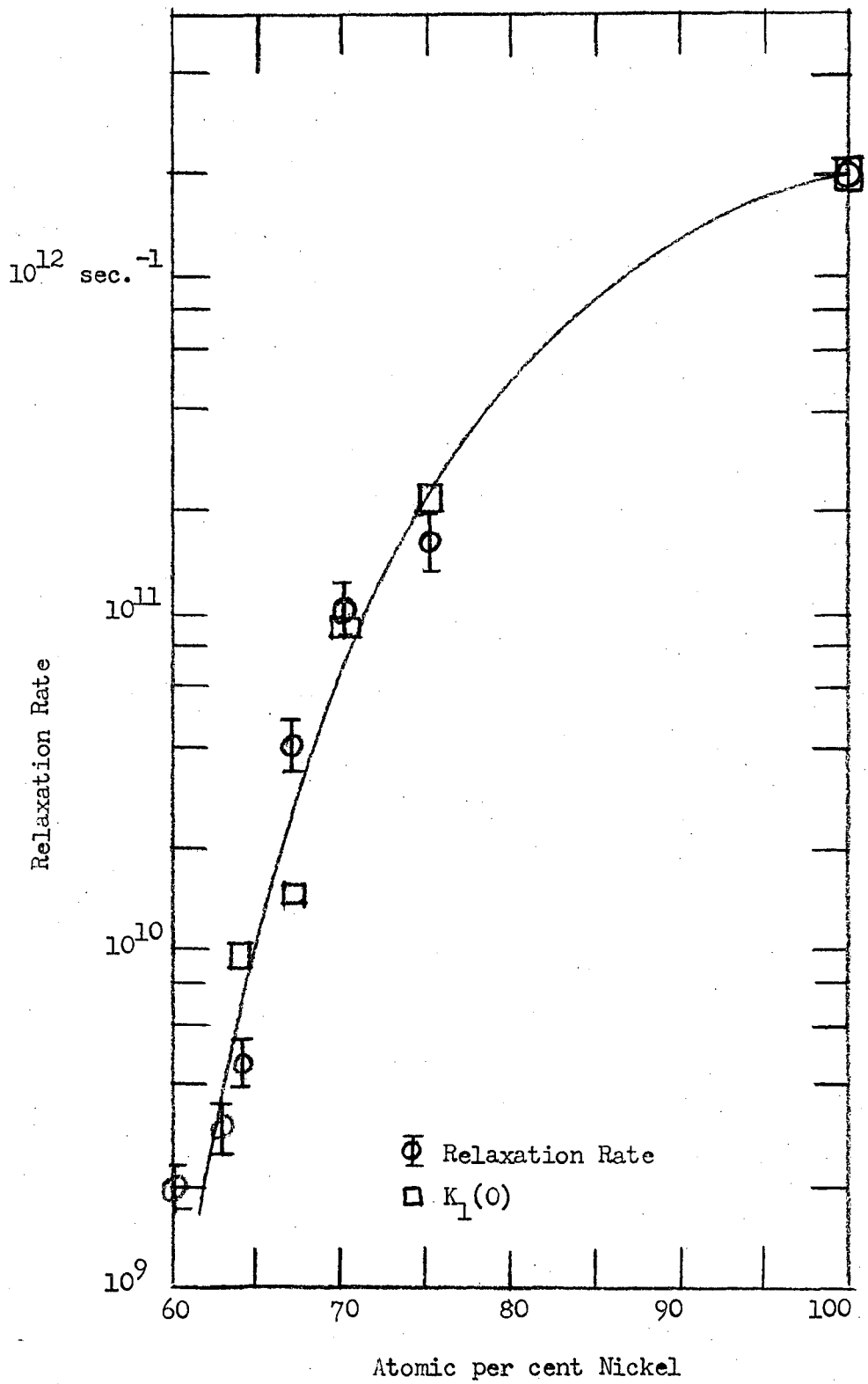
10^{12} sec.$^{-1}$
10^{11}
10^{10}
10^{9}
Relaxation Rate
60
70
80
90
100
Atomic per cent Nickel
Φ Relaxation Rate
□ $K_1(0)$

Fig. 23

important modifications in our microscopic model of our ferromagnet. First, we must acknowledge the fact that we are dealing with a band of electrons constructed from localized d-states which overlap in space with their nearest neighbors. Thus, there are, in reality, two types of exchange in our system. The first is the large intra-atomic exchange, resulting from the intra-atomic Coulomb interaction between all the d-electrons associated with an atomic site. This interaction tends to lead to the formation of local moments. This was discussed by Anderson[93] when he attempted to explain the formation of local moments in dilute alloys of magnetic elements in non-magnetic hosts.

The second type of exchange is the inter-atomic type, resulting from overlap of neighboring atomic wave functions. It is much weaker than the first type, and is responsible for the ferromagnetic alighment of the local moments.

We will discuss this model further, but first we will consider the consequences of such a model with respect to the relaxation rate.

Let us assume that the intra-atomic exchange results in the formation of localized magnetic moments, which, for certain ranges of the parameters describing the system, may have small amplitude. That is,

5.2.1 $$\langle \vec{S}_i \rangle = \xi \, \vec{S}_i$$

5.2.1a $$|\vec{S}_i| = 1/2$$

5.2.1b $$\langle \vec{\mu}_{loc} \rangle_i = g \, \mu_b \langle \vec{S}_i \rangle$$

where i denotes a random lattice site.

We further assume that these moments remain constant in magnitude as the temperature is increased to above the Curie temperature, but are allowed to become disordered. Then the dipolar interaction of these reduced moments

between neighboring sites can be written in the form (following equations 4.4.16, 18, and 25)

5.2.2 $$\mathcal{H}_{Dip} = D \langle \vec{S}_i \rangle \cdot \langle \vec{S}_2 \rangle f(\alpha_i, i = 1,2,3)$$

where $f(\alpha_i)$ is the appropriate function of the direction cosines α_i between the spin directions and the crystallographic axes. Or, re-ordering the terms

5.2.2a $$\mathcal{H}_{Dip} = \langle \vec{S}_i \rangle \cdot \{D \cdot \langle \vec{S}_2 \rangle \times f(\alpha_i)\}$$

It is the quantity in the brackets which causes the diploar precession of the random spin site $\langle \vec{S}_1 \rangle$. We see that the precession rate $\omega_D(\xi)$ is reduced from the value corresponding to $\xi=1$ by a factor of ξ. That is

5.2.3 $$\omega_D(\xi) = \xi \cdot \omega_D$$

where $\omega_D = \frac{1}{\hbar} D$.

Of course, these reduced moments now arise from very rapid fluctuations of localized atomic wave functions. The magnitude of the moment associated with one of these instantaneous state is $g \mu_b \vec{S}$, but these states fluctuate at the very high intra-atomic exchange rate, $\omega_{intra} = J_{intra}/\hbar$, and time-average to the smaller, observed state with moment, $\xi \cdot g \mu_b \vec{S}$.

One might then expect that each magnetic site is influenced by the large dipolar interaction with its nearest neighbors. The precession rate due to the instantaneous dipole moment is the full dipolar rate, $\omega_D = D/\hbar$. However, this moment is modulated at the very high rate, ω_{intra}, which is so rapid, that the overall contribution to the relaxation rate, $1/T_2 = (1/\hbar)(D^2/J_{intra})$, is small enough to be dominated by the dipolar interaction between time-averaged quantum mechanical expectations of these localized states.

These reduced moments are modulated by the inter-atomic exchange couplings with their nearest neighbors. This modulation rate is given by

5.2.4. $$\omega_{ex} = \frac{\Delta E_{ex}}{\hbar}$$

where ΔE_{ex} is the energy difference between two localized states being in the parallel configuration, or the anti-parallel one. (This can be demonstrated by general uncertainty-principle arguments.) We showed during the discussion of the anisotropy, that

5.2.5 $$\Delta E_{ex} = k_b \theta' \xi^2 = J \xi^2$$

Then the relaxation rate between the reduced localized moments due to the inter-atomic exchange modulation of the dipolar interaction between these reduced moments is now

5.2.6 $$1/T_2 = \frac{\omega_D^2(\xi)}{\omega_{ex}(\xi)} = \frac{1}{\hbar} D^2/J$$

This is essentially the same result we obtained from equation 5.1.26, during whose derivation the intra-atomic exchange was neglected.

However, the formation of these localized states also changes the value of the Curie constant C appearing in equation 5.1.20 which we used to calculate T_2 from ΔH.

The expression for C is given by

5.2.7 $$C = N \mu^2 / 3 k_b$$

In the Stoner model, the electrons acted independently, and their magnetic moment, per magnetic carrier, was $\vec{\mu} = g\mu_b \vec{S}$. In the present model, the electrons associated with a lattice site are coupled to a state with reduced moment $\langle \vec{\mu} \rangle = \xi g\mu_b \vec{S}$. We assume this coupling to be independent of T, so these states maintain a constant amplitude as the temperature is increased above the Curie temperature. The observed decrease in magneti-

zation arises from the disordering among the localized states, as in any other localized moment magnetic material. It is clear that the Curie constant for such a system is determined by the reduced moment. Then we write, using the fact that $\xi(T) = \xi_o$:

5.2.8 $$C(\xi) = C(\xi_o) = N(\xi_o g\mu_b S)^2/3k_b = \xi_o^2 \cdot C(\xi=1)$$

Then equation 4.1.20 becomes

5.2.9 $$\Delta H = \gamma \frac{C(\xi_o)}{T} \cdot \frac{H}{M} \frac{1}{T_2}$$

5.2.10 $$\Delta H = \gamma \frac{C(\xi_o=1)}{T} \cdot \frac{H}{M} \frac{1}{T_2} \cdot \xi_o^2)$$

It is the quantity in the parenthese which was determined by applying equation 5.1.20 to the observed linewidth data, using the value of C appropriate to the Stoner model (i.e. $C(\xi=1)$). Thus, according to the present model, we have actually determined $(\frac{1}{T_2} \cdot \xi_o^2)$.

The discussion of the anisotropy, which was based on the average value of the localized moment was independent of how this reduced average localized moment arises, i.e., whether it is due to inter-atomic hopping or intra-atomic coupling, Thus, the results of that discussion are valid in this model also. Then combining equations 4.4.30 and 5.2.6., we see that equation 5.1.30 is still valid. We re-write this equation in the form

5.2.10 $$(\frac{1}{T_2} \cdot \xi_o^2) = K_1(0) \cdot f(T)$$

which now agrees with the experiment (figure 23). Thus, with the assumption of a localized state, and consideration of the effect of this assumption on the Curie constant, we obtain excellent agreement between the expected variation in the anisotropy and the observed linewidth.

The two assumptions central to this result are:

1. Very strong intra-atomic exchange, which provides localized moments which vary with alloy composition. This interaction also provides a very rapid modulation of the individual atomic states forming these moments, which masks the effects of the dipolar interaction between the instantaneous values of the local moment.

2. These local moments remain essentially constant in amplitude as the temperature is increased. This contributes a Curie-Weiss term to the paramagnetic susceptibility, but with an amplititude corresponding to the small localized moments. Since these moments remain constant in amplitude, ω_D remains essentially constant as T is increased.

Such a microscopic model of a ferromagnet has been discussed by a number of authors.

Lederer and Blandin[94] described one such model. They present a Hartree-Fock description of the magnetic electrons in which both the intra-atomic exchange and the ordinary exchange stemming from the inter-atomic interaction are included. They showed the intra-atomic coupling contributes a term to the total energy of the system which makes it favorable to create local moments, and the inter-atomic exchange makes it favorable to align these moments. They discuss three possibilities:

1. Both of these terms are weak. This case leads to a non-magnetic state.

2. Intra-atomic exchange is just below the value necessary to produce a local moment, but the extra energy gained by the coupling between such moments when they exist is enough to cause the unmagnetized state to decrease its energy and produce ordered localized states. They then consider the wave vector dependence of this inter-atomic coupling, whose

magnitude depends on the wave vector describing the distribution of these local moments. (That is $|\bar{q}| = 0$ corresponds to ferromagnetism, $|\bar{q}| = \pi/(\text{lattice constant})$ corresponds to the classical anti-ferromagnetic distribution, and other values of $\bar{q}$ describe various anti-ferromagnetic spin density wave states.)[95] By raising the temperature in this type of substance, one destroys the order and therefore one loses its contribution to the energy. Thus, above the transition temperature, the system becomes non-magnetic, with no localized moments. They suggest that this describes the case of chromium, which is a spin density wave anti-ferromagnet below its transition temperature, but has no local moments above this temperature.[96]

3. The intra-atomic exchange is very strong. This leads to localized moments at all temperatures. These moments order below a critical temperature depending on the strength of the inter-atomic exchange. Above this temperature, one obtains a disordered array of local moments.

A similar model was also discussed by Liu.[97] This author generalizes the Anderson model, which we have mentioned. The Anderson model explains the existence of magnetic moments in certain dilute alloys of magnetic solutes in non-magnetic hosts. According to this model, the d-electrons interact with each other at a particular atomic site via the intra-atomic Coulomb interaction, and with the conduction electrons via the s-d exchange interaction. The d-states are broadened by admixture with the conduction electron states into a band as a result of J_{sd}, and split (up states from down states) by the intra-atomic exchange. Anderson showed that for certain ranges of the parameters describing these interactions, there is a net difference in the occupation numbers of the spin directions associated with each atom. This difference in occupation numbers gives rise to the localized moment associated with the atom, and may be non-

integral, as in the band picture. Then at low temperatures, when the spins order (assuming there is an additional interaction present to cause them to do so), the magnetic moment per site may be a (small) non-integral number of Bohr magnetons.

Liu demonstrated an interesting feature of this model. He calculated the magnetic susceptibility from this model and showed that in the paramagnetic region the number of Bohr magnetons associated with each site, as determined by the magnitude of the Curie constant describing the observed susceptibility, can be greater than that deduced from saturation magnetization measurements. The ratio of these two quantities depends in a complicated way on the values of the parameters describing the system. Basically, this arises from the fact that the external field causes an enhancement of the magnitude of these local moments. This fits in very nicely with our observed magnetostatic measurements.

He then extends the Anderson picture to a collection of dense (rather than dilute) Anderson local moments, and includes the effects of the overlap of neighboring wave functions. He shows that this overlap leads to an exchange interaction between these moments of the Heisenberg type between neighboring moments:

5.2.11 $$\mathcal{H}_{exch} = -2\,J\,\langle\vec{S}_1\rangle\cdot\langle\vec{S}_2\rangle$$

He also shows that this model gives rise to spin waves and critical fluctuations. He present additional evidence favoring this model, based on Fermi surface measurements which he relates to predictions of this model. The reader is referred to this paper for further details about this model.

However, our data seems to indicate that this is the type of band approach necessary to explain the magnetic behavior of our system.

C. Spectroscopic Splitting Factor

The g-value for free electrons is about 2.00. In a free atom, the g-factor differs from this value, due to the spin-orbit interaction, which couples the spin moment, with g=2, to orbital moment with g=1. In a ferromagnetic metal, the orbital angular momentum is quenched.[4] However, as we have discussed, the spin orbit interaction is still present. It is still able to change the energy splitting between adjacent Zeeman levels from the value corresponding to the g=2 case. This change is treated for the localized moments case by Slichter[75] and for the band model by Brooks.[79] The fractional shift in g in both cases is of the order $\Delta g/g \approx A/\Delta$, where A is the spin orbit coupling parameter and Δ is the splitting between the originally degenerate orbital states, which are mixed and split by the crystalline field.

Another mechanism causing g-shift is the s-d exchange interaction. It occurs in a manner analagous to the Knight shift in NMR.[98] The fractional g-shift from this mechanism is about J_{sd}/E_f.

We present our spectrographic splitting factors for our samples in table I. We note that there is relatively little change in it over the entire range of composition covered in our experiments. This would indicate that the band structure is relatively constant.

Table I. Spectroscopic splitting factor as a function of alloy composition.

Nickel concentration (at.%)	g-factor
100.	2.22 ± .03
90.	2.40 ± .10
80.	2.32 ± .05
70.	2.26 ± .08
66.7	2.30 ± .05
64.	2.30 ± .10
60.	2.40 ± .15

VI. SUMMARY AND CONCLUSIONS

We have seen that in order to explain some of the magnetic properties of the nickel-rhodium system, i.e., the continuously decreasing saturation moment, relatively large paramangetic susceptibility, and low temperature high field differential susceptibility, we must abandon the traditional or localized moment description in favor of a band approach.

The simplest such approach has been treated by Stoner, and his results have been expanded by many subsequent authors. This approach treats the magnetic electrons as a conduction electron gas, but account is taken of the exchange arising from the electron-electron interaction, as well as the Fermi statistics required to describe these electrons. However, we have demonstrated that this approach is an over simplication in the case of Ni-Rh, although it has met with a great deal of success in describing the weakly ferromagnetic intermetallic compound, $ZrZn_2$. In the case of our system, the predictions of this theory do not agree with the experimental observations of the composition dependence of the saturation magnetization and the paramagnetic susceptibility. Like the Stoner model, a more accurate description must associate a small magnetic moment, whose magnitude varies with alloy composition, with each atomic site. This assumption is supported by our anisotropy data, and is consistent with the other magneto-static data. By examining the electron spin relaxation rate as a function of alloy composition, and comparing it with the observed variation in the magneto-crystalline anisotropy, we can draw certain conclusions about the microscopic nature of the magnetic state.

Our data has indicated that central to this problem is the intra-atomic exchange interaction, which is responsible for the formation and composition dependence of localized magnetic moments. This interaction,

in addition to the inter-atomic exchange interaction, which causes these localized moments to order into a ferromagnetic state at sufficiently low temperature, is responsible for the magnetic behavior of the system.

Our system, then, may be thought of as being distinct from $ZrZn_2$, the latter seeming to be well described by the more simple Stoner model. This is understandable, as $ZrZn_2$ is composed of two non-magnetic elements. Neutron diffraction studies have demonstrated that the spin density is quite large between lattice sites. Thus it may well be that it is simply a fortuitous accident that the density of states at the Fermi level and the exchange parameter for this material have the necessary values to creater ferromagnetism in the way described by the Stoner model.

In the case of Ni-Rh, however, the alloys are composed of one magnetic element, diluted with a non-magnetic one. In the case of pure nickel, the magnetic electrons, while certainly mobile and band-like, retain a tight binding form. They are, therefore, to be considered as being strongly associated with the individual nickel lattice sites. Thus, as rhodium is added to pure nickel, one might expect that the magnetic moments are still closely related to the lattice sites (whether only the nickel sites, or both the nickel and the rhodium sites), and the description of our system should really start with this idea as a basis. This is indeed the basis of the Anderson model, and the generalization upon which we have based our purposed description of Ni-Rh.

ACKNOWLEDGMENTS

I would like to thank Professor A. M. Portis who suggested this research topic and provided invaluable help in interpreting the results. It is a pleasure to acknowledge Dr. E. Nembach, Mr. L. Johnson, and Mr. G. Georgakopoulos, for their help in preparing and analyzing the samples.

I am grateful to the National Science Foundation and the United States Atomic Energy Commission for their generous financial support.

Finally, I would like to thank my wife, Barbara, for all her support, both moral and material, during the experiments and preparation of this thesis.

REFERENCES

1. C. Herring, Magnetism IV, edited by George T. Rado and Harry Suhl, Academic Press, New York (1966).
2. E. P. Wohlfarth, Phys. Letters 3, 17 (1962).
3. E. Fawcett and W. A. Reed, Phys. Rev. 131, 2463 (1963).
4. C. Kittel, Introduction to Solid State Physics, 3rd. edition, John Wiley and Sons, New York (1966).
5. H. L. Luo and P. Duwez, J. Less Common Metals 6, 245 (1964).
6. E. Bucher, W. F. Brinkman, J. P. Maita and H. J. Williams, Phys. Rev. Letters 18, 1125 (1967).
7. J. Crangle and D. Parsons, Proc. Roy. Soc. (London) 259, 509 (1960).
8. M. B. Salamon, Ph.D. Thesis, University of California, Berkeley (1967).
9. B. R. Cooper and F. Keffer, Phys. Rev. 125, 896 (1962).
10. M. B. Salamon, Phys. Rev. 155, 224 (1967).
11. Chemical Rubber Company, Handbook of Chemistry and Physics, 46th. edition, 1965-66.
12. G. Feher, Bell Technical Journal 36, 449 (1957); also Bell System Monograph 2782.
13. J. Siebert.
14. C. Kittel, Phys. Rev. 73, 155 (1948).
15. Charles P. Slichter, Principles of Magnetic Resonance, Harper and Row, New York (1963), p. 33 ff.
16. R. M. Bozorth, Ferromagnetism, Van Nostrand Co., New York (1951), p. 846.
17. P. Weiss and R. Forrer, Ann. de Phys. 5, 153 (1926).
18. F. Bloch, Z. Physik 57, 545 (1929).

19. L. M. Roth, J. Appl. Phys. 38, 1065 (1967).

20. G. Kemeny, Phys. Letters 25A, 307 (1967).

21. S. Alexander and G. Horwitz, Phys. Rev. 164, 642 (1967).

22. J. Hubbard, Phys. Letters 26A, 709 (1967).

23. A. W. Overhauser, Phys. Rev. 167, 691 (1968).

24. D. R. Penn, Phys. Rev. 142, 350 (1965).

25. C. Kittel, Quantum Theory of Solids, John Wiley and Sons, New York (1964).

26. E. C. Stoner, Proc. Roy. Soc (London) A154, 656 (1936).

27. C. Kittel, op. cit., p. 446 ff.

28. E. C. Stoner, Proc. Roy. Soc. (London) A154, 656 (1936).

29. E. C. Stoner, Proc. Roy. Soc. (London) A165, 372 (1938).

30. E. C. Stoner, Proc. Roy. Soc. (London) A169, 339 (1939).

31. E. P. Wohlfarth, Phil. Mag. 40, 1095 (1949).

32. K. L. Hunt, Proc. Roy. Soc. (London) A216, 103 (1953).

33. E. P. Wohlfarth and R. Rhodes, Phil. Mag. 7, 1817 (1962).

34. S. Ogawa and N. Sakamoto, Phys. Letters, 23, 199 (1966).

35. S. J. Pickart, H. A. Alperin, G. Shirane, and R. Nathans, Phys. Rev. Letters 12, 444 (1964).

36. S. Foner, E. J. McNiff, Jr., and V. Sadagopan, Phys. Rev. Letters 19, 1233 (1967).

37. H. J. Blythe, J. Phys. C. (Proc. Phys. Soc. ser 2) 1, 1604 (1968).

38. E. P. Wohlfarth, Phys. Letters 3, 17 (1962).

39. E. P. Wohlfarth, J. Appl. Phys. 39, 1061 (1968).

40. P. Rhodes and E. P. Wohlfarth, Proc. Roy. Soc. (London) A273, 247 (1963).

41. E. P. Wohlfarth, Proc. Roy. Soc. (London) A195, 434 (1949).

42. W. Band, Proc. Cambr. Phil. Soc. 42, 139, 144 (1946).

43. A. B. Lidiard, Proc. Cambr. Phil. Soc. 49, 115 (1953).

44. E. W. Elcock, P. Rhodes and A. Teviotdale, Proc. Roy. Soc. (London) A221, 53 (1954).

45. D. M. Edwards and E. P. Wohlfarth, Proc. Roy. Soc. (London) A303, 127 (1968).

46. E. P. Wohlfarth, J. Appl. Phys. 39, 1061 (1968).

47. J. Mathon, Proc. Roy. Soc. (London) A306, 355 (1968).

48. H. Hurwitz, Ph.D. Thesis, Harvard University, (1941).

49. J. H. Van Vleck, Rev. Mod. Phys. 17, 42 (1945); Physica 15, 204 (1949).

50. J. H. Van Vleck, Rev. Mod. Phys. 25, 220 (1953).

51. J. M. Ziman, Principles of Theory of Solids, Cambridge University Press, Cambridge (1964).

52. C. Herring, J. Appl. Phys. 31, 3S (1960).

53. L. Pauling, Phys. Rev. 54, 899 (1938).

54. R. M. Bozorth, op. cit., p. 441.

55. E. D. Thompson, E. P. Wohlfarth, and A. C. Bryan, Proc. Phys. Soc. 83, 59 (1964).

56. L. Hodges, H. Ehrenreich, and N. D. Lang, Phys. Rev. 152, 505 (1966).

57. F. M. Mueller, Phys. Rev. 153, 659 (1967).

58. Conyers Herring and Charles Kittel, Phys. Rev. 81, 869 (1951).

59. Conyers Herring, Phys. Rev. 87, 60 (1952).

60. R. J. Elliott and W. Marshall, Rev. Mod. Phys. 30, 75 (1962).

61. R. Kubo, T. Izuyama and Duk-Joo Kim, J. Phys. Soc. Japan suppl. B1 (Proc. Int. Conf. on Magnetism and Crystallography) 67 (1962).

62. T. Izuyama, Duk-Joo Kim, and R. Kubo, J. Phys. Soc. Japan 18, 1025 (1963).

63. R. Kubo, J. Phys. Soc. Japan 12, 570 (1957).

64. R. J. Elliott, Proc. Roy. Soc. (London) A235, 289 (1956).

65. E. D. Thompson, Ann. Phys. 22, 309 (1963).

66. D. M. Edwards, Proc. Roy. Soc. (London) A269, 338 (1962).

67. D. C. Mattis, Phys. Rev. 132, 2521 (1963).

68. D. M. Edwards, Proc. Roy. Soc. (London) A300, 373 (1967).

69. T. Izuyama and R. Kubo, J. Appl. Phys. 35, 1074 (1964).

70. S. Doniach and E. P. Wohlfarth, Phys. Letters 18, 209 (1965).

71. D. M. Edwards, Phys. Letters 24A, 350 (1967).

72. S. Ogawa and N. Sakamoto, J. Phys. Soc. Japan 22, 1214 (1967).

73. R. M. Bozorth, Ferromagnetism, Van Nostrand Co., New York (1951).

74. R. Becker and W. Doring, Ferromagnetismus, Berlin (1939).

75. C. P. Slichter, Principles of Magnetic Resonance, Harper and Row, New York (1963), p. 46.

76. J. H. Van Vleck, Phys. Rev. 52, 1178 (1937).

77. R. J. Elliott, Phys. Rev. 96, 266 (1954).

78. H. J. Williams and R. M. Bozorth, Phys. Rev. 55, 673 (1939).

79. H. Brooks, Phys. Rev. 58, 909 (1940).

80. A. M. Portis and D. Teaney, J. Appl. Phys. 29, 1692 (1958).

81. J. C. Slater, Rev. Mod. Phys. 18, 441 (1946).

82. C. P. Slichter, op. cit., p. 31.

83. M. Sparks, Ferromagnetic-Relaxation Theory, McGraw-Hill Book Company, New York (1964).

84. D. S. Rodbell, Phys. Rev. Letters 13, 471 (1964).

85. B. R. Cooper and F. Keffer, Phys. Rev. 125, 896 (1962).

86. P. G. De Gennes, C. Kittel, and A. M. Portis, Phys. Rev. 116, 323 (1959).

87. H. Mori and K. Kawasaki, Progr. Theor. Phys. 27, 529 (1962).

88. N. Bloembergen, E. M. Purcell, and R. V. Pound, Phys. Rev. 73, 679 (1948).

89. J. H. Van Vleck, Phys. Rev. 74, 1168 (1948).

90. J. H. Van Vleck, Phys. Rev. 78, 266 (1950).

91. F. Keffer, Phys. Rev. 88, 686 (1952).

92. P. W. Anderson and P. R. Weiss, Rev. Mod. Phys. 25, 269 (1953).

93. P. W. Anderson, Phys. Rev. 124, 41 (1961).

94. P. Lederer and A. Blandin, Phil Mag. 14, 363 (1966).

95. A. W. Overhauser, Phys. Rev. 128, 1437 (1962).

96. G. Shirane and W. J. Takei, J. Phys. Soc. Japan 17, 35 (1962).

97. S. H. Liu, Phys. Rev. 163, 472 (1967).

98. D. Shaltiel, J. H. Wernick, H. J. Williams, and M. Peter, Phys. Rev. 135, A1364 (1964).

99. L. I. Schiff, Quantum Mechanics, McGraw-Hill Book Company, New York, (1955), p. 286.

FIGURE CAPTIONS

Fig. 1 Microwave cavity and temperature control unit.

Fig. 2 Faraday's Law magnetization measurement unit.

Fig. 3 Figure 3 has been deleted.

Fig. 4 Schematic representation of the distribution of electrons in the spin-up and spin-down states. a. non-magnetic case. b. strongly ferromagnetic case. c. weakly ferromagnetic case.

Fig. 5 Schematic representation showing the transfer of electrons necessary to proceed from the non-magnetic state to a magnetic state.

Fig. 6 Relative magnetization and Curie temperature vs. relative exchange parameter in the Stoner model. a. Relative magnetization, ξ_0, versus relative exchange interaction strength, $k_b\Theta'/E_f$, with fourth order exchange coefficient, A = .10.
b. Same as (a), except A = 0.
c. Relative Curie temperature, k_bT_c/E_f versus relative exchange interaction strength.

Fig. 7 $3n_{sat}/\langle q_c^2\rangle$ versus the relative magnetization, ξ_0, in the Stoner model. Here n_{sat} is the magnetic moment per atom in units of Bohr magnetons as determined by saturation magnetization measurements and q_c is the magnetic moment per atom as determined by fitting the paramagnetic susceptibility to a Curie-Weiss law. Upper curve is evaluated at $T = 2T_c$ and the lower curve is evaluated at $T = 1.5\,T_c$, where T_c is the Curie temperature.

Fig. 8 Saturation magnetization at $T = 0$ vs. nickel concentration for Ni-Rh. Saturation magnetization is expressed in units of Bohr magnetons per atomic site.

Fig. 9 Curie temperature vs. nickel concentration for Ni-Rh.

Fig. 10 Saturation moment per atom vs. Curie temperature for Ni-Rh. Saturation moment is in units of Bohr magnetons.

Fig. 11 Relative magnetization, ξ_0, vs. nickel concentration. ξ_0 is determined by assuming each Rh atom added to the alloy contributes one magnetic carrier to the magnetic band.

Fig. 12 Relative magnetization, ξ_0, vs. nickel concentration. ξ_0 is determined by assuming each Rh atom added to the alloy contributes 1.5 magnetic carriers to the magnetic band.

Fig. 13 Relative magnetization, ξ_0, vs. Curie temperature for Ni-Rh is determined by assuming each atom of Rh added to the alloy contributes one hole to the magnetic band.

Fig. 14 Magnetic moment per atom of alloy vs. nickel concentration. n_b is the number of Bohr magnetons associated with each atomic site, as determined by the paramagnetic susceptibility. Here, $\langle q_c^2 \rangle$ is the square of the Curie magneton number, which is determined from the slope of the inverse susceptibility vs. temperature curves.

Fig. 15 Relative positions of spin-up sub-band and spin-down sub-band for a band ferromagnet. (a) Strong ferromagnet. Shows energy gap, Δ, between top of majority carrier sub-band and minority carrier Fermi level. (b) Weak ferromagnet. There is no such band in this case.

Fig. 16a Square of magnetization vs. square of temperature for $Ni_{.667}$-$Rh_{.333}$. Here T_c is the Curie temperature and M_o is a convenient normalizing constant, chosen near M(T=0).

Fig. 16b Magnetization vs. $(T/T_c)^{3/2}$ for $Ni_{.667}$-$Rh_{.333}$.

Fig. 16c Same as Fig. 16a, except alloy composition is $Ni_{.70}$-$Rh_{.30}$.

Fig. 16d Same as Fig. 16b, except alloy composition is $Ni_{.70}$-$Rh_{.30}$.

Fig. 16e Same as Fig. 16a, except alloy composition is $Ni_{.75}$-$Rh_{.25}$.

Fig. 16f Same as Fig. 16b, except alloy composition is $Ni_{.75}$-$Rh_{.25}$.

Fig. 17 Anisotropy constant vs. nickel concentration for Ni-Rh. Numbers on figure denote temperature at which the anisotropy was determined.

Fig. 18 Anisotropy constant (at 4.2°K) vs. alloy composition.

Fig. 19 Anisotropy constant (at 4.2°K) vs. square of saturation magnetization.

Fig. 20a Magnetic resonance linewidth vs. temperature for $Ni_{.667}$-$Rh_{.333}$.

Fig. 20b Magnetic resonance linewidth vs. temperature for $Ni_{.70}$-$Rh_{.30}$.

Fig. 20c Magnetic resonance linewidth vs. temperature for $Ni_{.75}$-$Rh_{.25}$.

Fig. 20d Magnetic resonance linewidth vs. temperature for $Ni_{.80}$-$Rh_{.20}$.

Fig. 21a Relaxation rate vs. temperature for $Ni_{.667}$-$Rh_{.333}$. Determined using Eq. 5.1.20.

Fig. 21b Relaxation rate vs. temperature for $Ni_{.70}$-$Rh_{.30}$.

Fig. 21c Relaxation rate vs. temperature for $Ni_{.75}$-$Rh_{.25}$.

Fig. 22 Paramagnetic spin relaxation rate vs. alloy composition. Also shown is the function of anisotropy, $K_1(0)/\xi_0^2$ to compare with Eq. 5.1.30.

Fig. 23 Paramagnetic spin relaxation rate vs. alloy composition. Also shown is the anisotropy constant $K_1(0)$ as a function of alloy composition.

LEGAL NOTICE

This report was prepared as an account of Government sponsored work. Neither the United States, nor the Commission, nor any person acting on behalf of the Commission:

A. Makes any warranty or representation, expressed or implied, with respect to the accuracy, completeness, or usefulness of the information contained in this report, or that the use of any information, apparatus, method, or process disclosed in this report may not infringe privately owned rights; or

B. Assumes any liabilities with respect to the use of, or for damages resulting from the use of any information, apparatus, method, or process disclosed in this report.

As used in the above, "person acting on behalf of the Commission" includes any employee or contractor of the Commission, or employee of such contractor, to the extent that such employee or contractor of the Commission, or employee of such contractor prepares, disseminates, or provides access to, any information pursuant to his employment or contract with the Commission, or his employment with such contractor.

TECHNICAL INFORMATION DIVISION
LAWRENCE RADIATION LABORATORY
UNIVERSITY OF CALIFORNIA
BERKELEY, CALIFORNIA 94720